Phenotypic and molecular characterization of human SPG10 model in *Drosophila melanogaster* and its link to BMP signaling.

Dissertation

zur Erlangung des Grades eines

Doktors der Naturwissenschaften

der Mathematisch-Naturwissenschaftlichen Fakultät

und

der Medizinischen Fakultät

der **Eberhard-Karls-Universität Tübingen**

vorgelegt von

Vrinda Sreekumar

Trivandrum, India.

February – 2015

Tag der mündlichen Prüfung:	30/06/2015
Dekan der Math.-Nat. Fakultät:	Prof. Dr. W. Rosenstiel
Dekan der Medizinischen Fakultät:	Prof. Dr. I. B. Autenrieth
1. Berichterstatter:	PD Dr. Bernard Moussian
2. Berichterstatter:	Prof. Dr. Hansjürgen Volkmer
Prüfungskommission:	Prof. Dr. Ludger Schöls
	Prof. Dr. Hansjürgen Volkmer
	Prof. Dr. Robert Feil
	PD Dr. Bernard Moussian

I hereby declare that I have produced the work entitled:

"Phenotypic and molecular characterization of human SPG10 model in *Drosophila melanogaster* and its link to BMP signaling,"

submitted for the award of a doctorate, on my own (without external help), have used only the sources and aids indicated and have marked passages included from other works, whether verbatim or in content, as such. I swear upon oath that these statements are true and that I have not concealed anything. I am aware that making a false declaration under oath is punishable by a term of imprisonment of up to three years or by a fine.

Tübingen, _____ _____

Date Signature

Acknowledgement

First and foremost, I would like to thank my mentor Dr. Tobias.M.Rasse for giving me the opportunity to work on this project and guiding me through, allowing me to grow as a research scientist. I would like to express my special appreciation and gratitude towards my thesis committee members Prof. Dr. Ludger Schöls and Prof. Dr. Hansjürgen Volkmer for their immense support, guidance and valuable suggestions. I would also take this opportunity to thank DZNE and Hertie Institute for clinical brain research for providing me with the fellowships to complete my PhD.

No words can express my thanks and gratitude towards my lab mates for their constant support, help, encouragement and for all the fun I had in and out of lab. Special thanks to Dr. Petra Füger, Dr. Yao Zhang, Dr. Jeannine Kern, Dr. Bronwen Lasky for introducing me to the field of *Drosophila* research and teaching me the basics of fly genetics. I am truly grateful to Dr.Junyi Zhu for his immense support and willingness to help me with my experiments as a double blind candidate. Special thanks to Dr. Jeannine Kern, Shabab Hannan, Junyi Zhu Carola Schneider for taking care of my flies during my maternity leave and supporting me throughout. My heartfelt thanks to Dr. Natasha Veresceaghina, who to me was like a second mentor in lab, supporting me professionally and personally. I am very happy and grateful to have worked with Dr Doychin Stanchev, Josephine Ng, Stanley Dinesh, Katharina Daub, Raphael Zinser. Thank you all for being such wonderful colleagues and letting me overcome my homesickness. The great times spent together with you all would be remembered forever.

I am extremely happy to be blessed with a wonderful family. I am forever indebted to my parents who have been and still would be my greatest strength in life. No words can express my love and respect for their sacrifices, constant support, love, care and understanding. A blessing in disguise is my better half, my husband Anoop, who has constantly encouraged and helped me evolve as an independent and confident human. Thank you for being a wonderful husband and for finding time after a hard day's work to read my thesis, providing valuable tips and scientific inputs. Last but not the least I would like to thank almighty for gifting me with my precious daughter Vaiga who completes me. Thank you for being such a wonderful and understanding baby and co-operating with me throughout pregnancy while I had to work in the lab. You came into my life as a bundle of joy and very willingly let your mother take some time away from you to write her thesis and complete her PhD. Thank you for making me a proud mother.

Table of Contents

Common Abbreviations

A	alanine
AD	alzheimer disease
ADP	adenosine diphosphate
ALS	amyotrophic lateral sclerosis
ANF	atrial natriuretic peptide
ANOVA	analysis of variance
APP	amyloid precursor protein
AT	anterograde transport
ATG8	autophagy related protein 8
ATP	adenosine-5- triphosphate
AZ	active zone
BMP	bone morphogenetic protein
Brp	bruchpilot
C	cysteine
CAZ	cytomatrix active zone
CD8	cluster of differentiation 8
CNS	central nervous system
CSP	cysteine string protein
DIC	dynein intermediate chain
Dlg	disc large
DNA	deoxyribonucleic acid
Dpp	decapentaplegic

DV-Glut	*drosophila* vesicular glutamate transporter
Dvl	dishevelled
EM	electron microscopy
EP	electro potential
Eve	even skipped
FMI-43	styryl pyridinium dye
Fz	frizzled
GB	gaussian blur
Gbb	glass bottom boat
GDP	guanosine diphosphate
GFP	green fluorescent protein
GluR	glutamate receptor
GMR	glass multimer reporter
GSK	glycogen synthase kinase
GTP	guanosine triphosphate
HD	huntington disease
HEPES	4-(2-hydroxyethyl)-1-piperazineethanesulfonic acid
Hiw	highwire
HL3	hemolymph-like solution 3
HRP	horse raddish peroxidase
HSP	hereditary spastic paraplegia
Kcl	potassium chloride
Khc	kinesin heavy chain

KIF	Kinesin super family protein
KLC	kinesin light chain
L1	first instar larvae
L2	second instar larvae
L3	third instar larvae
LAMP	lysosome associated membrane protein
m RFP	monomeric red fluorescent protein
MAP1B	microtubule -associated protein 1B
MAPK	mitogen-activated protein kinase
$Mgcl_2$	magnesium chloride
MKK	mitogen activated protein kinase kinase
MT	microtubule
MV	mutivesicular
N	asparagine
NaCl	sodium chloride
$NaHC0_3$	sodium bicarbonate
NGS	normal goat serum
NIPA-1	non imprinted in Prader-Willi/Angelman syndrome 1
NMJ	neuro muscular junction
p	probability
PBS-T	phosphate buffered solution with triton-X
PD	parkinson disease
PFA	paraformaldehyde

PLV	poly lysosomal vesicles
pMad	phosphorylated mothers against decepentaplegic
PNS	peripheral nervous system
PolyQ	polyglutamine
R	arginine
REP	rough eye phenotype
RFP	red flourescent protein
RNA	ribonucleic acid
RNAi	messenger ribonucleic acid interference
RT	retrograde transport
S	serine
Sax	saxophone
Scw	scew
Sd	standard deviation
Sem	standard error of mean
SMA	spinal muscular atrophy
SNARE	soluble N-ethylmaleimide-sensitive factor attachment protein receptor
SPG10	spastic paraplegia type 10
SV	synaptic vesicle
TGF-ß	transforming growth factor-ß
Tkv	thickveins
Tkv-CA	thickveins constitutively active

TPR	tetratricopeptide
UAS	upstream activating sequence
V	valine
VNC	ventral nerve cord
Wit	wishful thinking
Wnd	wallenda
WNT	wingless
YFP	yellow fluorescent protein

1 Summary

Hereditary spastic paraplegia (HSP) is a group of genetically heterogeneous neurodegenerative disorders characterized by progressive spasticity of lower extremities as a consequence of axonopathy of the longest cortico spinal tract. Defects in axonal transport, ER membrane modeling, mitochondrial function, DNA repair, autophagy, lipid metabolism and myelination have been linked to HSP. SPG10, a subtype of HSP is caused due to mutations in the anterograde microtubular motor protein kinesin. Kinesin mutation impairs axonal transport leading to synaptic dysfunction.

My study was aimed at the phenotypic and molecular characterization of the human SPG10 model in *Drosophila melanogaster* and to investigate its suspected interplay with BMP signaling. The mutation in kinesin protein in human SPG10 has been mapped to position N256S. This point mutation was inserted into *Drosphila* kinesin heavy chain (Khc) at the N262S position and the mutated kinesin protein was ectopically expressed using tissue specific drivers. The *Drosophila* Khc^{N262S} mutants were characterized by reduced survival, behavioral impairments, axonal swellings, synaptic protein depletion at distal NMJs, cytoskeletal disability, developmental delay, and synaptic degeneration. Ectopic overexpression of wild type kinesin alongside mutated kinesin ($Khc^{N262S+wt}$) partially rescued the HSP pathology thus revealing the dominant negative nature of this mutation. Khc^{N262S} mutation affected both anterograde and retrograde transport in *Drosophila* larvae. Impairment of long distance transport within axons directly contributes to synaptic defects by perturbing the BMP signaling pathway which is essential for synapse maintenance and function. Till date a common pathological mechanism in HSPs remains to be identified. Atleast 4 human SPGs have been linked to altered BMP signaling. The key pathological features of downregulated BMP signaling in *Drosophila* resemble that of the Khc^{N262S} *Drosophila* model. A previous study in the lab show reduced pMad (transcription factor of BMP target gene, Trio) levels in Khc^{N262S} larval motor neuron cell bodies. Assuming that the phenotypical defects in the Khc^{N262S} *Drosophila* model may be due to altered BMP signaling, we hypothesized that upregulation of BMP signaling in Khc^{N262S} mutants could rescue the synaptic and behavioral defects via cytoskeletal stabilization. However, neither the overexpression of constitutively active BMP receptor Tkv-CA nor the overexpression of target gene Rac-GEF Trio was able to rescue the Khc^{N26S} pathology significantly. *In- vivo* study using YFP tagged Tkv showed impairments in retrograde transport of Tkv which was consistent with reduced pMad

levels observed in motor neuron cell bodies of $Khc^{N262S+TkV-CA}$ larvae. Though overexpression of Trio in mutants partially rescued the cargo trafficking it did not suffice synaptic or behavioral rescue owing to its tight regulation and influence on numerous other genes. Since Trio is the only BMP target gene known, it does not rule out regulation of other unidentified genes. Finally, molecular mechanism involved in Khc^{N262S} induced SPG10 pathology is quite complex since both anterograde and retrograde transport is impaired, hence BMP signaling could only be one among the many signaling pathways affected, and sole upregulation of which alone does not suffice rescue.

My study has successfully characterized the severity of the SPG10 model in *Drosophila* at the molecular level as well as behavioral level. After testing our hypothesis, arising from similarity of phenotypes and previously described interplay at molecular level, a connection between SPG10 pathology and BMP signaling seems highly plausible, yet our proposed mechanism of rescue was only partially successful.

2 Introduction

2.1 Axonal transport in neurons

Neurons, the core component of the nervous system, are electrically excitable cells that process and transmit information through chemical and electrical signals. Neurons connect to each other via synapses to form neural networks that act as information highways between different areas of the brain (Lodish H 2000). Sensory neurons carry information from the sensory receptors of the body to the brain. Motor neurons transmit information from the brain to the muscles of the body for muscular activity and glandular outputs. Interneurons are responsible for communicating information between different neurons in the body.

A typical neuron possesses a cell body (soma), dendrites and an axon (**Figure 1**). The cell body contains all the cellular organelles and is also the site of most protein synthesis and degradation. Dendrites are thin structures that arise from the cell body which then extends and branches giving rise to a complex "dendritic tree" which acts as major input sites for information. An axon is a special cellular extension that arises from the cell body at a site called the axon hillock and can extend several times the diameter of the soma in length (Lodish H 2000). The information from the cell body is transmitted along the axon to its terminus which contains specialized structures called synapses which communicate with target cells through the release of neurotransmitters.

The vast majority of axonal proteins are synthesized in the neuronal cell body and transported along axons. Axonal transport occurs throughout the life of a neuron and is essential for its growth and survival. Axonal transport is a cellular process responsible for the movement of mitochondria, lipids, synaptic vesicles, proteins, and other organelles between the cell body and synapses through the axoplasm. Proteins that are synthesized in the cell body are transported along the axon to its terminus and the residual proteins are transported back to the cell body for degradation (Karle, Mockel et al. 2012).

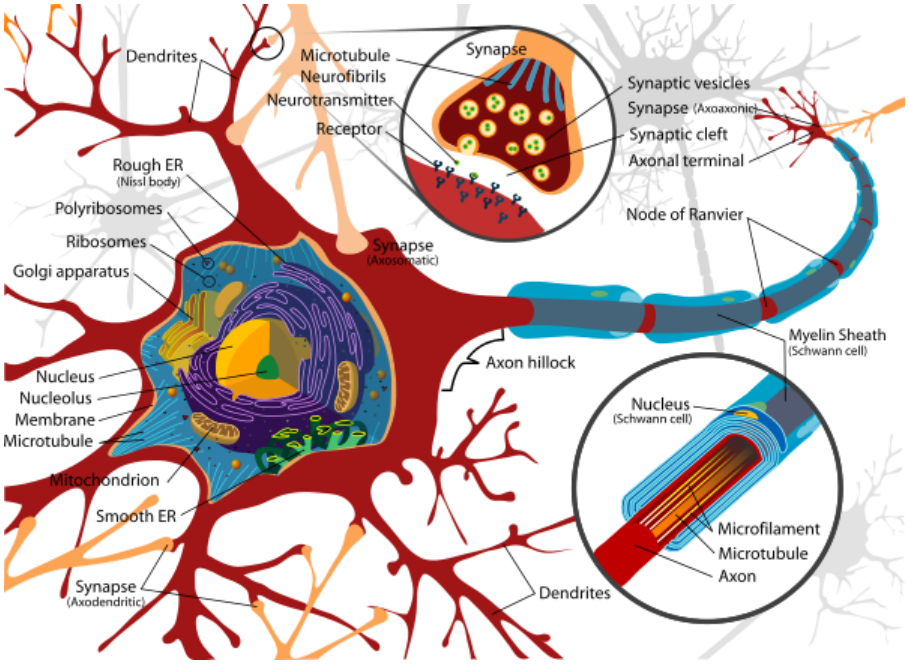

Figure 1: Structure of a neuron. (en.wikipedia.org)

Axonal transport occurs along the cellular cytoskeleton which provides the neuron with structural support that allows the cell to grow or change in size and shape over time. There are three major components of the axonal cytoskeleton—microtubules, actin, and intermediate filaments (**Figure 2**).

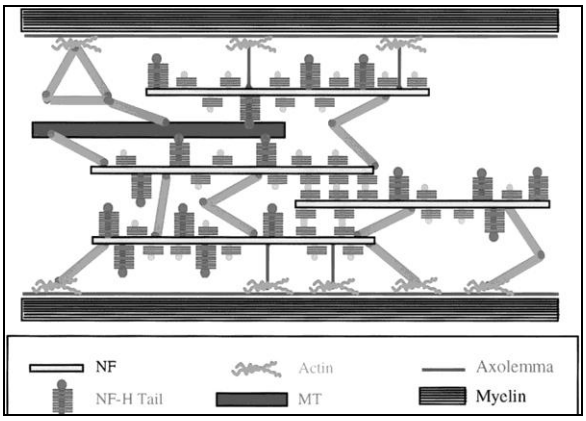

Figure 2: Cytoskeletal arrangement in axons. The axonal cytoskeleton is shown comprising microtubules, neurofilaments and actins. (Image source- *Rao et al, The journal of cell biology, 1998*)

Axonal transport is bidirectional and based on the direction of transport can be classified as anterograde or retrograde. Proteins and membranes that are required for renewal of the axon, synapse formation and neurotransmission as well as various signaling molecules are synthesized

in the cell body assembled into membranous vesicles or multiprotein particles and are transported to the axonal terminus by a process called anterograde transport (Chevalier-Larsen and Holzbaur 2006). This transport is mediated via microtubular motors called kinesins (Goldstein 2001). On the other hand, damaged membranes, proteins, vesicles, signaling molecules and organelles are transported back from the axonal terminus to the cell body (for degradation) by a process called retrograde transport. It is mediated via microtubular motors called dynein-dynactin complex (Hirokawa, Nitta et al. 2009; Hirokawa, Niwa et al. 2010) (**Figure 3**). Based on the rate of transport, axonal transport can be classified as fast or slow. Proteins that are required for the maintenance of axonal cytoskeleton like microtubules, neurofilaments and actin filaments move slowly along the axon at speeds of 0.1-3mm/day (Hirokawa, Nitta et al. 2009; Terada, Kinjo et al. 2010). While, membrane vesicles are carried by fast axonal transport at a rate up to 400mm/day (Hirokawa, Nitta et al. 2009; Terada, Kinjo et al. 2010). Fast transport is critical during development especially for the growth of axons and dendrites by adding new material to their tips (Karle, Mockel et al. 2012).

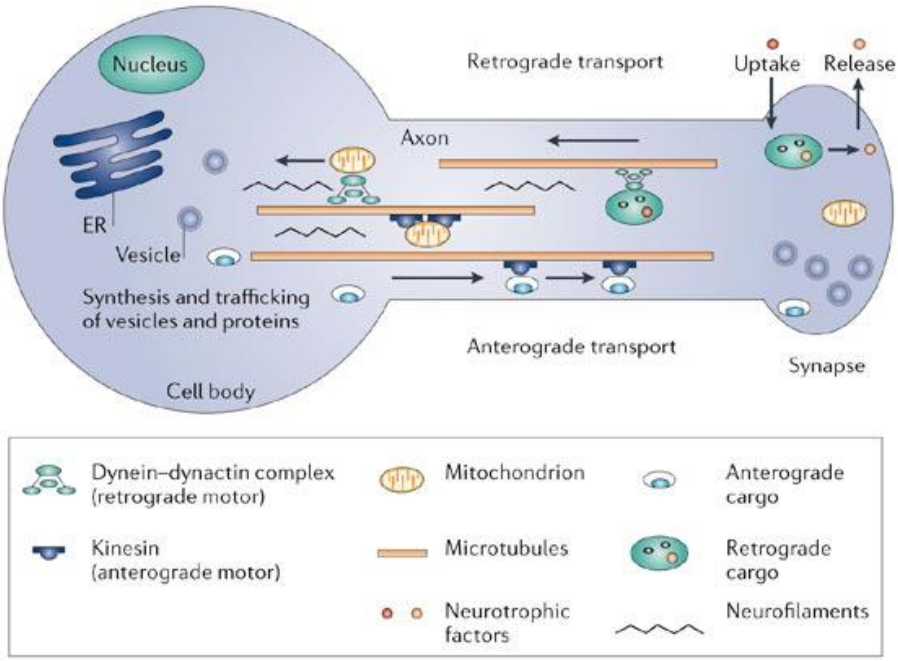

Figure 3: Axonal transport. Schematic representation of bi- directional axonal transport. Anterograde transport of various cargos from cell body to synapse along microtubule is mediated by the anterograde motor– kinesin. Retrograde transport of cargos from synapse to cell body is mediated via retrograde motor- dyenin-dynactin complex. (Image source - *Piera Pasinelli and Robert H. Brown, Nature Reviews Neuroscience, 2006*)

Microtubules run along the length of the axon that provides the main cytoskeletal track for transportation mediated via specialized microtubular motors (Hirokawa, Nitta et al. 2009; Hirokawa, Niwa et al. 2010; Karle, Mockel et al. 2012; Kang, Hansen et al. 2014).

2.1.1 Microtubules

Microtubules along with microfilaments and intermediate filaments form the eukaryotic cellular cytoskeleton which is involved in various processes like cell motility, intracellular transport, mitosis, secretion, cell shape maintenance, cell polarization and positioning of membrane vesicles and organelles (Hirokawa 1994; Joshi 1994; Mandelkow and Mandelkow 1995; Conde and Caceres 2009). In neurons, microtubules function in the initial steps of polarization, organization of intracellular compartments, remodelling of dentritic spines and trafficking of cargos to the pre and post synaptic membranes (Conde and Caceres 2009). Microtubules are composed of α and β-tubulin dimers. These dimers polymerize end to end with the α-subunit of one contacting the β-subunit of the other to form protofilaments. For polymerization to occur, the dimers must be present at a concentration above a threshold called the critical concentration (Walker, O'Brien et al. 1988; Desai and Mitchison 1997; Vale 2003).

13 such protofilaments associate laterally to form a single microtubule which is then extended by the addition of more protofilaments. Microtubules have a distinct polarity that is important for their biological function. Therefore, in a protofilament, one end will have the α- subunits exposed while the other end will have the β-subunits exposed. These ends are designated as the slow growing (−) and fast growing (+) ends, respectively. The elongation of microtubules typically only occurs at the (+) end (Walker, O'Brien et al. 1988; Desai and Mitchison 1997; Vale 2003).

One of the most striking features of microtubules is their rapid turnover (which potentiates reorganization) and their ability to undergo cycles of rapid growth and disassembly known as dynamic instability (**Figure 4**). Individual microtubules exist in either polymerized or depolymerized states. The transition from growing to shrinking state is called catastrophe, whereas the transition from shrinking to growing is called rescue (Conde and Caceres 2009).

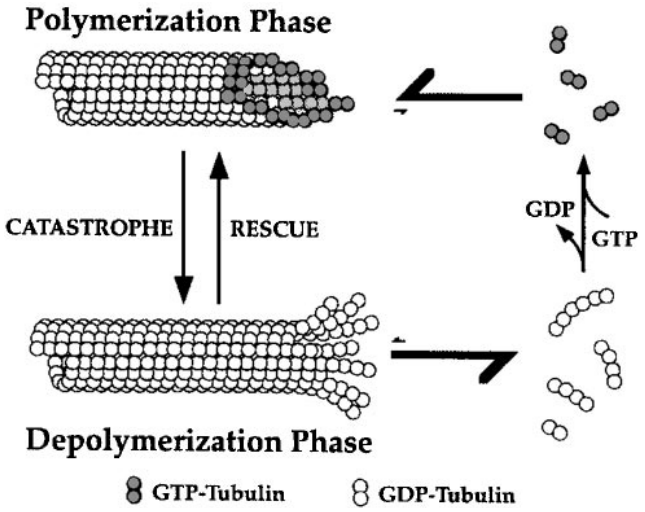

Figure 4: Microtubule dynamic instability characterized by the co existence of polymerizing and depolymerizing microtubules. GTP-tubulin is incorporated at polymerizing microtubular ends; the bound GTP subsequently hydrolyzed releasing an inorganic phosphate group. Polymerizing microtubules infrequently transit into the depolymerization phase (catastrophe). Depolymerization is characterized by the very rapid loss of GDP-tubulin subunits and oligomers from the MT end. Depolymerizing MTs can also infrequently transit back to the polymerization phase (rescue). (Image source - *Arshad Desai and Timothy J. Mitchison, Annu. Rev. Cell Dev. Biol. 1997*)

The transport of membrane vesicles and organelles in both directions along axonal microtubules can be visualized by video-enhanced microscopy. Members of two large families of motor proteins—the kinesins and the dyneins generate movements along the microtubules using the chemical energy of ATP hydrolysis (**Figure 5**). Conventional kinesin and other plus end-directed members of the kinesin family carry their cargo toward the cell periphery, whereas cytoplasmic dyneins and minus end-directed members of the kinesin family transport materials toward the cell body (Grafstein and Forman 1980; Brady, Lasek et al. 1982; Hirokawa 1982; Hirokawa, Pfister et al. 1989). The motors bind to the microtubule using the motor head region while the tail end binds with the cargo and carries it along the microtubule.

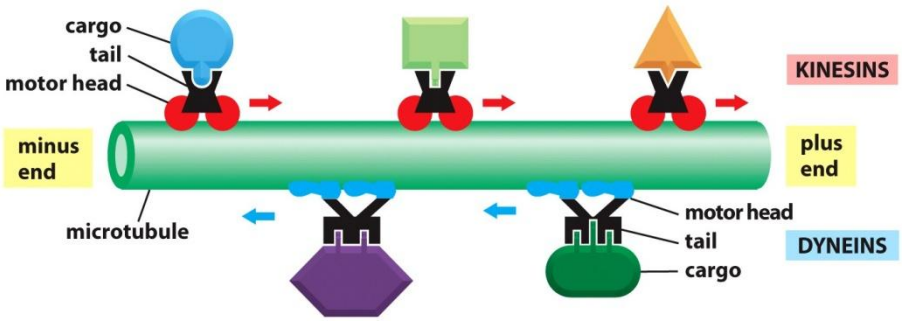

Figure 5 : Microtubular motors. Schematic representation of the microtubule showing the minus and plus ends with the motors kinesin and dynein carrying the cargo anterogradely and retrogradely. Motor heads bind to the microtubule and tail end binds the cargo. (Image source – *Essentail Cell biology 3/ Garland science 2010*).

Motor proteins travel in a specific direction along the microtubule. This is because the microtubule is polar and the motor heads can only bind to the microtubule in one orientation, meanwhile ATP binding gives each step its direction through a process known as neck linker zippering (Hirokawa 1998; Hirokawa, Noda et al. 1998).

Microtubules undergo post translational modifications like detyrosination, glutamylation, acetylation and glycylation (Desai and Mitchison 1997; Conde and Caceres 2009). The post translational modification of microtubules, which leads to its stabilization, plays an important role in the binding of the motor proteins to the microtubules. It has been shown that detyrosination, polyglutamylation and acetylation could guide selected motors and their respective cargos along specific microtubule tracks (Schulze, Asai et al. 1987). Likewise, the conventional kinesin (kinesin-1) binds preferentially to detyrosinated tubulin which has important consequences for its subcellular distribution in the neurons (Liao and Gundersen 1998; Kreitzer, Liao et al. 1999; Dunn, Morrison et al. 2008; Konishi and Setou 2009). Kinesin also shows high specificity binding to polyglutamylated tubulin (Larcher, Boucher et al. 1996; Bonnet, Boucher et al. 2001). Similarly, microtubule acetylation stimulates anterograde and retrograde transport by increasing the binding of kinesin and dynein to microtubules. Consequently, acetylation of microtubules could selectively stimulate intracellular dynamics and cargo distribution (Reed, Cai et al. 2006; Dompierre, Godin et al. 2007; Cai, McEwen et al. 2009). Collectively, the microtubules serve as an excellent path for kinesin binding and function.

2.1.2 Kinesins

Kinesins are microtubule-associated motor proteins which convert chemical energy released from nucleoside triphosphates (ATP) into mechanical energy.

Conventional kinesins move towards the plus end of microtubules, however members of kinesin 14 family (e.g. Ncd in *Drosophila*) moves towards the minus end of microtubules (Grafstein and Forman 1980; Brady, Lasek et al. 1982; Vale, Reese et al. 1985; Hirokawa 1998; Hirokawa, Noda et al. 1998; Hirokawa and Noda 2008; Hirokawa, Nitta et al. 2009; Hirokawa, Noda et al. 2009). By the position of the motor domain in the polypeptide chain, kinesins are classified as N-

terminal, internal, or C-terminal. Based on their variable polypeptide chain composition kinesins can be classified as monomers, homodimers or heterodimers (Hirokawa and Noda 2008). Kinesins are structurally related to G proteins, which uses the energy by hydrolyzing GTP instead of ATP. Several structural elements like the Switch I and Switch II domains are shared between the two families (Vale 1996).

Human kinesin superfamily members include proteins which are organized into 14 families from kinesin-1 through kinesin-14 (Dagenbach and Endow 2004). Kinesin-1 is the prototypical conventional kinesin.

2.1.2.1 Kinesin 1

Members of the kinesin superfamily vary in shape but the prototypical kinesin-1 is a hetero tetramer whose motor subunit kinesin heavy chain (KHC) (denoted Khc in *Drosophila*) forms a protein dimer that binds two light chains (KLC) **(Figure 6)** (Hirokawa and Noda 2008).

The heavy chain of kinesin-1 comprises a globular head (the motor domain) at the amino terminal end. This is connected via a short and flexible neck linker to the stalk which is a long, central alpha-helical coiled-coil domain. This further terminates in a carboxyl terminal tail domain which associates with the light-chains. The stalks of two KHCs intertwine to form a coiled-coil that directs dimerization of the two KHCs **(Figure 7)** (Hirokawa, Pfister et al. 1989; Hirokawa 1998; Hirokawa, Nitta et al. 2009; Hirokawa, Noda et al. 2009; Hirokawa, Niwa et al. 2010).

The globular motor domain of the kinesin heavy chain generates force that binds ATP and microtubules. Each head has two separate binding sites- one for the microtubule and the other for ATP. ATP binding and hydrolysis (which releases ADP), changes the conformation of the microtubule-binding domains and the orientation of the neck linker with respect to the head and thus enabling kinesin walking. The amino acid sequence of the head motor domain is well conserved among various kinesins. Several structural elements in the head region, including a central beta-sheet domain and the Switch I and II domains have been implicated in mediating the interactions between the two binding sites and the neck domain (Kozielski, Sack et al. 1997) . The helical stalk domain acts as a spacer and force transducer.

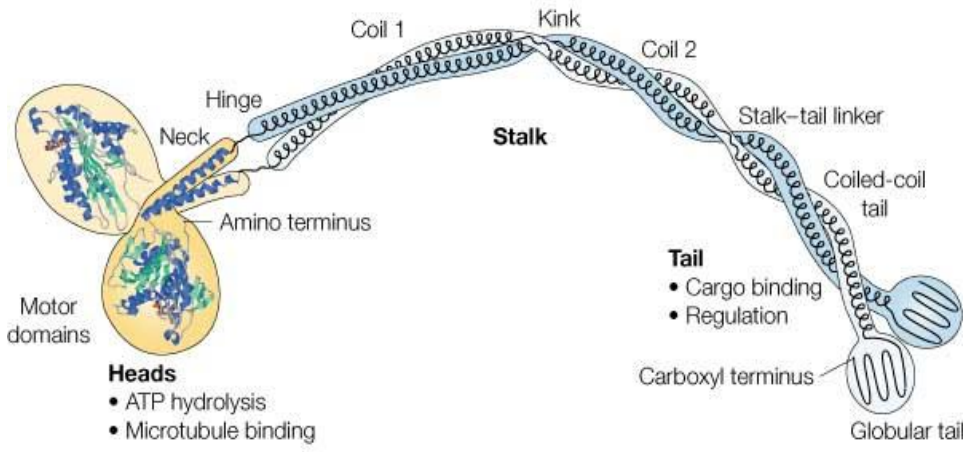

Figure 6: Kinesin-1 structure. Schematic representation of Kinesin-1 structure. Motor domain is involved in microtubule binding at the expense of ATP hydrolysis. The tail region binds the cargo. The neck connects the motor head domain to the globular tail. (Image source - *Günther Woehlke & Manfred Schliwa, Nature Reviews Molecular Cell Biology, Oct 2000*)

The globular tail domain which binds the light chains connects the complex to the cargo (e.g. vesicles or organelles) (Vale, Reese et al. 1985; Kozielski, Sack et al. 1997; DeBoer, You et al. 2008; Hirokawa and Noda 2008; Hirokawa, Nitta et al. 2009; Hirokawa, Noda et al. 2009; Karle, Mockel et al. 2012). Cargo binds to the kinesin light chains, at the tetratricopeptide repeat (TPR) motif sequence of the KLC. But in some cases cargo also binds to the C-terminal domains of the heavy chains (Hirokawa, Pfister et al. 1989). Kinesin heavy chains and light chains only homodimerize, whereas the interaction between heavy and light chains has shown no specificity. (DeBoer, You et al. 2008; Karle, Mockel et al. 2012).

The vertebrate genome of Kinesin-1 contains three isoforms of kinesin heavy chain (KIF5A, KIF5B and KIF5C) and three isoforms of kinesin light chain (KLC1, KLC2, KCL3). Of these, KIF5B, KLC1 and KLC2 are expressed ubiquitously. KIF5A and KIF5C are expressed specifically in neurons (Niclas, Navone et al. 1994; Kanai, Okada et al. 2000). The *Drosophila* genome contains one kinesin heavy chain (Khc) isoform and one isoform of kinesin light chain (Klc), which are ubiquitously expressed (Yang, Saxton et al. 1988). Kinesin-1 acts as a motor for fast axonal transport of membranous organelles as well as for slow axonal transport of cytoplasmic proteins.(Terada, Kinjo et al. 2000; Terada, Kinjo et al. 2010; Karle, Mockel et al. 2012).

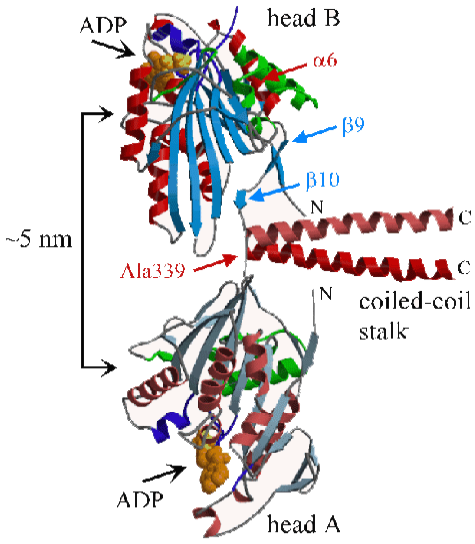

Figure 7: Crystal structure of Kinesin motor: The motor domain contains a central β-sheet of eight strands surrounded by six α-helices. The presumptive microtubule-binding region is coloured green. The nucleotide binding region is coloured purple, the nucleotide (ADP) is shown in yellow. The linker region (β9-β10) connects the core motor domain and the neck region. Dimerization is achieved by the coiled-coil interaction between the two neck helices at α7. (Iamge source - *Kozielski et al., Cell 1997*)

Kinesin-1 cargo include mitochondria, synaptic proteins, vesicular glutamate transporter, lysosomes, membrane associated Soluble N-ethylmaleimide-sensitive factor attachment protein receptor (SNARE) proteins, syntaxin-1-containing vesicles, tubulin, apolipoprotein E receptor 2, phosphorylated amyloid precursor protein (APP) etc (Tanaka, Kanai et al. 1998; Verhey, Meyer et al. 2001; Inomata, Nakamura et al. 2003; Su, Cai et al. 2004; Kimura, Watanabe et al. 2005; Morton, Cunningham et al. 2010; Karle, Mockel et al. 2012). Transport of these cargos is indispensable for the functioning of neurons. Consequently, impairments of axonal transport have serious consequences and are linked to the development of many neurodegenerative diseases.

2.2 Axonal transport defect and neurodegenerative diseases

The intracellular transport of organelles along an axon is crucial for the maintenance and function of a neuron. Disruption of axonal transport is an early and also causative event in many neurodegenerative diseases. Axonal transport defects can be due to mutations in motor proteins like kinesin and dynein or in the cytoskeletal proteins (**Figure 8**). Diffuse axonal injury that interrupts the transport will cause the distal axon to degenerate and this process is called Wallerian degeneration (Wang, Medress et al. 2012). Axonal transport defects are the underlying

cause for many motor neuron diseases like spinal muscular atrophy (SMA), hereditary spastic paraplegias (HSPs), amylotrophic lateral sclerosis (ALS) etc (Chevalier-Larsen and Holzbaur 2006).

Defects in axonal transport have also been indirectly linked to a number of progressive human neurodegenerative diseases including Alzheimer disease (AD), Huntington disease (HD) (De Vos, Grierson et al. 2008). These diseases display axonal pathologies including abnormal accumulations of proteins and organelles. The proteins encoded by genes linked to these diseases are transported in the axon, and manoeuvring these genes also disrupts transport (Chevalier-Larsen and Holzbaur 2006). Axonal transport defects are most obvious in the neurons with long axons where long distance transport is required. Hereditary spastic paraplegia is one such neurodegenerative disease where long distance axonal transport is perturbed.

Axonal transport in human disease

	Disease name	Mutant protein	Cellular pathology relevant to transport deficits
Motor mutations	CMT type 2A	KIF1B beta	reduced transport of synaptic vesicle proteins
	spastic paraplegia	KIF5A	altered microtubule/motor interaction
	CFEOM type1	KIF21A	predicted to disrupt anterograde transport of vesicles
	distal SBMA	$p150^{Glued}$	reduced microtubule/$p150^{Glued}$ interaction
			p150 aggregation
Cytoskeletal mutations	CMT type 2	HSP27	disruption of neurofilament formation
			p150 mislocalized and aggregated
	HRD	TBCE	disruption of microtubule stability
	CMT type 2	NF-L	disruption of anterograde and retrograde transport
Neurodegenerative diseases involving axonal transport	Huntington's disease	huntingtin	disruption of anterograde and retrograde transport
			axonal swellings
	SBMA	AR	disruption of anterograde and retrograde transport
	Alzheimer's disease	APP/PS1	disruption of anterograde transport
			axonal blockage
	ALS	SOD1	deficits in anterograde and retrograde transport
			dynein/SOD1 aggregates

Figure 8: Axonal transport defects and neurodegenerative diseases. (Image source - *E. Chevalier-Larsen, E.L.F. Holzbaur et al, Biochimica et Biophysica Acta 2006*)

2.3 Hereditary spastic paraplegia

Hereditary spastic paraplegia (HSP) is a group of genetically heterogeneous neurodegenerative disorders characterized by progressive spasticity and weakness of the lower extremities (Harding 1983). It occurs as a consequence of axonopathy of the longest cortico spinal tract resulting in pyramidal tract dysfunction (Finsterer, Loscher et al. 2012). Age of onset is anywhere from early childhood to above 70 years and progresses slowly over many years (Lo Giudice, Lombardi et al. 2014).

HSP is clinically divided into pure and complicated forms. While the pure form presents spasticity of lower extremities leaving upper limbs unaffected , the complicated from displays a wide range of neurological and systemic features like ataxia, mental retardation, dementia, epilepsy, visual and speech impairment, deafness and difficulty in swallowing and breathing. Based on the mode of inheritance HSPs are classified as autosomal dominant, autosomal recessive or X-linked. To date, 71 spastic gait disease-loci and 54 spastic paraplegia genes (SPGs) have been identified (Lo Giudice, Lombardi et al. 2014). 19 SPGs follow an autosomal dominant (AD, AD-SPG) mode of inheritance, 27 show autosomal recessive (AR, AR-SPG) and 5 are X-linked (XL, XL-SPG) (Salinas, Proukakis et al. 2008).

Several aberrant cellular processes are involved in the pathogenesis of HSP (**Figure 9**). Defects in membrane and axonal transport, endoplasmic reticulum membrane modelling and shaping, mitochondrial function, DNA repair and autophagy as well as abnormalities in lipid metabolism and myelination have been linked to HSP (Reid 2003; Dion, Daoud et al. 2009; Blackstone, O'Kane et al. 2011). Moreover, recent studies indicate that impairment of endosome membrane trafficking in vesicle formation, oxidative stress and mitochondrial DNA polymorphisms can also result in the onset of the disease (Atorino, Silvestri et al. 2003; Reid 2003; Blackstone, O'Kane et al. 2011; Sanchez-Ferrero, Coto et al. 2012).

One of the subtypes of HSP is SPG10 that is caused as a result of a mutation in the microtubular motor protein kinesin which interferes with axonal transport and thus leading to further complications.

2.3.1 Spastic paraplegia subtype 10 - SPG10

SPG10 is an autosomal dominant form of HSP due to point mutations in *KIF5A*, a gene encoding the neuronal kinesin heavy chain implicated in anterograde axonal transport. The SPG10 locus maps to chromosome 12q13. KIF5A (12q13.3) which was subsequently identified as the gene involved (Reid, Dearlove et al. 1999; Reid, Kloos et al. 2002). *KIF5A* mutations were found in both pure and complicated forms of the disease. SPG10 is implicated in approximately 3% of autosomal dominant HSPs. Mutations in KIF5A represent the major cause of the complicated form of autosomal dominant HSP (Goizet, Boukhris et al. 2009).

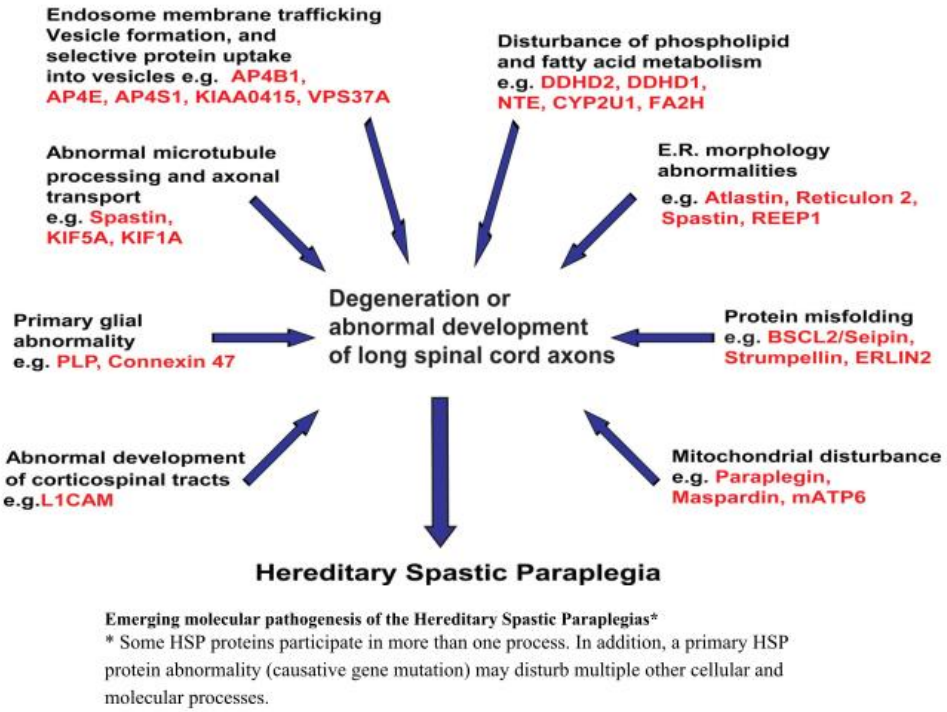

Figure 9: Factors involved in HSP pathogenesis: (Image source - *John K. Fink, Acta Neuropathol. 2013*)

Around 15 missense mutations and one deletion have been reported in KIF5A. All mutations are located within or close to the switch clusters into the motor domain. But exceptions are the point mutations p.A361V and p.E755K which falls within the neck region of the protein, adjacent to the globular motor domain (Goldstein 2001; Song, Marx et al. 2001). Functional analysis of 4 *KIF5A* mutations located in the motor or neck domains of kinesin revealed that *KIF5A* mutations affect axonal transport by reducing the cargo flux leading to deficient supply of essential proteins to the synapse (Ebbing, Mann et al. 2008). When the motility of kinesin in 4 KIF5A mutations (p.K253N, p.N256S, p.R280C, and p.A361V) was analyzed, the A361V mutation did not change the gliding properties in vitro, whereas the others either reduced microtubule affinity or gliding velocity or both (Ebbing, Mann et al. 2008; Kawaguchi 2013). Furthermore, optical tweezer assays demonstrated the inability of mutant kinesins to move along the microtubules, indicating an almost complete abrogation of KIF5A function due to the point mutations (Ebbing, Mann et al. 2008; Kawaguchi 2013). All known SPG10 patients are heterozygous for the *KIF5A* allele and hence the axonal transport is affected gradually and not abruptly. This is due to the dominant-negative effect of mutated KIF5A on the wild-type protein which blocks the microtubule binding of the latter gradually. This results in delayed arrival of mitochondria to the

synapse which further depletes the synapse of proteins and ATP which in turn affects synaptogenesis and synapse maturation (Karle, Mockel et al. 2012). Furthermore, Kinesin-1 and Kinesin-2 mediates the anterograde transport of the retrograde motor complex (dynein-dynactin complexes) (Deacon, Serpinskaya et al. 2003; Hirokawa, Niwa et al. 2010; Yamada, Toba et al. 2010). Thus impairment of kinesin mobility indirectly affects retrograde transport. Several studies have demonstrated that the frequency and velocity of neurofilament movements are affected in both anterograde and retrograde directions by KIF5A mutations, strengthening the theory that KIF5A is required for retrograde transport (Uchida, Alami et al. 2009; Wang and Brown 2010). Since kinesin-1 transports both fast and slow cargo (Hirokawa, Niwa et al. 2010; Terada, Kinjo et al. 2010), it is very likely that impairment of kinesin leads to the disrupted transport of cytoplasmic protein needed for homeostasis resulting in the pathogenesis of SPG10 (Barry, Millecamps et al. 2007; Uchida, Alami et al. 2009; Wang and Brown 2010). In order to understand the SPG10 pathology in depth, it is important to study the disease progression in vivo. *Drosophila melanogaster* serves as a very simple *in- vivo* model to study pathology involved in many neurodegenerative diseases.

2.4 *Drosophila melanogaster*- a simple model organism

Drosophila melanogaster, one of the first organisms with a fully sequenced genome serves as an excellent experimental model owing not only to its simplicity but also because of the many advantages (genetic, anatomic, behavioural, methodical and economic) over other vertebrate model systems. The fly genome has been completely sequenced and annotated, and encodes for more than 14,000 genes (Reiter, Potocki et al. 2001). Of these, the bulk of the genome is carried by only three chromosomes.

It has been estimated that nearly 75% of disease-related genes in humans have functional orthologs in the fly (Reiter, Potocki et al. 2001). There is approximately 40% similarity between homologs of protein sequences and around 80-90% homology in conserved functional domains between fly and mammal (Pandey and Nichols 2011). It is possible to create a *Drosophila* ortholog of a gene of unknown function found to be mutated in human disease which enables to study its normal physiological function. Meanwhile, it is also possible to induce the disease-specific mutation into that ortholog to unravel the pathological effect of the mutation on the functionality of that gene. Alternatively, gene function can be studied by creating a transgenic

model expressing the mutant human gene in the *Drosophila* and facilitate understanding of the pathological mechanism behind the development of the disease. Another advantage of using the *Drosophila* system is the spatial and temporal control over the expression of desired gene using a tissue specific upstream activating sequence UAS-Gal4 expression system (Prussing, Voigt et al. 2013).

It is possible to carry out high throughput genetic and drug screens to identify enhancers and suppressers of the phenotype (physiological or behavioural) caused by the expression of the mutated gene in *Drosophila* (Pandey and Nichols 2011). The compound eye of *Drosophila* allows easy access for phenotypic characterization of the gene under study by allowing its expression using an eye tissue specific driver (e.g. GMR-Gal4) (Prussing, Voigt et al. 2013). *Drosophila* can also be used to study various behavioural aspects of the disease. The fly's behaviour ranges from simple avoidance to learning and memory (McGuire, Deshazer et al. 2005). Another advantage of using *Drosophila* is the short lifespan of the organism, which enables to carry out life-long studies in a short period of several days instead of months or years as with rodents. Depending on diet and stress their lifespan ranges up to an average maximum of 120 days (Pandey and Nichols 2011).

Defined by developmental stage, *Drosophila* serves as multiple model organisms, each with its own specific advantages. The various developmental stages are - embryo, larva, pupa, and adult. The embryo is often used in fundamental developmental studies like examining pattern formation, cell fate determination, organogenesis, neuronal development and axon path finding (Lawrence and Johnston 1989; Panzer, Weigel et al. 1992; Newsome, Asling et al. 2000; Bhat, Gaziova et al. 2007). Wandering third instar larva is routinely used to study development and physiology as well as some simple behaviour. The visualization of fluorescently tagged cargos and proteins in real time is possible by *in-vivo* imaging of intact larvae, which is largely used to study axonal transport, protein targeting and signaling pathways. The sophistication and complexity of the fly is evident by the presence of its various structures that perform the equivalent functions of the mammalian heart, lung, kidney, gut, and reproductive tract (McClung and Hirsh 1998; Moore, Broihier et al. 1998; Bainton, Tsai et al. 2000; Nichols, Bendena et al. 2002; Satta, Dimitrijevic et al. 2003; Andretic, Kim et al. 2008). The visual system of the adult fly is extensively studied to understand vision (Ready, Hanson et al. 1976; Montell 2005) and other signaling pathways (Raftery, Twombly et al. 1995; Lindsay and Wasserman 2014). Another big advantage of using the fly model is the availability of a wide variety of well-established

molecular genetics tools due to its long history as an animal model in research. It is possible to include 'marker' genes in *Drosophila* which allows tracking the inheritance of the gene of interest through many successive generations. Using these markers and microinjection techniques desired transgenic *Drosophila* lines can be created (Pandey and Nichols 2011).

2.4.1 Genetic tools in *Drosophila*

2.4.1.1 UAS/Gal4 expression system

The UAS-Gal4 expression system has been used extensively to express endogenous and exogenous sequences in the tissues of interest (Phelps and Brand 1998). Two fly lines are used for this purpose. One of which is a driver line and the other is an upstream activator sequence (UAS) line. The driver flies contains a Gal4 coding sequence inserted downstream of a promoter of an endogenous gene. Gal4 is a transcription factor originating from *Saccharomyces cerevisiae* (Lohr, Venkov et al. 1995). It specifically binds to promoter elements or upstream activating sequence (UAS), thus activating expression of the downstream target sequence (Ptashne 1988; Lohr, Venkov et al. 1995) (**Figure 10**). A collection of Gal4 driver lines are available that drive the expression in specific tissues. Some examples are the *glass multimer reporter* (GMR-Gal4) driver inducing retinal expression, the (Elav-Gal4) driver inducing pan-neuronal expression,

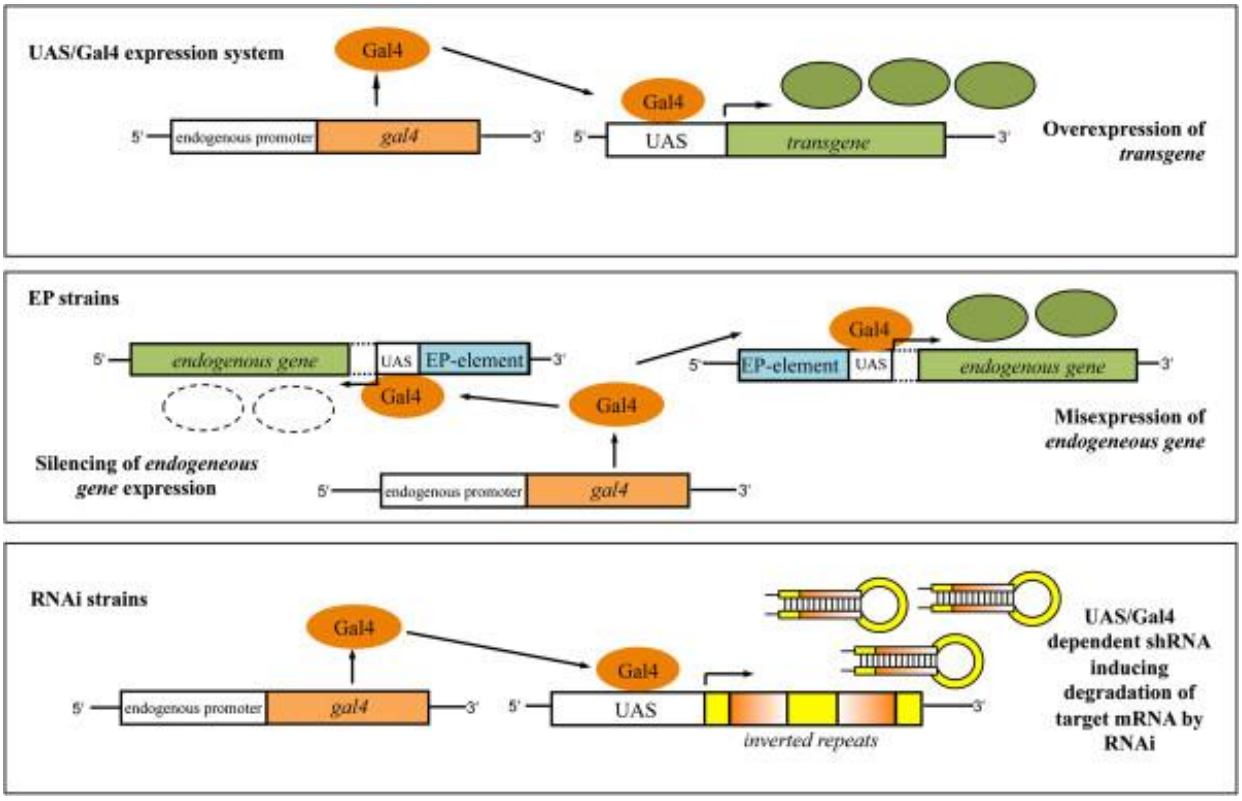

Figure 10: Genetic tools in *Drosophila* – The figure shows the various expression systems in *Drosophila*. The overexpression of the transgene using an upstream activator sequence called as the UAS/GAL4 expression system. Another method involves the silencing of the endogenous gene function using randomly inserted sequence. Silencing of the endogenous DNA using short inverted repeat sequences under UAS control. (Image source: *Prüßing et al. Molecular Neurodegeneration* 2013)

(D42-Gal4) driver inducing motor neuron expression etc (Moses, Ellis et al. 1989; Brand and Perrimon 1993). After crossbreeding the Gal4 driver and the UAS flies, the UAS target sequences will be expressed in a spatiotemporal manner. Gal4 activity is temperature dependent as minimal Gal4 activity is present at16°C, while at 29°C there is maximal Gal4 activity but still ensures minimal effects on fertility and viability due to growth at high temperature. Wide range of expression levels of desired genes can be achieved by altering the temperature and thereby makes the system quite flexible.

There is a variant of this system where the expression is controlled in a temperature sensitive manner by introducing the Gal80 yeast protein, which is a negative regulator of Gal4. This negative regulation is achieved by binding with Gal4 and thereby hindering the expression of UAS-constructs. The temperature sensitive variant of Gal80 (Gal80ts) only renders a functional Gal80 protein at a permissive temperature while at a restrictive temperature no functional Gal80 is produced (Zeidler, Tan et al. 2004). Thus at a permissive temperature of 18°C functional Gal80 is produced that binds Gal4 and thereby hindering the expression of UAS-constructs at this temperature. At a restrictive temperature of 29-30°C, no functional Gal80 is produced, thus enabling Gal4 to activate UAS sequence and inducing expression of the constructs at these temperatures.

2.4.1.2 EP-elements

These are sequences containing UAS sites which are randomly inserted in the fly genome leading to a misexpression of genes. These EP- elements facilitate activation of neighbouring gene depending on the orientation. It might facilitate activation (if the same orientation) or inactivation (if in reverse orientation). It acts in a Gal4-dependent manner. Wide collections of EP strains are available that allows misexpression of a large number of fly genes (Brand and Perrimon 1993; Rorth 1996).

2.4.1.3 RNAi lines

These fly lines express short inverted repeat sequences that correspond to an endogenous gene of interest and is under UAS control. Gal4-dependent expression of the inverted repeats result in the formation short hairpin RNAs (shRNAs) whose presence promotes a series of cellular mechanisms which eventually causes the silencing of the corresponding endogenous gene through RNA interference (RNAi) (Dietzl, Chen et al. 2007).

2.4.2 *Drosophila* neuromuscular junction

The *Drosophila* larval neuromuscular junction (NMJ) shares many structural and functional similarities to animal and human synapses. These include the basic features of synaptic transmission, as well as the molecular mechanisms regulating the synaptic vesicle cycle and moreover serves as an excellent model system for dissecting the cellular and molecular mechanisms of synaptic transmission. Owing to its large size, easy accessibility and the well characterized genetics it is a very simple and yet reasonable model. Another advantage of *Drosophila* NMJ is that the identical NMJs can be easily identified among different larvae and at the same time it is also possible to identify specific NMJ within one particular larva at several time points. Therefore, it is possible to follow a defined NMJ and its population of synapses over time. Each synapse consists of a presynaptic active zone (AZ), a postsynaptic density (PSD), and a synaptic cleft separating them. The AZ is defined as the presynaptic region in which SVs fuse with the presynaptic membrane and releases their neurotransmitters into the synaptic cleft. The AZ can be further subdivided into the protein-rich cytomatrix (CAZ), formed by several specialized proteins that play a role as a scaffold for other protein and also contains the associated machinery for the exocytosis and endocytosis of synaptic vesicles (Siksou, Rostaing et al. 2007). Cytoplasmic pool of SVs is associated within the AZ. A very prominent structure of *Drosophila* AZs is an electron-dense projection called T-bar which is marked by the presence of a particular protein called Bruchpilot (Brp), a member of the Cast/ERC/ELKS family (Ohtsuka, Takao-Rikitsu et al. 2002). Brp is required for the formation of T-bars (100). The clustering of postsynaptic proteins requires the innervations of the motor neuron terminal (Saitoe, Schwarz et al. 2001). The prevalence of well-organized postsynaptic disc large protein (Dlg) lying unopposed to a presynaptic terminal indicates that the presynaptic terminal has been retracted from the site of its abode (Bulat, Rast et al. 2014) .

The simplicity of *Drosophila* NMJ permits sophisticated genetic manipulations and diverse *in-vivo* experiments. Proteins can be expressed specifically at the pre or post synapse in a mutant background to understand its role in synaptogenesis and neurotransmission (Bellen, Tong et al. 2010; Bayat, Jaiswal et al. 2011). Information regarding vesicle release, endocytosis and post synaptic receptor function can be elucidated by performing electrophysiological experiments on individual nerves (Imlach and McCabe 2009; Bayat, Jaiswal et al. 2011). Specific experiments (FM1–43 dye uptake) allows one to establish the amount of membrane that is taken up and released during endocytosis and exocytosis, thus providing real-time analysis of vesicle trafficking (Verstreken, Ohyama et al. 2008). Antibodies against numerous pre and post synaptic proteins help assess the role of these proteins in synaptogenesis. Furthermore, Transmission Electron Microscopy and Immuno-EM studies provide ample information about the number, distribution and size of SV as well as active zones (Venken and Bellen 2007; Yao, Lin et al. 2009; Bayat, Jaiswal et al. 2011).

2.4.3 *Drosophila* as a model organism to study neurodegeneration

Drosophila is widely used as a model system to study neurodegenerative diseases. It serves as an excellent platform to indentify and validate cellular pathways that contribute to neurodegeneration which further helps in identifying promising therapeutic targets by using various approaches from screens to target validation.

When compared to millions of neurons found in mammalian brain, *Drosophila* nervous system is composed of only around 200,000 neurons and supporting glia. However the neurophysiology of fly brain is very similar to its mammalian counterpart. Flies also exhibit complex behaviours like circadian rhythms, sleep, learning and memory, courtship, feeding, aggression, grooming, and flight navigation which are mediated by discrete neural circuits (Newsome, Asling et al. 2000; McGuire, Deshazer et al. 2005; Collins and DiAntonio 2007; Desset, Buchon et al. 2008; Bellen, Tong et al. 2010). Visual and olfactory sensory inputs are processed in the optic and antennal lobes. The mushroom bodies deal with memory, and the central complex provides the motor output after the completion of sensory integration. The neurons of *Drosophila* and humans share neuronal similarities with respect to shape, synaptic intercommunications and their biochemical nature (Strauss 2002; Vosshall and Stocker 2007). Genes, cellular processes and basic building blocks of the nervous system are conserved in flies (Yoshihara, Ensminger et al. 2001). Several signaling cascades involved in neurodegeneration are conserved in flies. Likewise, the

neurotransmitters, synaptic proteins, receptors and ion channels that are involved in synaptic plasticity are similar in both fly and mammals (Takasu-Ishikawa, Yoshihara et al. 2001; Yoshihara, Ensminger et al. 2001). Flies also exhibit an age dependent deterioration of complex behaviours like learning, memory, motor ability, etc (Mockett, Radyuk et al. 2003; Simon, Liang et al. 2006). Till date, fly models exists for many neurodegenerative diseases like Huntington's disease, a range of related polyQ expansion disorders, transthyretin-linked amyloidotic polyneuropathy, Parkinson's disease, motor neuron disease and spinal muscular atrophy (Jackson, Salecker et al. 1998; Warrick, Chan et al. 1999; Feany and Bender 2000; Chan, Miguel-Aliaga et al. 2003; Mudher, Shepherd et al. 2004; Pokrzywa, Dacklin et al. 2007; Cao, Song et al. 2008; Watson, Lagow et al. 2008; Berg, Thor et al. 2009).

2.5 Signaling pathway regulating synaptic development in *Drosophila*

The development and growth of *Drosophila* NMJ requires an anterograde as well as a retrograde input from the muscles. Several developmental signaling pathways like Wnt ligand Wingless (Wnt), Mitogen activated protein kinase (MAPK) and Bone morphogenic protein (BMP/TGF-β) signaling play important role in the formation and growth of the *Drosophila* NMJ (Collins and DiAntonio 2007). The anterograde signaling is primarily mediated by the Wnt ligand Wingless (Wnt), whereas retrograde signaling occurs mostly by a bone morphogenetic protein (BMP) (Speese and Budnik 2007; Bayat, Jaiswal et al. 2011).

2.5.1 Wnt signaling

Wnt signaling plays an important role in axon path finding, dendritic development, and synapse assembly in both central and peripheral nervous systems. Wnts also modulate basal synaptic transmission, the structural and functional plasticity of synapses in the central nervous system (Speese and Budnik 2007; Salinas 2012).

In the Wnt pathway, Wnt binds to its receptor Frizzled (Fz) leading to the activation of downstream Dishevelled (Dvl) which in turn inhibits phosphorylation of β-catenin. Phosphorylation of β-catenin protects it from degradation and translocates to the nucleus to regulate gene expression (Speese and Budnik 2007; Salinas 2012).

Wnt signaling promotes the terminal remodeling of axons before synapses begin to assemble. In cerebellar mossy fiber axons and DRG neurons, activation of the Wnt pathway induces growth

cone pausing, axon branching and extensive enlargement of growth cones (Hall, Lucas et al. 2000; Krylova, Herreros et al. 2002; Salinas 2012). Studies using Wnt-null mutant mice have shown that Wnts promote synapse formation. Blocking Wnt7a activity impairs the normal patterning of mossy fibers and also inhibits synapse formation in the cerebellum (Roos, Hummel et al. 2000; Salinas 2012). Wnt7a functions in microtubule stability by inhibiting GSK-3β which in turn decreases the phosphorylation of microtubule associated protein 1B (MAP1B) and thus plays an indirect role in growth cone dynamics as well as formation of synaptic boutons in *Drosophila* NMJ (Roos, Hummel et al. 2000; Salinas 2012).

2.5.2 Mitogen activated protein kinase (MAPK) pathway

MAPK (Mitogen-Activated Protein Kinase) signal transduction pathways are evolutionarily conserved in eukaryotic cells and transduce signals in response to a variety of extracellular stimuli. Each pathway is composed of three classes of protein kinase: MAPK, MAPKK (MAPK Kinase) and MAPKKK (MAPK Kinase Kinase). Expression of many MAPK regulators and components has been shown to be enriched in the nervous system, and furthermore MAPK signaling has been shown to be involved in neural development. Disruption of this MAPK pathway is linked to many neurological diseases. MAP Kinase pathway is regulated by Highwire (Hiw), a putative RING finger E3 ubiquitin ligase that controls NMJ growth and branching (Collins and DiAntonio 2007; Bayat, Jaiswal et al. 2011).

2.5.3 BMP signaling pathway

BMP signaling is a highly conserved pathway that has been shown to play an important role in the organization and assembly of synapses (Bayat, Jaiswal et al. 2011). It is also critical for coordinated growth of neurons during development in both invertebrates and vertebrates. Synaptic terminal growth and electrophysiological refinement during *Drosophila* larval development is regulated by BMP signaling (Bayat, Jaiswal et al. 2011; Kang, Hansen et al. 2014).

Bone morphogenetic proteins (BMPs) are morphogenes belonging to the transforming growth factor-β (TGF-β) superfamily. Binding of the ligand activates BMP signaling pathway which brings together type I and type II BMP-receptors. In vertebrates, the type I receptor is phosphorylated by the type II receptor, which further activates receptor mediated Smads or R-

Smads (e.g. Smad 1 or Smad 5). These phosporylated R-Smads bind to Co-Smad, (eg Smad 4) and this complex gets translocated and acts as a transcription factor in the nucleus.

Three BMP-type ligands are present in *Drosophila* - Decapentaplegic (Dpp), Glass bottom boat (Gbb), and Screw (Scw), a distantly related family member (Newfeld, Wisotzkey et al. 1999). Generally during the signaling process, the muscle-derived BMP ligand, Glass bottom boat (Gbb), signals through the neuronal BMP receptors like Wishful thinking (Wit, type II), Thick veins (Tkv, type I) and Saxophone (type I) (Aberle, Haghighi et al. 2002; Marques, Bao et al. 2002; McCabe, Marques et al. 2003; Rawson, Lee et al. 2003; McCabe, Hom et al. 2004; Bayat, Jaiswal et al. 2011). Binding of Gbb to its receptor can either activate the Williams Syndrome-associated kinase LIMK1 which promotes stabilization of the synapse or effects the receptor-mediated phosphorylation of the Smad family transcription factor Mothers against decapentaplegic (Mad) (**Figure 11**). Recently, phosphorylated Mad (pMad) been shown to bind to the promoter of the *trio* gene, which encodes an activator of the *Rac* GTPase, essential for MT bundle formation and bouton growth (Ball, Warren-Paquin et al. 2010).

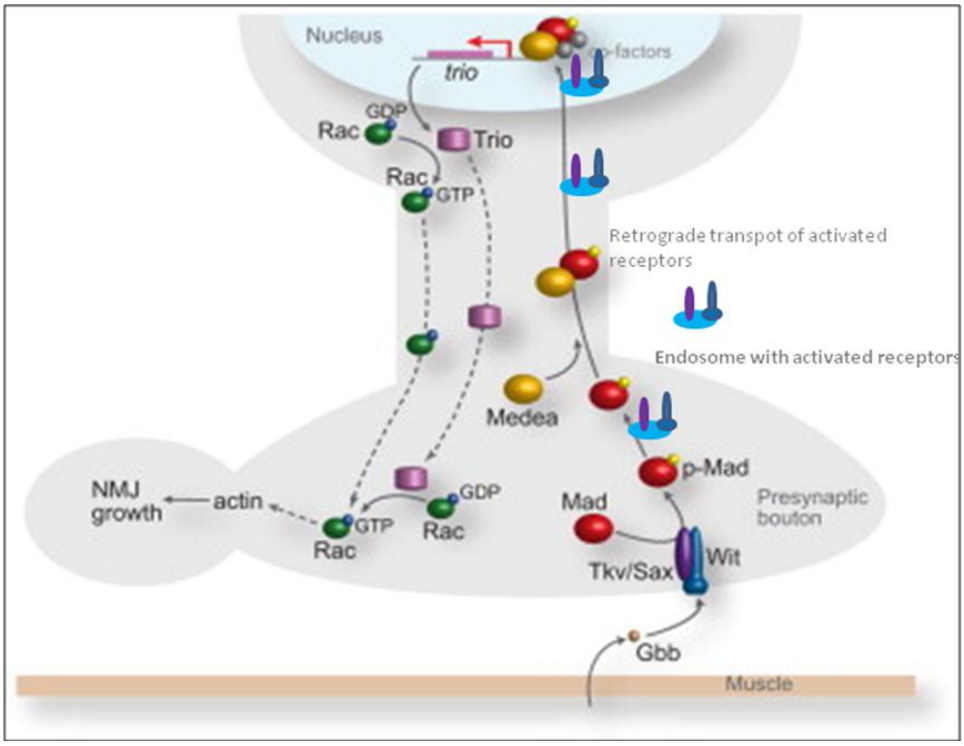

Figure 11: BMP signaling in *Drosophila*. The figure depicts the BMP signaling in neurons. Gbb acts as the ligand to activate the BMP receptors like Tkv/Sax or Wit which in turn phosphorylates Mad to p-Mad at the NMJ and similarly the activated receptors are carried via endosomes to the cell bodies where it activates mad to p-Mad. Phosphorylated Mad acts as transcription factor for the gene Trio which further is

required for NMJ growth mediated via downstream activators like Rac. (Image source: Modified image- *Robin.B.Wall et al, Neuron 2010)*

BMP signaling is tightly regulated and disruption of this tight regulation affected the structure and function of synapses in *Drosophila*. Absence of BMP signaling molecule LIMK1 was characterized by the clustering of postsynaptic proteins like Discs Large (Dlg) in the absence of any presynaptic molecules which led to synaptic retraction (Eaton and Davis 2005). In the absence of retrograde BMP signaling, very little Trio (target gene) was transcribed that led to very little Rac activation which finally disrupted the cytoskeletal arrangements in neurons (Ball, Warren-Paquin et al. 2010; Bayat, Jaiswal et al. 2011). *Drosophila* larvae developed small NMJs with reduced neurotransmission in the absence of key components of the pathway like Wit and Gbb, and on the other hand, in the absence of negative pathway components such as Daughters against decapentaplegic (Dad), the NMJs overgrew characterized by 'satellite boutons' which appeared to be disconnected from the other boutons (Keshishian and Kim 2004). Impaired long distant transport within axons directly contributed to synaptic defects by perturbing the BMP signaling pathway which is essential for synapse maintenance and function.

2.6 BMP signaling and axonal transport

BMP signaling and axonal transport follows a vicious cycle. For proper BMP signaling, its mediators requires to be transported anterogradely and retrogradely (Marques, Bao et al. 2002; McCabe, Marques et al. 2003; McCabe, Hom et al. 2004; Ball, Warren-Paquin et al. 2010; Bayat, Jaiswal et al. 2011; Kang, Hansen et al. 2014). Anterograde motor transports BMP receptors from the soma to the nerve terminal, while retrograde motors contribute to the delivery of activated BMP signals from the nerve terminal towards the cell body to activate gene expression. BMP receptors are endocytosed at the NMJ and are transported along the axon, as concluded from studies that have shown vesicles staining positive for BMP receptors and endosome markers like Rab (Smith, Machamer et al. 2012). At the same time BMP signaling through its downstream players like Trio, Rac, Raf etc stabilizes microtubules and actin filaments and thus maintains the dynamics of the cytoskeleton(Ball, Warren-Paquin et al. 2010) (**Figure 12**). Cytoskeletal dynamics and axonal transport are directly linked as proper cytoskeleton is necessary for an undisrupted axonal transport especially the fast axonal transport (Ball, Warren-Paquin et al. 2010; Bayat, Jaiswal et al. 2011; Kang, Hansen et al. 2014).

Components of the BMP pathway genetically interact with both kinesin-1 and dynein motor proteins. Neuronal derived BMP receptors (Wit, Tkv, Sax) and ligands (Mad, Med) functionally interact with both kinesin-1 and dynein motors signifying that these components can be transported within the axon via these molecular motors (Marques, Bao et al. 2002; McCabe, Marques et al. 2003; McCabe, Hom et al. 2004; Ball, Warren-Paquin et al. 2010; Bayat, Jaiswal et al. 2011; Kang, Hansen et al. 2014).

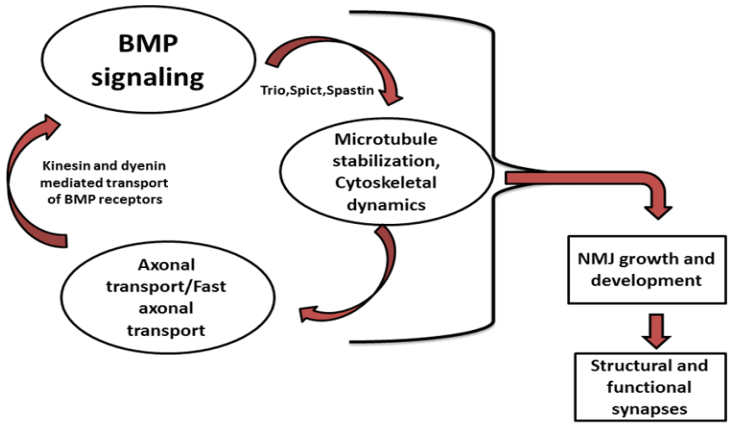

Figure 12: Schematic representation of interdependence of BMP signaling and axonal transport.

Expression of DN-Glued, which blocks the BMP pathway, inhibited axonal transport of the receptors. Likewise, BMP signaling was downregulated by the inhibition of dynein since the activated receptors of the BMP pathway could not be retrogradely trafficked from synaptic terminal to the cell body and nuclei to relay the signaling event at the NMJ (**Figure 13**) (Ball, Warren-Paquin et al. 2010; Bayat, Jaiswal et al. 2011; Kang, Hansen et al. 2014).

Trio, the Rho-type guanyl-nucleotide exchange factor (GEF) is under the transcriptional control of BMP signaling and together with Rac is involved in MT bundle formation and cytoskeletal dynamics, which further ensures presynaptic growth and regulation of neurotransmitter release. (Aberle, Haghighi et al. 2002; Marques, Bao et al. 2002; McCabe, Marques et al. 2003; Rawson, Lee et al. 2003; McCabe, Hom et al. 2004; Wang, Shaw et al. 2007; Ball, Warren-Paquin et al. 2010). Vice versa, disruption of BMP signaling reduces *Drosophila* Futsch/MAP1B levels and microtubule stability in motor axons and NMJ terminals (Wang, Shaw et al. 2007) . Defects in BMP signaling as a pathological mechanism has been proposed in several neurodegenerative diseases. BMP signaling has been reported to be down regulated in Amyotrophic lateral sclerosis (ALS), Spinal muscular atrophy (SMA) and Huntington's disease (HD), and quite conversely, BMP signaling was up regulated in Hereditary spastic paraplegia (HSP) and Multiple sclerosis

(MS) (Bayat, Jaiswal et al. 2011). Since these neurodegenerative diseases also exhibit axonal transport defects in addition to alterations in BMP signaling, hence it could be concluded that these BMP signaling alterations could likely occur via perturbations in long distance transport (Li, Li et al. 2001; Wang, Shaw et al. 2007; Zhao and Hedera 2013; Kang, Hansen et al. 2014).

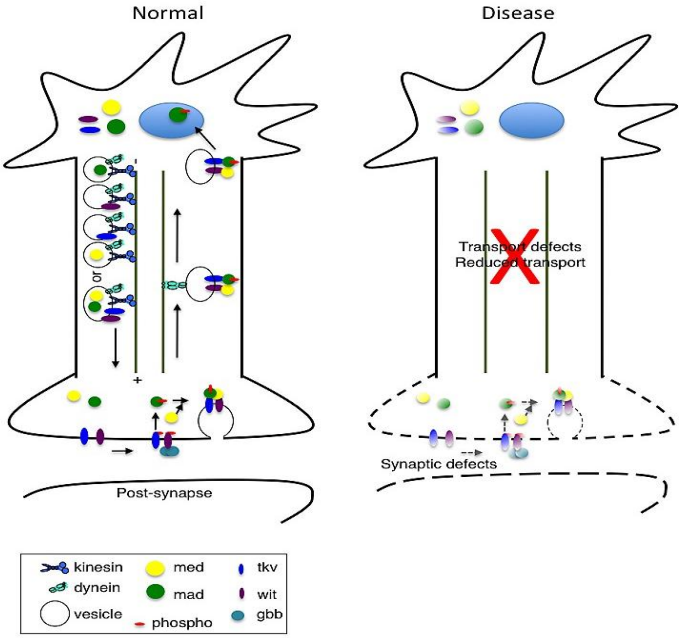

Figure 13: BMP signaling with intact and disrupted axonal transport- The figure depicts the loss of BMP signaling in conditions with reduced transport in contrast to the unperturbed transport. The BMP receptors like Tkv and Wit are transported to the synapse via kinesins and activated receptors are delivered to the soma via dynein to trigger gene expression. In conditions of reduced transport, the signaling is inhibited. (Image source: *Kang et al, PLoS one, 2014*).

2.6.1 BMP signaling and heriditary spastic paraplegias

Impaired BMP signaling has been reported in at least four HSP associated proteins, atlastin-1 (causing SPG3A), non-imprinted in Prader Willi/Angelman syndrome1 (NIPA1) (causing SPG6), spastin (causing SPG4) and spartin (causing SPG20). Fly larvae lacking the *Drosophila* homologue of NIPA1 and spichthyin are characterised by increased number of synaptic boutons at neuromuscular junctions and an upregulation of BMP signaling was observed (Wang, Shaw et al. 2007; Tsang, Edwards et al. 2009). Spict overexpression results in loss of boutons, which resembles the cellular pathology observed in mutants of either BMP signaling ligands or receptors like *gbb*, *sax*, and *tkv*. Spict mutants are also characterized by increased neuronal

concentrations of downstream messenger of BMP signaling p Mad, and are suppressed by blocking BMP signaling (Wang, Shaw et al. 2007; Tsang, Edwards et al. 2009). NIPA1and spichthyin binds to the type II BMP receptor promoting its endocytic internalization and degradation in lysosomes and thus inhibits BMP signaling (Blackstone, O'Kane et al. 2011). Knockdown of Spartin and spastin also resulted in increased pMad levels (Bayat, Jaiswal et al. 2011). Mutations in Atlastin-1, another HSP gene, exhibited a dominant-negative effect on the trafficking of BMPRII (wit) and thereby disrupted BMP signaling (Zhao and Hedera 2013; Kang, Hansen et al. 2014). These HSP gene mutants also exhibited axonal transport defects suggesting that perturbations in long distant transport likely affects BMP signaling both of which results in HSP disease pathology (Fuger, Sreekumar et al. 2012; Zhao and Hedera 2013; Kang, Hansen et al. 2014).

2.7 SPG10 *Drosophila* model Khc^{N262S} used in my study

The aim of my study was to characterise human SPG10 model in *Drosophila* and to investigate the underlying mechanism leading to its pathology. Since BMP signaling perturbations were linked to many HSPs, it was interesting to test if our *Drosophila* model of SPG10 also showed altered BMP signaling, which could then be an additional step towards establishing BMP signaling as a common pathological mechanism causing HSP.

Location of Khc^{N262S} mutation in *Drosophila*

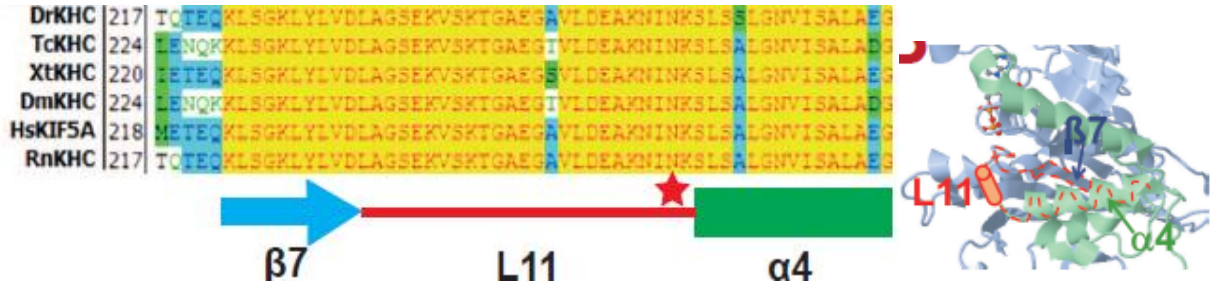

Figure 14: Location of Khc^{N262S} mutation. The figure depicts the aligned conserved sequences of KHC across species. The mutation which occurs at 256 amino acid (a.a) position in human KIF5A corresponds to 262 a.a position in *Drosophila melanogaster*. The mutation is located in the loop 11 that connects the beta sheet (β7) and alpha helix (α4) in the kinesin heavy chain. This mutation is located near the ATP binding site and the microtubule binding site.

The N256S mutation which is implicated in human SPG10 was selected to generate the first *in-vivo Drosophila* model for SPG10 (Fuger, Sreekumar et al. 2012). The KIF5A N256S mutation, which corresponds to the amino acid exchange N262S in *Drosophila* kinesin heavy chain, connects the microtubule and the ATP-binding site of Khc (Fuger, Sreekumar et al. 2012). Alignment of the Khc protein across species (*Danio rerio* (Dr), *Tribolium castaneum* (Tc), *Xenopus tropicalis* (Xt), *Drosophila melanogaster* (Dm), *Homosapiens* (Hs), *Rattus norvegicus* (Rn)) (**Figure 14**) shows unique conservation of the amino acids in this loop (Fuger, Sreekumar et al. 2012). The mutated kinesin was expressed ectopically in the mutant flies (Khc^{N262S}) using tissue specific drivers.

3 Materials and methods

3.1 Fly stocks

Flies were maintained at 25°C on standard fly media (0.8% agar, 14.3% dried yeast, 10% soy flour, 21.3% treacle, 8% malzin, 8% corn meal,0.63% propionic acid in water) and seeded with fresh live yeast if not otherwise indicated. Flies were raised at 18°C, 25°C or 29°C according to the expression mode (low temperature ensures mild expression and high temperature ensures higher expression of proteins) required in experiments. Fly strains used in this study are shown in **Table 1**. Transgenic stocks UAS-Khc^{wt} and UAS-Khc^{N262S} were created by BestGene (Chino Hills, USA) using integrase mediated site-specific transgenesis at cytological position 86F (Fly strain BDSC 23648). The fly stocks were obtained from Bloomington *Drosophila* stock center if otherwise indicated D42-Gal4 (BL8816), UAS-CD8-GFP (BL5130), UAS-Trio (BL9513),UAS-LacZ (BL1777), Trio6A (BL8595), Wit^{A12} (BL5173), Wit^{B11} (BL5174), Tkv^{7} (BL3242). The following stocks were kindly provided by W1118 (Castiglioni), Gbb94 (Hermann Ablere), UAS-Tkv-CA (Hermann Ablere), UAS-ANF-GFP (William Saxton), UAS-Wit-GFP (Mike O Conner) UAS-LAMP-GFP (Helmet Kramer), UAS-ATG-mRFP (Ernst Hafen), UAS-Tkv-YFP (Guillermo Marques). The RNAi fly stocks were kindly gifted by Aaron Voigt. All other fly stocks were created by me by either combining (gene on different chromosomes) or recombining (gene on same chromosome) of desired fly stocks.

Table 1

Genotypes expressed by motor neuron driver	Fly genotype refered to as
w-/w-;+/+;D42-Gal4/+	w^{1118}
w-/w-;+/+;UAS-khc^{N262S}/ D42-Gal4	Khc^{N262S}
w-/w-;+/+;UAS-khc^{wt}/ D42-Gal4	Khc^{wt}
w-/w-;UAS-Khc^{wt} /+;UAS-khc^{N262S}/ D42-Gal4	$Khc^{N262S+wt}$
w-/w-;+/+;UAS-$Khc^{N262S+LacZ}$/ D42-Gal4	$Khc^{N262S+LacZ}$
w-/w-;+/+;UAS-$Khc^{N262S+Cd8-GFP}$/ D42-Gal4	$khc^{N262S+CD8-GFP}$
w-/w-;+/+;UAS-$Khc^{N262S+Trio}$/ D42-Gal4	$Khc^{N262S+Trio}$
w-/w-;+/+;UAS-$Khc^{N262S+Tkv-CA}$/ D42-Gal4	$Khc^{N262S+Tkv-CA}$
w-/w-;+/+;UAS-$Khc^{Tkv-YFP+N262S}$/ D42-Gal4	$khc^{N262S+Tkv-YFP}$
w-/w-;+/+;UAS-$Khc^{Mad-GFP+N262S}$/ D42-Gal4	$Khc^{N262S+Mad-GFP}$
w-/w-;+/+;UAS-$Khc^{RacV12+N262S}$/ D42-Gal4	$Khc^{N262S+RacV12}$
w-/w-;+/+;UAS-$Khc^{Trio6A+N262S}$/ D42-Gal4	$Khc^{N262S+Trio6A}$
w-/w-;Tkv7/+;UAS-Khc^{N262S}/ D42-Gal4	$Khc^{N262S+Tkv7}$
w-/w-;WitA12/+;UAS-Khc^{N262S}/ D42-Gal4	$Khc^{N262S+WitA12}$
w-/w-;WitB11/+;UAS-Khc^{N262S}/ D42-Gal4	$Khc^{N262S+WitB11}$
w-/w-;+/+;UAS-$Khc^{N262S+Gbb-94}$/ D42-Gal4	$Khc^{N262S+Gbb94}$
w-/w-;P50-RNAi/+;UAS-Khc^{N262S}/ D42-Gal4	$Khc^{N262S+P50-RNAi}$
w-/w-;P150-RNAi/+;UAS-Khc^{N262S}/ D42-Gal4	$Khc^{N262S+P150-RNAi}$

Fly Genotype refered to as	Feature
w^{1118}	native wild type kinesin expression
Khc^{N262S}	ectopic expression of mutated kinesin+native kinesin
Khc^{wt}	ectopic expression of wild type kinesin+native kinesin
$Khc^{N262S+wt}$	ectopic expression of mutated and wild type kinesin+native kinesin
$Khc^{N262S+LacZ}$	ectopic expression of mutated kinesin and lacZ control+native kinesin
$khc^{N262S+CD8-GFP}$	ectopic expression of mutated kinesin and CD8-GFP control+native kinesin
$Khc^{N262S+Trio}$	ectopic expression of mutated kinesin and BMP target gene trio+native kinesin
$Khc^{N262S+Tkv-CA}$	ectopic expression of mutated kinesin and BMP receptor active Tkv+native kinesin
$khc^{N262S+Tkv-YFP}$	ectopic expression of mutated kinesin and YFP tagged Tkv+native kinesin
$Khc^{N262S+Mad-GFP}$	ectopic expression of mutated kinesin and BMP mediator Mad-GFP +native kinesin
$Khc^{N262S+RacV12}$	ectopic expression of mutated kinesin and constututively active Rac +native kinesin
$Khc^{N262S+Trio6A}$	ectopic expression of mutated kinesin and Trio mutant +native kinesin
$Khc^{N262S+Tkv7}$	ectopic expression of mutated kinesin and Tkv mutant+native kinesin
$Khc^{N262S+WitA12}$	ectopic expression of mutated kinesin and BMP receptor Wit mutant +native kinesin
$Khc^{N262S+Gbb94}$	ectopic expression of mutated kinesin and BMP ligand mutant Gbb+native kinesin
$Khc^{N262S+P50-RNAi}$	ectopic expression of mutated kinesin and RNAi dynactin+native kinesin
$Khc^{N262S+P150-RNAi}$	ectopic expression of mutated kinesin and RNAi dynactin+native kinesin

3.1.1 Complementary expression systems of Khc^{N262S} mutation

Two complementary expression systems were used to study the phenotypic and molecular characteristics of the *Drosophila* model of Khc^{N262S}.

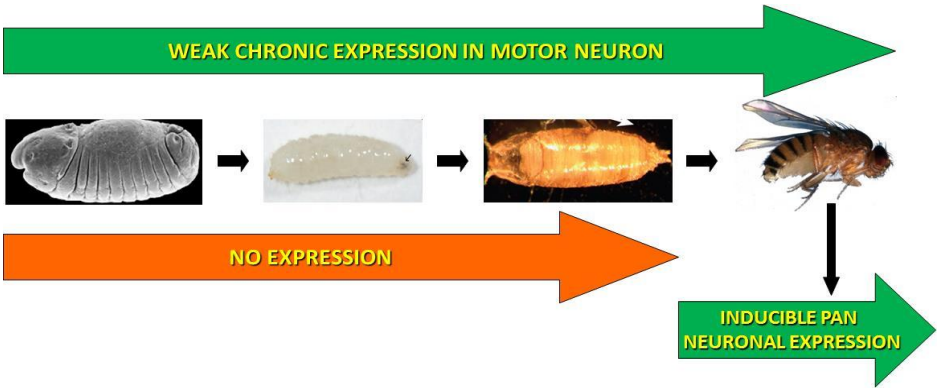

The weak chronic expression in motor neuron was mediated via D42-Gal4 driver that specifically drives the mutated protein in the motor neurons throughout development, from embryo to adult stage. This model system helps in understanding the step by step progression of the disease during each developmental stage. On the other hand, in the inducible pan neuronal expression, the mutated protein was expressed in both sensory and motor neurons by Elav X-Gal4 driver. Advantage of this system was the expression of mutated protein specifically at the adult stage so as to study the toxicity of the mutated protein.

3.2 Survival assay

Khc^{N262S}, Khc$^{N262S+wt}$, Khc^{wt} or w^{1118} flies were crossed with motor neuron specific D42-Gal4 driver flies at 18°C and were raised on standard fly media. Off springs were collected on the day of eclosion. From each of these, 15 -20 males were transferred into fresh vials containing standard fly media. Total of 100 flies per genotype were used for this assay. The flies were transferred to vials with fresh fly media every 3 days. Live and dead flies in each of the vials were assessed daily and the respective survival was plotted on a Kaplan-Meier plot.

3.3 Climbing assay

Khc^{N262S}, Khc^{wt} and W^{1118} strains were crossed with motor neuron specific D42-Gal4 driver flies at 18°C. Male off springs from each crossing were split into 2 batches of 50 flies each within 24

hours of eclosion. One batch was raised at 18°C while the other at 29°C to induce either low or high expression of the wild type and/or mutated kinesins respectively for 16 days. Then, the motor function of the flies was assessed by analyzing the ability of the flies to climb a distance of 6 cm along the walls of a vertical plastic tube within 15 seconds (standardized time period). Most of the w^{1118} control flies could climb the distance within the time span of 15 seconds and hence these values were used as measurement standards. A successful trail was scored 1 and the unsuccessful trail 0. Each fly was allowed to climb 3 times and the average climbing score per fly was calculated.

3.4 Thorax resin sections

Thorax tissue was dissected from adult fly after careful removal of head,limbs,wings and abdominal parts. The tissue was pre-fixed using (4% PFA, 3% glutaraldehyde, 0.1% sodium cacodylate) at 4°C overnight and post-fixed with 1% osmium tetroxide for 3 hours at 4°C. Thorax tissues were washed with 30%, 50%, 70% and 100% ethanol for 10 min each .This was followed by washing with 100% acetone and (3:1) acetone: epon for 1 hour. Tissues were then immersed in (1:1) acetone: Epon and 100% Epon for 24 hours each. The Epon was polymerized for 48 hours at 60°C. Semi-thin sections (2 µm) were prepared on a Reichert-Jung Supercut 2050 microtome with glass knife. The semi-thin sections were stained with Toluidine blue solution (0.5% Toluidine blue O [C.I 52040, Roth] in 1% [w/v] disodium tetraborate buffer) for 1 min and then washed under running water. The semi-thin sections were documented on a Zeiss Imager.Z1m microscope using a 20× Zeiss Neofluar, 0.5 N.A objective. All washing, fixation, and staining procedures were performed at room temperature unless otherwise indicated.

3.5 Larval locomotion analysis

To monitor locomotion behavior, individual larvae were placed on a thin slice of apple juice agar. Locomotion was examined at 25°C at 70% humidity by using a DCM510 (ScopeTek, P.R. China) camera integrated in a custom-built stereomicroscope. Larval locomotion were recorded at a frame rate of 30 fps for 5 min. The videos were then converted into .avi format by using a Prism Video Converter, v 1.61 (NCH Software Inc., Australia). Finally, images were cropped and compressed by using VirtualDub 1.9.10 (http://www.virtualdub.org/).

3.6 Eye phenotype scoring

To examine the external *Drosophila* eye phenotype, desired fly strains were crossed to eye specific GMR-Gal4 driver at 29°C under 12-h day/night cycles.16 day old male flies from the subsequent generation were used for analysis. Before imaging, the flies were frozen at -20°C for not more than 6 days to avoid changes in the hue of eyes. For imaging, flies were first thawed and dried at room temperature for 10–15 min. Images were obtained with a DCM510 (ScopeTek, Hangzhou, P.R. China) camera mounted on a Zeiss Stemi 2000 stereomicroscope (Carl Zeiss, Oberkochen, Germany).Eye phenotype was scored double blind by Junyi Zhu . Scoring was done considering the extend of eye damage indicated by depigmentation and black spots resulting from the necrosis of omatidia. A total of 10 male flies were screened for each genotype.

3.7 Larval tail flip assay

This simple behavioral assay was performed to analyze the general health of larvae. Genotypes w^{1118}, Khc^{wt}, Khc^{N262S}, $Khc^{N262S+LacZ}$, $Khc^{N262S+CD8\text{-}GFP}$, $Khc^{N262S+Trio}$, $Khc^{N262S+TKVCA}$, $Khc^{N262S+wt+CD8\text{-}GFP}$,$Khc^{N262S+wt+Trio}$,$Khc^{N262S+wt+TKV\text{-}CA}$, $Khc^{N262S+wt+P150RNAi}$, $Khc^{N262S+wt+P50RNAi}$, $Khc^{wt+P50RNAi}$, $Khc^{wt+P150RNAi}$, $Khc^{N262S+wt+TKV7}$, $Khc^{N262S+wt+Trio6A}$, $Khc^{N262S+wt+Gbb94}$, $Khc^{N262S+wt+WitA12}$ were driven using a motor neuron specific driver (D42-Gal4) at 29°C. The third instar larvae that emerged were scored double blind for its tail flip severity on apple juice agar plates. Perfectly healthy larvae locomoted normally and were scored 0, fast movement accompanied with tail flip was scored 1, slow movement with tail flip was scored 2, sparse movement with tail flip was scored 3 and finally complete paralysis was scored 4.

3.8 Immunohistochemical analysis

3.8.1 Larval dissection

Mid third instar stage larvae (L3) were used for dissection if not otherwise indicated. The larvae were dissected on rubber dissection pads covered by a drop of Ca^{2+} free HL3 solution (70mM NaCl, 5mM KCl, 20mM $MgCl_2$, 10mM NaHCO, 35mM trehalose, 115mM sucrose and 5mM HEPES, pH adjusted to 7.2). Larvae were cut open through the midline (posterior to anterior), the body wall stretched out and pinned on the sides. Subsequently gut was removed. Brain and

axons were left intact for axonal staining but removed for NMJ staining. Dissected larvae were fixed in4% para-formaldehyde (PFA) in phosphate buffered saline (PBS) or Bouin´s fixative (For details see **Table 2**). After removing the fixative with phosphate buffered solution containing 0.05% Triton-X (PBS-T), antibody staining was ensued.

3.8.2 Antibody staining

The larval preparations were blocked for 30 min with PBS-T containing 5% normal goat serum (PBS-T/NGS). The PBS-T/NGS solution was refreshed; primary antibodies were added and incubated over night at 4°C. The next day the samples were washed with PBS-T three times for 20min. Aliquots of secondary antibodies (**Table 2**) in PBS-T and 5% NGS were then added and incubated at room temperature for two hours. Larval preparations were washed again three times for 20min each with PBS-T and mountedon a glass object slide using Vectashield Mounting medium (Vector Laboratories, Burlingame, USA). (Primary and secondary antibody are listed in **Table 2**)

3.8.3 Imaging

Axonal sections or NMJ images were captured using Zeiss LSM 710 confocal microscope, with a 40x plan appochromatic 1.3 N.A oil objectives. Pixel size of 0.1mmx0.1mm and 0.5 mm interval between the stacks were maintained during imaging. Pinhole was kept at 1AU. Laser intensities were adjusted to one genotype, depending on the analysis to be performed. Z-stacks of whole NMJs (muscle 6 and 7 of segment A5) and sections of segmental nerves, passing through segments A3-A4 were imaged. ImageJ 1.45S (NIH) software was used for image processing and analysis.

Table 2.

Primary antibodies					
Antigen	**Antibody**	**Host**	**Dilution**	**Fixation**	**Source**
DV-Glut	DV-Glut NH_2	Rabbit	1:1000	10 min 4%PFA	Hermann Aberle
Bruchpilot	Nc82	Mouse	1:100	10 min 4%PFA	DSHB*
CSP	DCSP-2	Mouse	1:50	10 min 4%PFA	DSHB
Even skipped	3C10	Mouse	1:10	30 min 4%PFA	DSHB
Glutamate receptor	GluR 11C	Rabbit	1:2000	10 min 4%PFA	S.Sigrist
Futsch	22C10	Mouse	1:150	3 min Bouins	DSHB
Pmad	PS1	Rabbit	1:500	30 min 4%PFA	P.ten Dijke
Dlg	4F3	Mouse	1:50	5 min 4%PFA	DSHB
α-Tubulin	12G10	Mouse	1:10	5 min 4%PFA	DSHB
Acetylated α-Tubulin	611B1	Mouse	1:250	5 min 4%PFA	Sigma Aldrich

DSHB-Developmental studies hybridoma bank

Secondary Antibodies				
Antigen	**coupled to**	**Host**	**Dilution**	**Source**
HRP	Cy3	Goat	1:500	DiAnova
HRP	Cy5	Goat	1:500	DiAnova
Mouse	Alexa 488	Goat	1:500	Molecular probes
Mouse	Alexa 568	Goat	1:500	Molecular probes
Rabbit	Alexa 488	Goat	1:500	Molecular probes
Rabbit	Atto 647	Goat	1:500	Sigma

3.9 Data Analysis

Image processing and quantification were performed using ImageJ 1.45S (NIH). All samples to be analyzed and compared were dissected on the same day, stained in the same tube, mounted on the same slide and imaged using the same settings to avoid any variation between genotypes. All images were uniformly processed for comparable visualization. In brief, the raw data stack was Guassian filtered (radius-2); brightness and contrast were appropriately adjusted and were maximally projected. A gamma adjustment of 0.75 was applied wherever necessary. For quantification, image processing was performed as described below.

3.9.1 Quantification of axonal swelling

Axonal swellings are defined as nerve segments characterized by bright HRP staining and simultaneous accumulation of cargo. The raw images were captured as slices or z stacks, which were then projected with maximum intensity as a single image. These maximum projected images were then Gaussian blurred and subjected to further processing depending on the type of quantification required. For quantifying the area of swellings in a nerve segment, the maximum intensity projections of HRP channel were used to create a binary mask using appropriate threshold values which were kept constant for all the genotypes to be compared. This binary mask was superimposed with maximum projections of HRP and cargo channels (BRP, DV-Glut, CSP, ANF-GFP) with threshold values that were again kept constant for all the samples quantified. The resultant minimally projected HRP and cargo channels images display swellings of HRP and cargo along the axons after being normalized with the mask. These HRP and cargo swelling images were further superimposed on each other to obtain axonal swellings (colocalised HRP and cargo swellings) in the segmental nerves. Area fraction swellings were computed by taking the ratio of area covered by swellings to the total HRP area in each of the segmental nerves. Swelling density was defined as the number of cargo accumulations per 1000 μm^2 of segmental nerves. The processing parameters and thresholds used are described in **Table 3**.

Table 3.

Quantification of HRP and DV-Glut axonal swellings

Channel	Gaussian Blur	Projection	Mask theshold	Channel threshold
HRP	4	maximum	12	65
DV-Glut	2	maximum	-	65

Quantification of HRP and BRP axonal swellings

Channel	Gaussian Blur	Projection	Mask theshold	Channel threshold
HRP	4	maximum	12	40
BRP	2	maximum	-	40

Quantification of HRP and CSP axonal swellings

Channel	Gaussian Blur	Projection	Mask theshold	Channel threshold
HRP	4	maximum	12	60
BRP	2	maximum	-	60

Quantification of HRP and ANF-GFP axonal swellings				
Channel	**Gaussian Blur**	**Projection**	**Mask theshold**	**Channel threshold**
HRP	4	maximum	12	45
ANF-GFP	2	maximum	-	45

Quantification of HRP and DV-Glut axonal swellings BMP signaling				
Channel	**Gaussian Blur**	**Projection**	**Mask theshold**	**HRP threshold**
HRP	2	maximum	Batch 1 (13)	80
	2	maximum	Batch 2 (12)	80
DV-Glut	2	maximum	Batch 1 (13)	10
	2	maximum	Batch 2 (12)	8

Quantification of HRP and CSP axonal swellings BMP signaling				
Channel	**Gaussian Blur**	**Projection**	**Mask theshold**	**HRP threshold**
HRP	2	maximum	Batch 1 (13)	80
	2	maximum	Batch 2 (12)	80
	2	maximum	Batch 3 (15)	100
	2	maximum	Batch 4 (8)	40
CSP	2	maximum	Batch 1 (13)	31
	2	maximum	Batch 2 (12)	22
	2	maximum	Batch 3 (15)	13
	2	maximum	Batch 4 (8)	30

Quantification of HRP and LAMP-GFP axonal swellings BMP signaling				
Channel	**Gaussian Blur**	**Projection**	**Mask theshold**	**HRP threshold**
HRP	2	maximum	Batch 1 (12)	83
	2	maximum	Batch 2 (12)	95
LAMP-GFP	2	maximum	Batch 1 (12)	16
	2	maximum	Batch 2 (12)	12

Quantification of HRP and ATG8-mRFP axonal swellings BMP signaling				
Channel	**Gaussian Blur**	**Projection**	**Mask theshold**	**HRP threshold**
HRP	2	maximum	Batch 1 (5)	18
	2	maximum	Batch 2 (12)	18
ATG8- m RFP	2	maximum	Batch 1 (5)	6+auto threshold/2
	2	maximum	Batch 2 (12)	10+auto threshold/2

3.9.2 Quantification of synaptic proteins in neuromuscular junction

The raw images were captured as slices or z stacks, which were then projected with maximum intensity as a single image. These maximum projected images were further Gaussian blurred and processed depending on quantification demands. For quantifying the intensity of synaptic proteins in NMJs (muscle 6/7, segment A5), the maximum intensity projections of HRP channel were used to create a binary mask using appropriate threshold values which were kept constant for all the genotypes to be compared. This binary mask was superimposed with maximum projections of cargo channels (BRP, DV-Glut and CSP) to quantify the average intensities of these synaptic proteins in NMJs. The parameters used are shown in table below:

Table 4.

Quantification of DV-GLUT intensities at NMJ

Channel	Gaussian filter	Brightness/Contrast	Binary mask threshold
HRP	2	-	28
DV-GLUT	2	-	-

Quantification of CSP intensities at NMJ

Channel	Gaussian filter	Brightness/Contrast	Binary mask threshold
HRP	2	-	28
CSP	2	-	-

Quantification of BRP intensities at NMJ

Channel	Gaussian filter	Brightness/Contrast	Binary mask threshold
HRP	2	-	22
BRP	2	-	-

Quantification of DV-GLUT intensities at NMJ BMP

Channel	Gaussian filter	Brightness/Contrast	Binary mask threshold
HRP	2	-	Batch 1 (30) Batch 2 (15)
DV-GLUT	2	-	-

Quantification of LAMP-GFP intensities at NMJ BMP			
Channel	**Gaussian filter**	**Brightness/Contrast**	**Binary mask threshold**
HRP	2	-	Batch 1 (8) Batch 2 (15) Batch 3 (6)
LAMP-GFP	2	-	-

Quantification of Dlg intensities at NMJ BMP			
Channel	**Gaussian filter**	**Brightness/Contrast**	**Binary mask threshold**
HRP	2	-	5
Dlg	2	-	-

3.9.3 Dissection, staining and quantification of pMad in motor neuron cell bodies

Mid third instar stage larvae were dissected on rubber dissection pads covered by a drop of Ca^{2+}free HL3 solution (70mM NaCl, 5mM KCl, 20mM $MgCl_2$, 10mM $NaHCO_3$, 5mM trehalose, 115mM sucrose and 5mM HEPES with pH adjusted to 7.2).The larvae were dissected carefully and the ventral ganglion or brain were left intact for staining. Larvae were fixed in 4% formaldehyde in phosphate buffered saline (PBS) for 30 min. After removing the fixative with PBS-T (0.05% Triton-X 100in PBS) larval body wall preparations were kept in PBS-T in ice. The larval preparations were blocked for 30 minutes with PBS-T/NGS solution. The PBS-T/NGS solution was refreshed, Evenskipped and pMad primary antibodies were added and incubated over night at 4°C.The following day, the samples were washed with PBS-T three times for 20min. Required aliquots (**Table 2**) of secondary antibodies (anti-HRPcy5,Alexa flour 488 and Alexa flour 633) in PBS-T and 5% NGS were then added and incubated at room temperature for two hours. Larval preparations were washed again three times for 20min each with PBS-T and mounted on a glass object slide (with their brain facing up) using VectaShield mounting medium (Vector Laboratories, Burlingame, USA).The raw images of the ventral ganglion were captured as slices or z stacks. For quantification of pMad levels in motor-neuron cell bodies the Even-skipped (eve) channel was used to create a binary mask, which was subsequently superimposed (minimum overlay) with the pMad channel and pMad fluorescence intensities of aCC and RP2 motor neurons were analyzed.

3.10 *Drosophila* genomic DNA isolation and PCR amplification of UAS driven Khc

The flies used in the study were created by recombining and combining different genotypes and the presence of UAS-Khc in these flies were confirmed by PCR. Flies were anesthetized and frozen at -80°C for 5 min, homogenized in 100µl of solution A (0.1M Tris hydrochloride (pH9.0), 0.1M ethylene diamine tetra acetate, 1% sodium dodecyl sulphate, 0.1M sodium chloride) and centrifuged at 13000 rpm for 15 min. 100 µl of isopropanol was added to the resultant supernatant and was centrifuged at 10000 rpm for 5 min. The pellet was washed with 500 µl of 70% ethanol, centrifuged additionally for 5 min at 13000 rpm, dried at room temperature for 30 min and resuspended in 20µl water. DNA content was quantified using nanodrop (Thermo scientific). 500 ng of DNA was used for the PCR amplification of the UAS-Khc gene using the following cycling conditions.

PCR cycling conditions: Denaturation: 94°C 30 sec, 40 cycles of annealing at 58.5°C, extension at 72°C for 10 min.

Primers used:

UAS Khc sense: 5'GTCGCTAAGCGAAAGCTAAGC3'

UAS Khc antisense: 5' CCAGGGCTGAAATTACGTTGC3'

3.11 Statistics

Statistical tests were performed using the freely available software PAST (http://folk.uio.no/ohammer/past/index.html). Survival assay was tested using Prism 6 (Graphpad software inc, California). Standard deviation (SD) and standard error of mean (SEM) were calculated for each study. Normality was tested using the Shapiro-Wilk test (α=0 .05). Normally distributed data were analyzed either by student's t-test (two groups) or by a one-way analysis of variance (ANOVA) followed by a Tukey-Kramer post-test for comparing multiple groups. Data that were not normally distributed were analyzed using Kruskal-Wallis H-test followed by a post-test for comparisons between multiple groups. The following alpha levels were used for all tests: * $p<0.05$; ** $p<0.01$; *** $p<0.001$.

4 Results

4.1 Khc^{N262S} expression resulted in human HSP like phenotype in *Drosophila*

4.1.1 Khc^{N262S} mutant larvae displayed tail flip phenotype

Ectopic expression of either mutated kinesin (Khc^{N262S}) or co- expression of mutated and wild type kinesin ($Khc^{N262S\ +wt}$) resulted in distal paralysis in larvae. When mutated kinesin was driven using the motor neuron specific D42-Gal4 driver at 25°C or 29°C, the mutant third instar (L3 stage) larvae displayed a characteristic tail flip phenotype which mirrored distal paralysis in human patients. Strong expression of Khc^{N262S} led to the progression of paralysis from the posterior to the anterior segments of the larvae, and finally paralyzed the whole body with mobility restricted to the head region. Nevertheless, death ensued in these larvae. The ectopic expression of wild type kinesin along with the mutated kinesin in $Khc^{N262S\ +wt}$ larvae significantly reduced the lethality. These larvae developed into viable adult flies at either 25°C or 29°C; however, the tail flip phenotype still persisted in these larvae. The average tail flip rate was lower in Khc^{N262S} mutants when compared to $khc^{N262S+wt}$ mutants since they were significantly weaker (**Table 5**). No tail flip or paralysis was observed in control animals that expressed native kinesin (w^{1118}) or those that overexpressed wild type kinesin (Khc^{wt}).

Table 5: Kinesin mutants display distal paralysis.

Genotype	Larval number	Larvae showing tail flip [%]	Completely paralyzed larvae [%]	Average tail flip rate
w^{1118}	50	0	0	0
Khc^{wt}	50	0	0	0
$Khc^{N262S+WT}$	31	100%	0	46 flips/min
Khc^{N262S}	44	57%	43%	2 flips/min

W^{1118},Khc^{wt},$Khc^{N262S+wt}$,Khc^{N262S} flies were mated with motor neuron specific D42-Gal4 flies at 25°C and the 4 day old third instar larvae that emerged were scored for distal paralysis by analyzing their movement on apple juice agar plates. $Khc^{N262S+wt}$ larvae showed rapid tail flipping (46 flips/min) but their moving ability was not affected. The Khc^{N262S} mutant larvae were much weaker and hardly showed any movement.

43% of the larvae were completely paralyzed and the other 57% showed tail flip (2 flips/min) but were unable to move. No tail flip was observed in control animals (Khc^{wt} and w^{1118})

4.1.2 Fly phenotype– Khc^{N262S} mutant flies displayed erect wing phenotype

Since D42-Gal4 expression system was temperature dependent (**Section 2.4.1.1**), strong expression of Khc^{N262S} proved lethal when driven by D42-Gal4 driver at 25°C and 29°C as no adult flies emerged. However, weaker expression using the same driver at 18°C enabled most of the flies to emerge alive.

Flies expressing Khc^{N262S} had deformed wings. At rest, they held their wings in an abnormal upright position, almost perpendicular to their body axis (**Figure 15A**). These flies did not fly unless forced, and when they did, they could not sustain stable flight. This defect has been attributed to apoptotic degeneration of indirect flight muscles in a previous study using Parkinson-related *Drosophila* pink-1 mutant flies (Falcon-Perez, Romero-Calderon et al. 2007).

To confirm if the abnormal wing posture was due to flight muscle degeneration, thorax sections of the flies were made. However, no signs of muscle loss in Khc^{N262S}-expressing flies were observed and the thoracic indirect flight muscles were intact (**Figure 15B**), suggesting that the abnormal wing posture was secondary to impaired motor neuron function and not a result of muscle degeneration.

4.1.3 Reduced Survival in Khc^{N262S} mutant flies.

Survival assay was carried out at 18°C by expressing the mutant and wild type proteins using the D42-Gal4 driver. While the median life expectancy of control w^{1118} and khc^{wt} flies were 124 and 116 days respectively, the Khc^{N262S} flies that emerged survived only for about 5 days, an extremely significant ($p<0.001$) reduction of median survival (**Figure 16**). However, a partial rescue of reduced survival was achieved by expressing an extra copy of wild type kinesin (in $Khc^{N2652S+wt}$ flies) where the median survival was increased to 100 days (still a reduction of 25% compared to control flies).

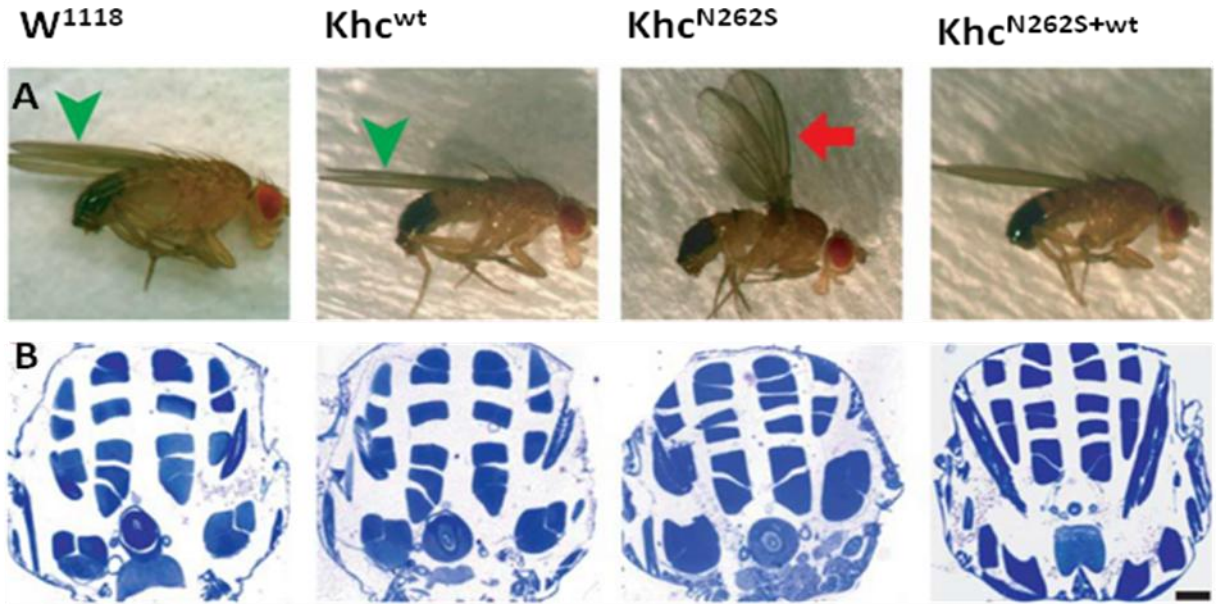

Figure 15: Characterization of adult *Drosophila* SPG10 model flies. (A) Analysis of wing posture of 2 day old W^{1118}, Khc^{wt}, Khc^{N262S}, and $Khc^{N262S + wt}$ adult flies driven by D42-Gal4 driver at 18°C is shown. At rest, control flies held their wings parallel to their body axis indicated by the green arrowhead. But the Khc^{N262S} mutant fly held their wings almost perpendicular to body axis indicated by the red arrow suggesting either degeneration or functional impairment of the indirect flight muscles. (B) However, analysis of thorax muscle integrity provided no evidence for the degeneration of the indirect flight muscles in Khc^{N262S} flies. Scale bar: 100 µm.

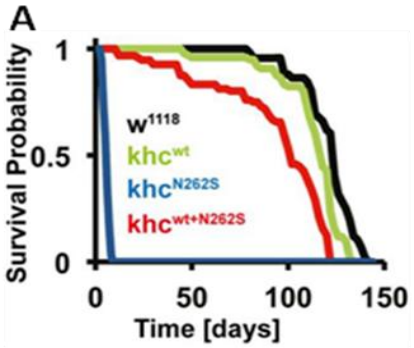

B

D42-Gal4 →	w^{1118}	khc^{wt}	khc^{N262S}	$khc^{wt+N262S}$
Flies assayed:	120	102	95	96
Life expectancy:	124 days	116 days	5 days	100 days

D42-Gal4 →	w^{1118}	khc^{wt}	khc^{N262S}	$khc^{wt+N262S}$
w^{1118}		***	***	***
khc^{wt}	***		***	***

Figure16: Survival ability. (A) Kaplan-Meier survival curve recorded at 18°C (Genotypes: black: D42>w^{1118}; Green: D42>Khc^{wt}; Blue: D42>Khc^{N262S}; Red: D42>$Khc^{wt+N262S}$). **(B)** Summary of the survival data. Statistical significance of data was determined by a series of Mantel-Cox tests. *** $p<0.001$

4.1.4 Impaired motor function observed in mutant flies - Khc^{N262S} displayed climbing defects.

To test whether conditional expression of Khc^{N262S} after development into flies was sufficient to cause neurodegeneration, the pan neuronal temperature sensitive Elav-Gal4, tub-Gal80^{ts} driver (**section 2.4.1.1**) was used to drive the mutated protein. Within 24 hours of eclosion, the flies were shifted from a temperature of 18°C to 29°C to induce the protein expression. 16 days after induction, the ability of the Khc^{N262S} flies to climb along vertical plastic vials were significantly impaired ($p<0.001$) when compared to controls (w^{1118} and Khc^{wt}) (**Figure 17**). On the other hand, the climbing ability of 16 day old Khc^{N262S} flies at 18°C with very mild expression of mutated protein were not significantly different from that of controls, validating that the expression of mutated protein in adult fly was enough to cause motor neuron defect.

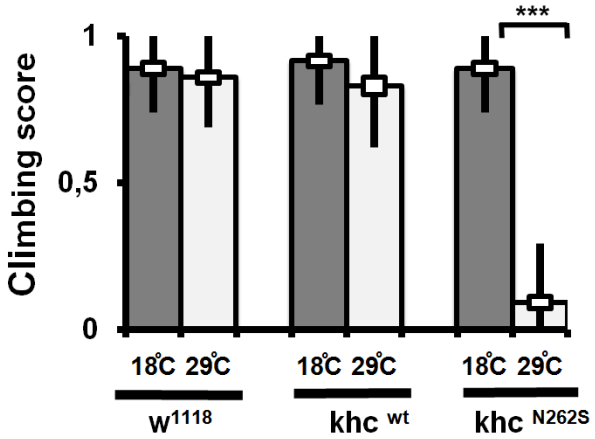

Figure 17: Climbing defects in Khc^{N262S} flies. Climbing assay of 16 days old mutated and control flies are shown. The desired proteins were expressed using Elav-Gal4, tub–Gal80^{ts}. Protein expression was induced in adult flies by shifting it from a temperature of 18°C (protein expression blocked) to 29°C (protein expression induced). A total of 50 flies per genotype were used in the study. Statistical significance was tested using an unpaired, two-tailed student's t-test (*** $p<0.001$). The standard error of the mean (s.e.m) is shown as a box, standard deviation (s.d.) as a black line.

4.1.5 Khc^{N262S} mutation resulted in lethality upon motor neuronal or pan neuronal expression.

The severity of mutated protein expression using various tissue specific drivers was analyzed. *Drosophila* undergoes various stages of development before emerging as adult flies –egg, larval (L1 or first instar, L2 or second instar and L3 or third instar larval stages) and pupa. Pan neuronal

expression of mutated protein using Elav-Gal4 driver at 29°C resulted in the death of mutated larvae in the second instar (L2) stage. When the mutated protein was expressed in the motor neurons, the larvae died at L3 stage. Driving it in tissues using the Actin-Gal4 also proved lethal as larvae died at L2 stage. Lethality was greatly reduced when the mutated protein was expressed in muscles using Mhc-Gal4 driver as viable adult flies eclosed. Owing to very low expression of mutated protein at 18°C, no lethality was observed in early stages of development and adult flies eclosed. Nevertheless the mutant adult flies driven under the control of Elav-Gal4, Actin-Gal4 or D42-Gal4 was much short lived when compared to Khc^{wt} control (**Table 6**). On the other hand tissue specific overexpression of wild type kinesin did not result in any lethality using any of these drivers at either temperature.

Table 6: Severity of Khc^{N262S} with various drivers.

Construct	**UAS-Khc^{wt}**		**UAS-Khc^{N262S}**	
Driver	**18°C**	**29°C**	**18°C**	**29°C**
Elav-Gal4	Viableadults	Viableadults	Viableadults	Died L2 stage
Mhc-Gal4	Viableadults	Viableadults	Viableadults	Viableadults
Actin-Gal4	Viableadults	Viableadults	Viableadults	Died L2 stage
D42-Gal4	Viableadults	Viableadults	Viableadults	Died L2-L3

4.2 Khc^{N262S} mutants are characterized by axonal swellings

4.2.1 Quantitative and qualitative analysis of axonal swellings in Khc^{N262S} mutants

Impaired kinesin function causes a general disruption of fast axonal transport that in turn leads to dystrophic neuron development, defective neurotransmission and progressive distal paralysis (Salinas, Proukakis et al. 2008). It has been shown in a previous study that kinesin mutation cause axonal swellings that are filled with cargos of fast axonal transport, membrane bound organelles and synaptic membrane protein (Hurd and Saxton 1996).

Axonal ultrastructure of mutant larvae (khc^6) have shown dramatically swollen regions that are packed with membrane bound organelles (Hurd and Saxton 1996). A similar cellular phenotype was observed in the segmental nerves of Khc^{N262S} mutant larvae. Axonal traffic jams in the segmental nerves of the D42-Gal4 driven mutant and control third instar larvae (raised at 29°C)

were qualitatively and quantitatively analyzed by immunostaining with various cargo specific antibodies. Anti-HRP antibody can recognize a neural specific carbohydrate moiety in *Drosophila* axons and hence it has widely been used as a neuron specific probe that stains the surface of individual neuron including axon (Snow, Patel et al. 1987).

Axonal swelling interpretation:

Swelling was defined by (a) the accumulation of cargo, (b) a local increase in anti-HRP staining intensity, and (c) a strong increase in axon diameter. The two main parameters analyzed were area fraction swelling and swelling densities. The area fraction swelling is defined as the ratio of area of colocalised bright HRP and cargo staining to the total HRP area of the nerve segment. The swelling density is the number of cargo swellings per 1000μm^2 of segmental nerves.

4.2.2 Kinesin-1 specific cargos CSP and DV-Glut trapped in nerve segments of Khc^{N262S} larvae

Axonal trafficking of two presynaptic proteins-cysteine string protein (CSP) and *Drosophila* vesicular glutamate transporter (DV-Glut) were analyzed since these proteins underwent high levels of microtubule based axonal transport.

In the khc null mutants axonal accumulation of CSP has been reported (Hurd and Saxton 1996). In a previous study by our lab, we have shown large immunoreactive clusters of CSP along the segmental nerves of khc null, Khc^{N262S} and Khc$^{N262S+wt}$ larvae (Fuger, Sreekumar et al. 2012). But on the other hand, no such clusters were observed in nerve segments of control animals. When the swellings were quantified, both area fraction swelling and swelling densities of CSP were significantly increased ($P<0.01$) in khc null mutant and Khc^{N262S} when compared to controls (**Figure 18**).Expression of wild type kinesin along with the mutant kinesin (Khc$^{N262S+wt}$) reduced the swellings considerably but nevertheless were still significantly more when compared to controls ($P<0.05$).

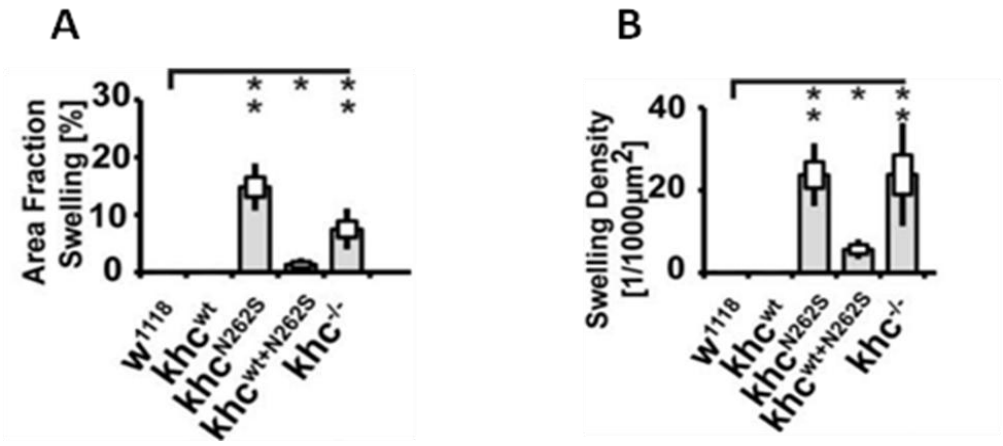

Figure 18: CSP axonal trafficking in segmental nerves. Analysis of axonal cargo accumulation was performed by staining segmental nerves of third instar larva (under the control of D42-Gal4 driver at 29°C) for the membrane marker anti-HRP and for synaptic vesicle marker CSP. **(A)** The graph represents the percentage of area fraction swelling for w^{1118}, Khc^{wt}, Khc^{N262S}, $Khc^{N262S+wt}$ and Khc null mutants. **(B)** The graph represents the swelling density per 1000 µm^2 axonal area. Both the area fraction of the nerve filled with cargo accumulations and the number of cargo accumulations per 1000 µm^2 of the nerve were significantly increased in larvae expressing khc^{N262S}, either alone, or in combination with Khc^{wt}. For all quantifications, n = 10 axons per genotype were used. Statistical significance **(A,B)** was determined by using a Kruskal-Wallis H-test for comparisons between multiple groups. The standard error of the mean (s.e.m.) is shown as a box, the standard deviation (s.d.) as a black line. * $p<0.05$; ** $p<0.01$, *** $p<0.001$.

Similarly, when the axonal trafficking of DV-GLUT was analyzed, swellings covered around 18% (**Figure 19B**) of total axonal area of the Khc^{N262S} mutants. An average of 20 such swellings (**Figure 19C**) were observed in the segment nerves which was significantly higher when compared to controls ($p<0.001$).

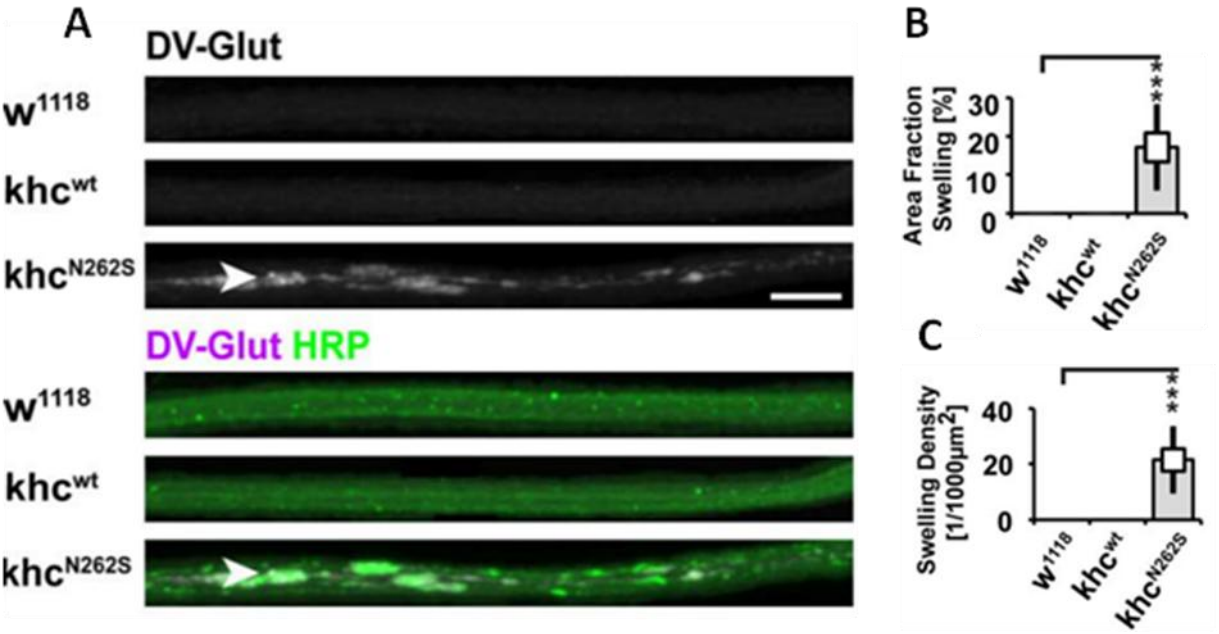

Figure 19: DV-Glut axonal trafficking in segmental nerves. Analysis of axonal cargo accumulation was performed by staining segmental nerves of third instar larva (under the control of D42-Gal4 driver, 29°C) for the membrane marker anti-HRP and DV-Glut **(A)** Confocal images of axonal segments immunostained with DV-Glut and membrane marker HRP is shown for w^{1118},Khc^{wt} and Khc^{N262S} larvae. Axonal accumulations are indicated by arrowhead. **(B)** Graph represents the percentage of area fraction swelling. **(C)** Graph represents the swelling density per 1000 micrometre axonal area of the above mentioned genotypes. For all quantifications, n = 10 axons per genotype were used. Statistical significance **(B, C)** was determined by using a Kruskal-Wallis H-test for comparisons between multiple groups. Scale bars in B–I: 10 µm.The standard error of the mean (s.e.m.) is shown as a box, the standard deviation (s.d.) as a black line. * $p<0.05$; ** $p<0.01$, *** $p<0.001$.

4.2.3 Khc^{N262S} axonal swellings stained positive for Kinesin-3 cargos.

Expression of Khc^{N262S} in the motor neurons not only affected the trafficking of Kinesin-1 cargo but also other motor protein cargos. The transport of dense core vesicles and the transport of the active zone protein Bruchpilot (Brp) was disturbed in Khc^{N262S} expressing larvae but not in controls (**Figure 19**). Both cargos are transported by the kinesin-3 family member unc-104(Mahr and Aberle 2006).

The accumulation of both ANF-GFP and Brp in the HRP swellings indicated that the fast axonal transport of not only kinesin-1 but also kinesin-3 cargoes were disturbed by the expression of Khc^{N262S} in nerve segments. Though the area fraction swellings of both ANF-GFP and Brp in

mutants were considerably less (2-3%) (**Figure 20B and 20E**) when compared to kinesin-1 cargos (18-20%) (**Figure 19B**), their mere presence suggests an early evidence for a generalized disruption of axonal transport in Khc^{N262S} *Drosophila* model. There could be two possible reasons for this. The slow moving mutant kinesin dimers could result in traffic block and thus prevent other motors to progress, or, it could be the consequence of destabilized microtubules.

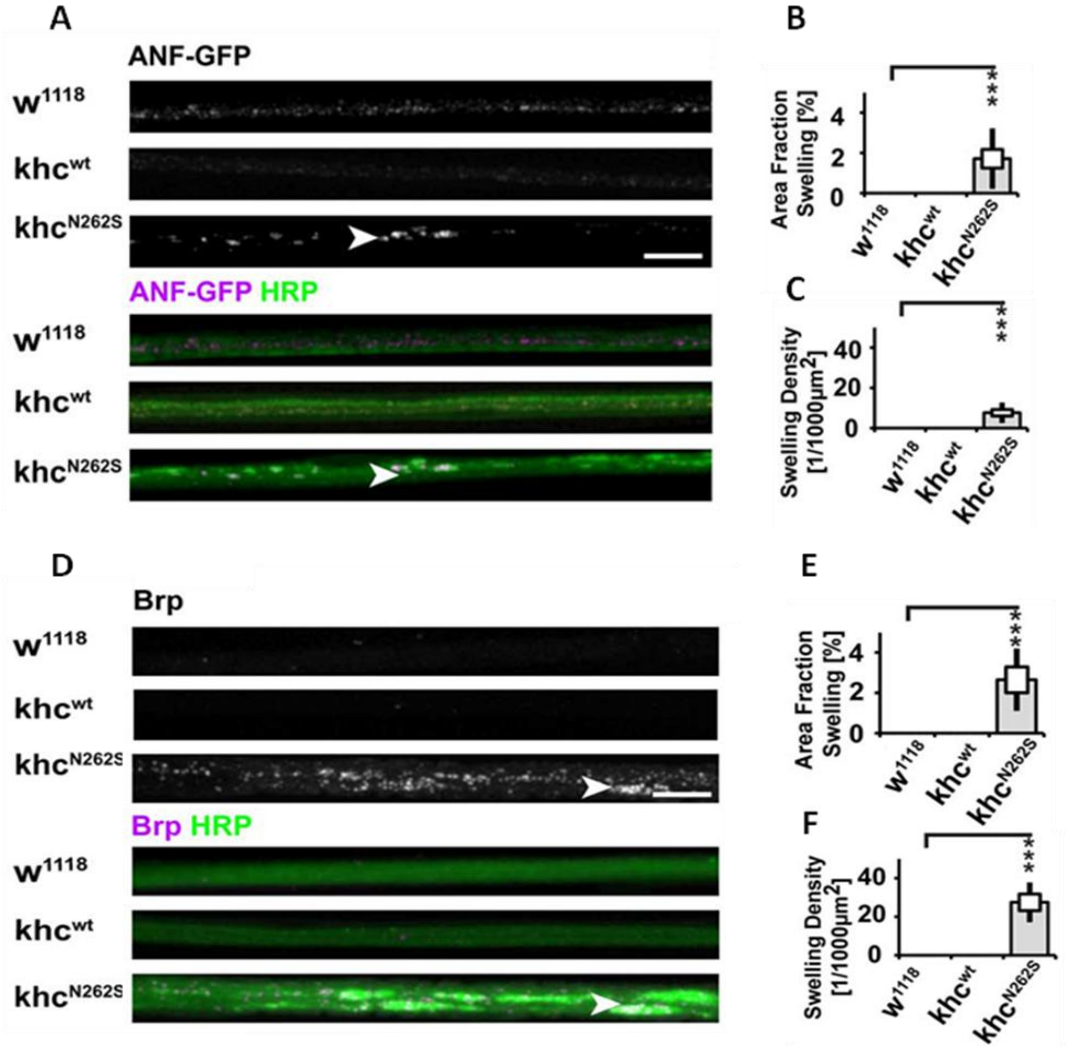

Figure 20: Trafficking of Kinesin-3 cargos in segmental nerves. Analysis of axonal cargo accumulation was performed by staining segmental nerves of third instar larva (under the control of D42-Gal4 driver, 29°C) for the membrane marker anti-HRP and for Kinesin-3 cargos ANF-GFP and Brp **(A)** Confocal images of axonal segments of w^{1118}, Khc^{wt} and Khc^{N262S} third instar larvae stained with ANF-GFP and membrane marker HRP. **(B, C)** Graph depicts the percentage of area fraction swelling and swelling density per 1000 micrometre area of axonal segments for Kinesin-3 cargo ANF-GFP. **(D)** Confocal images of axonal segments immunostained with Brp and HRP. **(E, F)** Graph depicts the

percentage of axonal swellings and swelling density per 1000 micrometre for Brp. Axonal cargo accumulations (arrowheads in A, D) were defined as segments of the nerve characterized by a bright anti-HRP staining and the simultaneous accumulation of cargoes. For all quantifications, n = 10 axons per genotype were used. Statistical significance **(B, C, E and F)** was determined by using a Kruskal-Wallis H-test for comparisons between multiple groups. Scale bar: 10 µm. The standard error of the mean (s.e.m.) is shown as a box, the standard deviation (s.d.) as a black line. * $p<0.05$; ** $p<0.01$, *** $p<0.001$.

4.2.4 Endosomal and autophagosomal markers trapped in the swellings of Khc^{N262S} axonal segments.

While lysosomal associated membrane protein (LAMP) is a marker for late endosomes and lysosomal compartments, autophagy-related protein 8 (ATG8) is a marker for autolysosomal compartments (Pulipparacharuvil, Akbar et al. 2005; Kohler, Brunner et al. 2009). Previously in our lab, ultrastructural analysis of the axons of larvae expressing Khc^{N262S} revealed the presence of dark staining organelles similar to multivesicular bodies, pre-lysosomal vacuoles (PLVs) and autophagosomes (Fuger, Sreekumar et al. 2012). To validate this finding further, GFP tagged LAMP and RFP tagged ATG8 was driven in the motor neurons of control and mutant animals using D42-Gal4 driver at 29°C. While no strong LAMP-GFP fluorescence was detected in control w^{1118} larvae, it was strongly enriched in axonal swellings (**Figure 21A-arrowhead**) of Khc^{N262S} expressing larvae. The autolysosomal marker ATG8-mRFP also localized in axonal swellings (**Figure 21B- arrowhead**). The accumulation of PLVs can be triggered by impairments in the retrograde transport of small pre-lysosomal organelles, which then fuse and mature, giving rise to the PLVs observed swellings (Hurd and Saxton 1996). Alternatively, stress-driven autophagy of the cytoplasm might further contribute to the formation of PLVs (Hurd and Saxton 1996). The fact that the swellings are positive for ATG8 is consistent with the hypothesis that stress-driven autophagy of the cytoplasm might contribute to the formation of PLVs (Hurd and Saxton 1996).

4.3 Synaptic protein depletion at distal NMJs of Khc^{N262S} mutants:

Since the trapping of synaptic proteins (CSP, DV-Glut, Brp) was observed in the swellings of nerve segments, it was interesting to check whether the impairment of axonal transport reflected on the distribution of these proteins at distal NMJs.

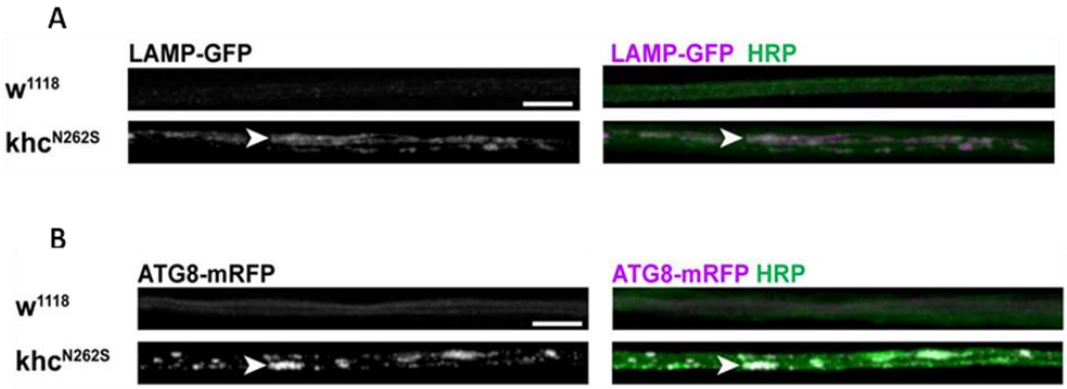

Figure 21: Trafficking of lysosomal and autopahgosomal molecules in Khc^{N262S} mutants. Confocal images of immunofluorescent staining showing segmental nerves of mid-third-instar *Drosophila* larvae (D42-Gal4 driver at 29°C). **(A)** Larvae were stained for the membrane marker anti-HRP as well as for the lysosome marker LAMP-GFP. **(B)** Staining for the autophagosome marker ATG8-mRFP and HRP. White arrowheads indicate axonal swellings that are positive for autophagosomes and lysosomal organelles. Scale bars in A and B: 10µm.

Degeneration of distal NMJs has been reported in the Khc^{N262S} mutants (Fuger, Sreekumar et al. 2012). To investigate if reduced synaptic protein distribution could be one factor responsible for the observed degeneration of synapses, NMJs (muscle 6/7, segment A5) were stained for CSP and DV-Glut as markers for synaptic vesicles (SVs) and Brp as a marker for active zones (AZs). CSP acts as molecular chaperons that are involved in the insoluble NSF Attachment Protein receptor (SNARE) complex assembly. Expression of DV-Glut determines the size and glutamate content of synaptic vesicles, and finally, the assemblies of active zone matrix T bar rely on Brp. Therefore the depletion of these presynaptic markers could be detrimental. There was a significant reduction of Brp and DV-Glut intensities in mutant NMJs when compared to wild type ($P<0.01$).The intensity of CSP in the mutant NMJ was reduced to a lesser extent than the other two synaptic protein, nevertheless it was still significantly less when compared to wild type ($P<0.05$). Confocal images revealed that DV-Glut and CSP abundance is increased in dystrophic boutons and reduced elsewhere at NMJs of D42< khc^{N262S} larvae (**Figure 22C and Figure 22E-arrows**). SV proteins were inhomogenously distributed in Khc^{N262S}expressing larvae. There was a strong correlation between the inhomogeneity observed in the staining for HRP and SV proteins. This inhomogeneous distribution might resemble defects in the delivery of SV, in endo-/exocytosis, or in membrane trafficking.

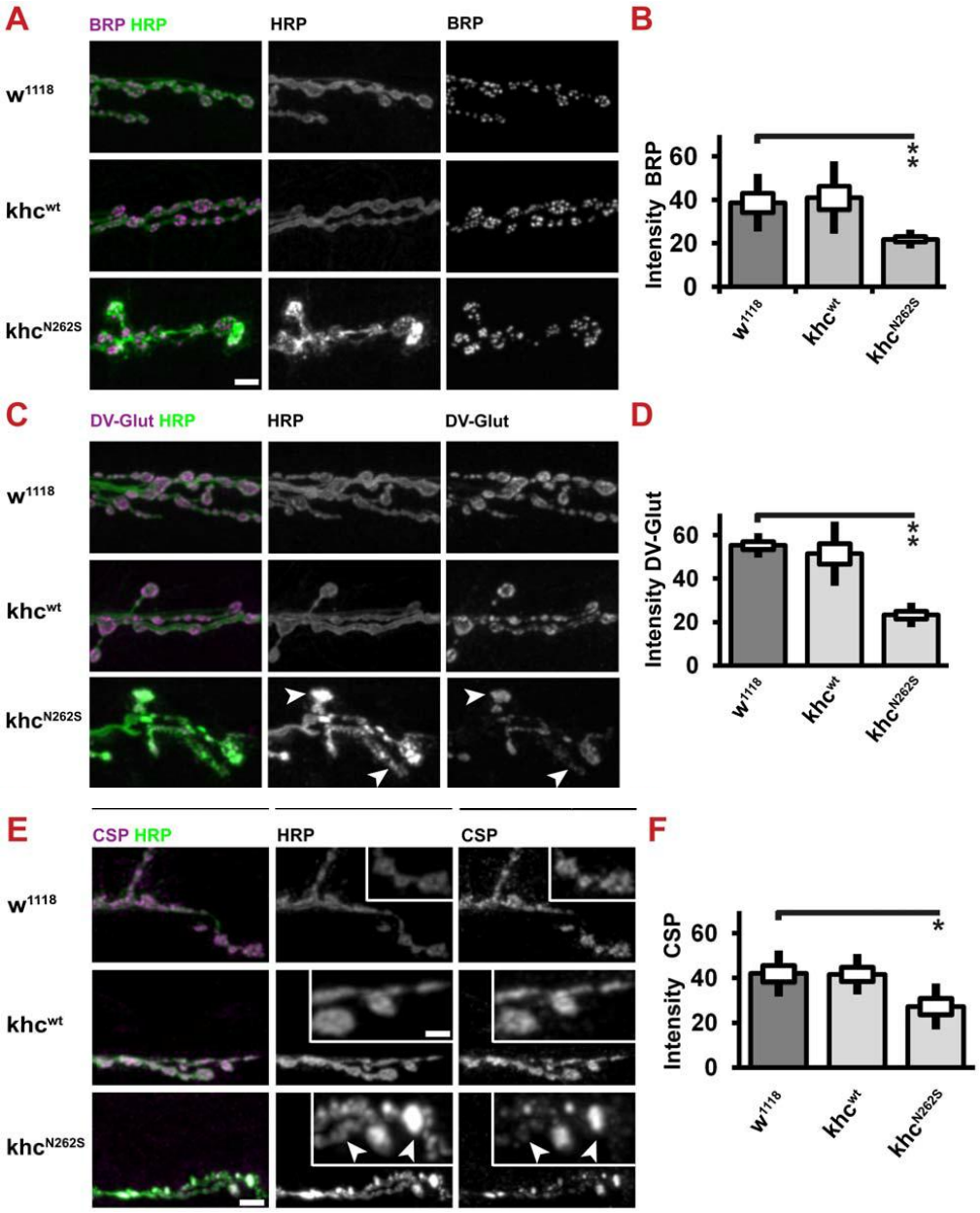

Figure 22: Expression of Khc^{N262S} causes length-dependent synaptic defects at the neuromuscular junction. Confocal images and quantification of immunofluorescent staining of synaptic marker proteins. NMJs 6/7, segment A5 of mid-third-instar *Drosophila* larva, were selected for analysis. D42<w^{1118} and D42<Khc^{wt} larvae were used as controls for the mutant phenotype D42<Khc^{N262S}. **(A,B)** NMJ staining for the active zone protein Brp and graph depicting the Brp intensity in the distal NMJs. **(C,D)** Staining for the synaptic vesicle proteins DV-Glut and quantification of DV-Glut intensities in NMJs. **(E,F)** Staining for synaptic protein CSP and its intensity quantification. **(A,C,E)** Confocal images revealed that DV-Glut and CSP abundance is increased in dystrophic boutons **(C,E arrows)** and reduced elsewhere **(C,E arrowheads)** at NMJs of D42<Khc^{N262S} larvae. Scalebar: 5 mm. For quantification, n = 8–10 NMJs were analyzed per genotype. Statistical significance was determined using a Kruskal-Wallis H-test for

comparisons between multiple groups. The standard error of the mean (s.e.m.) is shown as a box, the standard deviation (s.d.) as a black line. * p,0.05; ** p,0.01.

4.4 Destabilization of microtubules observed in distal NMJs of Khc^{N2626S} mutants.

Microtubules play key roles in the control of synaptic structure and function (Conde and Caceres 2009). Mutations perturbing microtubule dynamics are causatively linked to inherited neurological disorders. Microtubule destabilization and transport failure acts as an "early" pathogenic cascade leading to synaptic decline (Desai and Mitchison 1997). Prior studies in the lab to investigate the cytoskeletal integrity, has shown a significant decline in the futsch (N- and C-terminal domains of futsch are homologous to the vertebrate MAP1B microtubule-associated protein) staining especially at the synaptic terminals of mutant larvae when compared to controls (Fuger, Sreekumar et al. 2012). Therefore, analysis of microtubular dynamics at the NMJs could further strengthen this theory of cytoskeletal loss at distal NMJs of Khc^{N262S} mutants. Tubulins are carried by slow axonal transport and there are evidences that kinesin mutation does not seem to affect the slow axonal transport (Chevalier-Larsen and Holzbaur 2006). Hence the total tubulin intensities in the NMJ 6/7 of segment A5 of mutant and control third instar larvae driven by the D42Gal4 driver and raised at 29°C was analyzed. Though there was a reduction in the intensities of total tubulin in Khc^{N262S} NMJs, yet it was not significantly less when compared to control w^{1118} animals. It was interesting to further test whether the real issue was destabilization of microtubules since the total tubulin distribution was not significantly affected. The stability of microtubules depends on the post translational modification of tubulins. Acetylated microtubules are excellent indicators of stabilized microtubules. Microtubule stability was assayed locally within the synapse by using antibodies specific to acetylated tubulin, which label stable and long-lived microtubules. Not only that the intensity of acetylated microtubules were significantly reduced in the Khc^{N262S} animals when compared to controls ($p<0.001$), but the stabilized microtubule network was much thinner and fainter especially at the synaptic terminals when compared to controls (**Figure 23**). This typical phenotype of microtubular network has been previously observed in NMJ of spastin mutants characterized by severe microtubular destabilization (Sherwood, Sun et al. 2004).

4.5 KhcN^{262S} mutants show delayed pupation.

When driven by the Gal4 driver at 25°C Khc^{N262S} flies could not emerge and died in the pupal stage. Additionally, a delayed development was observed during progression from embryo to pupa. When compared to controls (w^{1118} or Khc^{wt}), the Khc^{N262S} mutant larvae took 24 hours longer for maximum pupa formation. The additional expression of wild type kinesin protein along with the mutant kinesin in (Khc$^{wt+N262S}$) compromised the delay in development. Maximum pupa was formed in the control groups 7 days past egg hatching. However, in Khc^{N262S} mutants maximum pupa formation took 8 days, a day longer than controls which were a significant delay with respect to the lifespan of *Drosophila*.

4.6 Khc^{N262S} mutants display defects in active zone development

Neuro developmental impairment was analyzed by testing the synapse maturity at L2 stage (an early stage in larval development) of mutant and control larvae. Synapse comprises of tightly apposed pre and postsynaptic membranes, a postsynaptic cluster of neurotransmitter receptors, and a presynaptic complex of proteins that promotes neurotransmitter release. For a synapse to function, the proper complement of proteins must localize to the presynaptic release machinery, and the protein composition at the release site is a likely determinant of its synaptic efficacy (Fejtova and Gundelfinger 2006). The active zones at the presynapse are opposed to postsynaptic glutamate receptor (GluR) clusters (Petersen, Fetter et al. 1997). In *Drosophila*, Bruchpilot localizes to every active zone which is opposed by the GluR at the post synapse which marks the maturity of the synapse (Wagh, Rasse et al. 2006). The animals were stained for the presynaptic active zone protein Bruchpilot (Brp) and the essential glutamate receptor subunit *Drosophila* glutamate receptor IIC (DGluRIIC). In Khc^{N262S} mutants there was reasonable increase of Brp-negative active zones, yet the morphology and number of DGluRIIC clusters appeared grossly normal (**Figure 24A and 24B**).

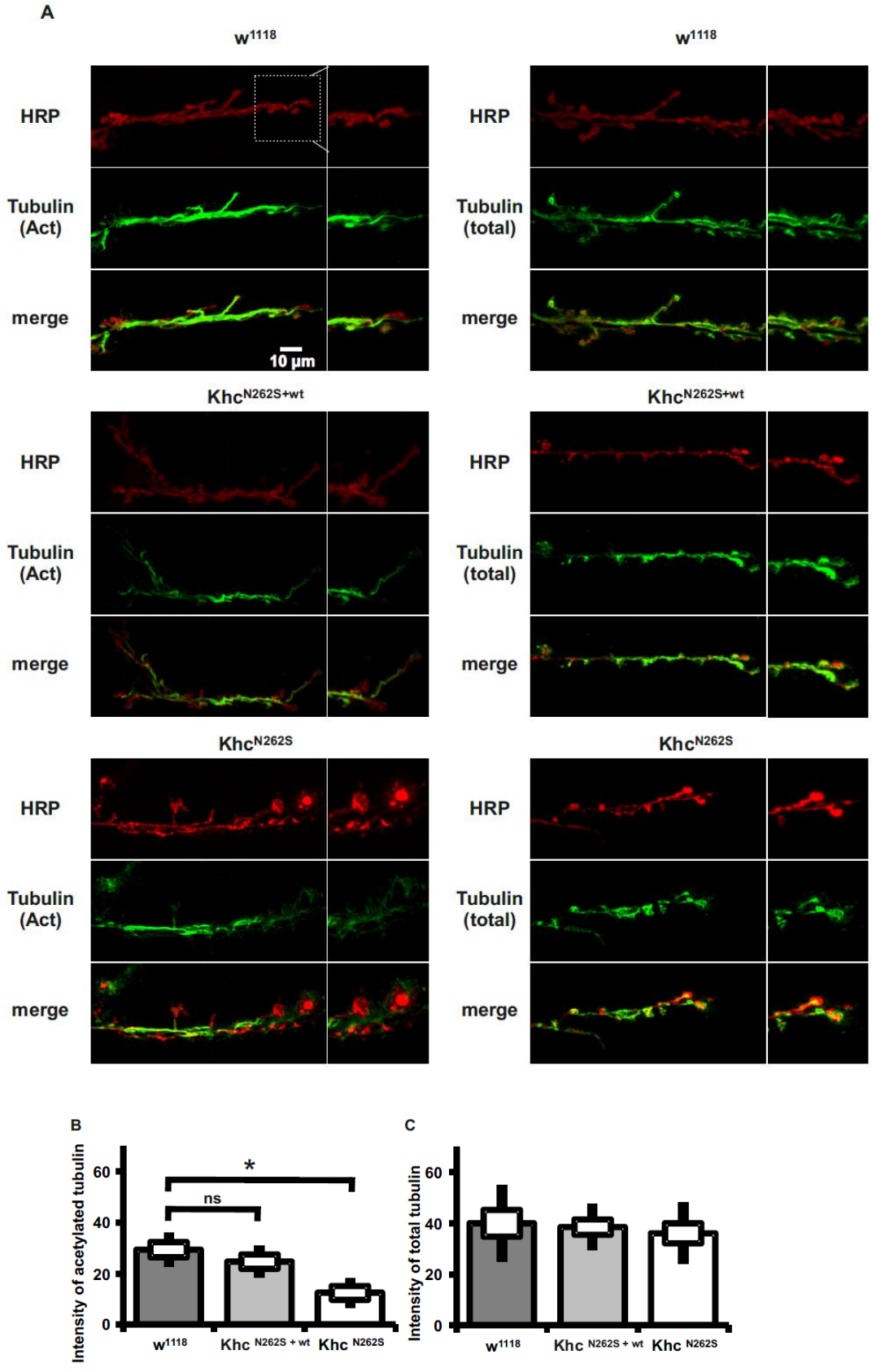
A
w1118
w1118
HRP
Tubulin (Act)
merge
10 µm
HRP
Tubulin (total)
merge
KhcN262S+wt
KhcN262S+wt
HRP
Tubulin (Act)
merge
HRP
Tubulin (total)
merge
KhcN262S
KhcN262S
HRP
Tubulin (Act)
merge
HRP
Tubulin (total)
merge
B
Intensity of acetylated tubulin
60
40
20
0
*
ns
w1118
Khc N262S + wt
Khc N262S
C
Intensity of total tubulin
60
40
20
0
w1118
Khc N262S + wt
Khc N262S

Figure 23: Khc^{N262S} mutant NMJs marked with destabilized microtubules. (A) Confocal images of immunofluorescent staining of acetylated and total tubulin. NMJs 6/7, segment A5 of mid-third-instar *Drosophila* larva, were selected for analysis. D42<w^{1118} was used as control for the mutants D42<Khc$^{N262S+wt}$ and D42<Khc^{N262S}. The magnified image shows the synaptic terminal staining. Acetylated tubulin intensity is severely reduced and thinned out in the terminal synaptic boutons of Khc^{N262S} NMJ. **(B)** Graph depicts the intensity of acetylated tubulin in NMJs. **(C)** Graph represents the intensity of total tubulin in the NMJs. Scale bar: 10µm. For quantification, n = 8–10 NMJs were analyzed per genotype. Statistical significance was determined using a Kruskal-Wallis H for comparisons between multiple groups. The standard error of the mean (s.e.m.) is shown as a box, the standard deviation (s.d.) as a black line.. * p<0.05; ** p<0.01, *** p<0.001.

GluR clusters that are unapposed to a Brp-positive active zone is called running unopposed phenotype has been previously reported in role of Rab3 in active zone formation (Graf, Daniels et al. 2009).

The increase in BRP negative synapses could be an indication of immature synapses but however since the GluIIc recptor distribution and Brp negative synapses (though reduced) are not significantly affected compared to w^{1118}, it rules out the possibility of neurodevelopmental issues. Khc^{N262S} mutation has more neurodegenerative nature. I also observed that in the nerve segments of mutant animals, there were early signs of cargo trafficking impairment. Even at the L2 stage in mutants, the nerve segments were positive for large clustering of Brp and to some extend the HRP swellings. However, the HRP swellings in the axonal segments of L2 Khc^{N262S} larvae (**Figure 24C**) were less when compared to HRP swellings observed in L3 stage of Khc^{N262S} (**Figure 20**) though the accumulation of Brp seemed to be almost comparable, hence it is probable that the swellings appear secondary to impaired cargo transport.

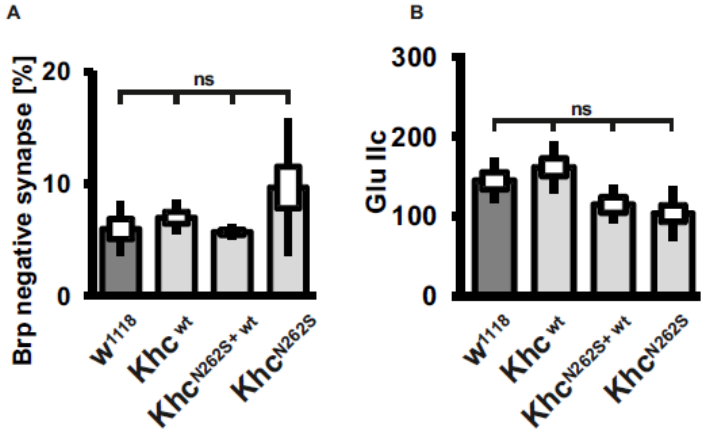

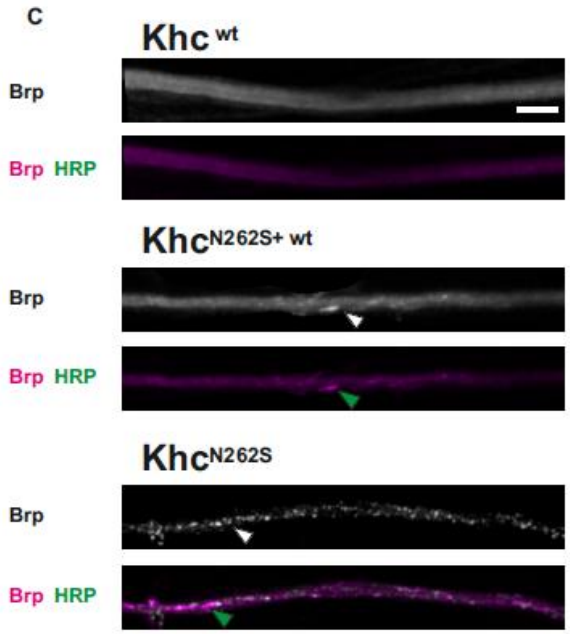

Figure 24: Active zone assembly and axonal trafficking in L2 stage Khc^{N262S} larvae. D42<w^{1118}, D42< Khc$^{N262S+wt}$, D42< Khc^{N262S} L2 stage larvae raised at 29°C was analysed for Brp and GluIIC distribution in NMJ 6/7 segment A5 as well as for presence of swelling in axons. (A) Graph represents the percentage of Brp negative synapses in the NMJs normalised to muscle length. (B) Graph represents the normalised GluIIC distribution in NMJs. (C) Confocal images showing the Brp and HRP staining of nerve segments in L2 larvae of the above mentioned genotypes. Brp accumulation indicated by white arrowhead and Hrp-Brp localization in swelling indicated by green arrowhead. Scale bar 10µm. For quantification, n = 8–10 NMJs were analyzed per genotype. Statistical significance was determined using a Kruskal-Wallis H for comparisons between multiple groups. The standard error of the mean (s.e.m.) is shown as a box, the standard deviation (s.d.) as a black line. * $p<0.05$; ** $p<0.01$, *** $p<0.001$.

4.7 Khc^{N262S} mutation also affects retrograde transport of cargos

Biochemical evidence for a direct interaction between conventional kinesin and cytoplasmic dynein, mediated by an interaction between dynein intermediate chain (DIC) and kinesin light chains (KLCs) was shown via immunoprecipitation studies using rat brain cytosol by Ligon *et al*. Studies in extruded squid axoplasm have indicated that the specific inhibition of either kinesin (7, 8) or dynein/dynactin (9) results in a bidirectional block in the transport of vesicles along microtubules.

Interdependence of anterograde and retrograde motors has also been noted genetically. Martin *et al* identified dominant genetic interactions between the kinesin, cytoplasmic dynein, and dynactin genes in *Drosophila*. Mutations in either motor resulted in an inhibition of axonal transport and caused accumulation of organelles in axonal swellings that stain for markers of both anterograde and retrograde motility (Chevalier-Larsen and Holzbaur 2006). Previously in our lab it was shown through in vivo studies of mitochondrial transport that Khc^{N262S} mutation significantly reduced the retrograde flux of mitochondria in nerve segments (Fuger, Sreekumar et al. 2012).

4.7.1 Co-expression of Khc^{N262S} and RNAi against retrograde motors worsened the mutant rough eye phenotype:

Dyneins and dynactins are the major retrograde transport motors. In *Drosophila*, P150 Glued and P50 dynamitin, subunits of dynactin assist retrograde transport by binding to dynein (Waterman-Storer and Holzbaur 1996). Genetic screens using the fly eye have been successful in the study of neurodegeneration as well as identifying genetic modifiers of disease. The compound eye of *Drosophila* contains around 800 repeating subunits, called ommatidia, disruption of which results in rough eye phenotype. Owing to the ease of viewing the retina under a dissecting microscope and the flexibility of manipulating the eye without compromising the overall health of the fly, it serves as an ideal tool for genetic screens (Prussing, Voigt et al. 2013). Expression of toxic gene products in the *Drosophila* compound eye causes rough eye phenotype (REPs) enabling an easy scoring system for genetic modifier screens.

Khc^{N262S}, RNAi against P50 , RNAi against P150 as well as RNAi against P150 and P50 along with Khc^{N262S} ($Khc^{N262S+RNAi\ P50}$, $Khc^{N262S+RNAi\ P150}$) was expressed using a GMR-Gal4 driver in the eyes of flies. After expressing the desired proteins using the GMR-Gal4 driver at 29°C for 12 days post eclosion, the severity of depigmentation and necrosis in fly eyes were scored The expression of mutated kinesin protein Khc^{N262S} resulted in depigmentation (**Figure 25, arrow heads**) of ommitidia and development of black spots which resembled necrosis (**Figure 25, arrows**). The inhibition of retrograde transporters P50 RNAi and P150 RNAi alone did not affect the eye structure significantly. However, expression of Khc^{N262S}along with P50 RNAi and P150 RNAi ($Khc^{N262S+RNAiP150}$, $Khc^{N262S+RNAiP50}$) worsened the mutant eye phenotype considerably (for this purpose, flies co-expressing GMR and Khc^{N262S} were mated with flies expressing RNAi against retrograde motors). In addition to depigmentation, degeneration of ommatidias was also observed which gave a glassy appearance to the eyes (**Figure 25**). Since a couple of genes were

driven under the control of GMR driver, it was required to test whether there was a possibility of gene dilution in the co expression model. For this purpose, an additional control was used ($Khc^{N262S+Lacz}$). LacZ gene was driven using the GMR-Gal4 driver in the mutant background which served as an ideal control. Expression of LacZ alone (in the absence of mutant background) did not create any distortion of the fly eye and does not induce any toxicity in flies. On the other hand, expression of Khc^{N262S} together with LacZ ($Khc^{N262S+LacZ}$) resulted in characteristic depigmentation **(Figure 25, arrowhead)** and black spots **(Figure 25, arrow)** as observed in the Khc^{N262S} mutants but the eye phenotype observed was significantly better than the $Khc^{N262S+RNAi\ P50\ /\ P150}$. As expected, the overexpression of wild type kinesin did not cause any distortion of eye. This additive nature of phenotypic severity upon co expression of Khc^{N262S} and retrograde transport block implicated a possible molecular interaction between anterograde and retrograde transport in Khc^{N262S} mutants.

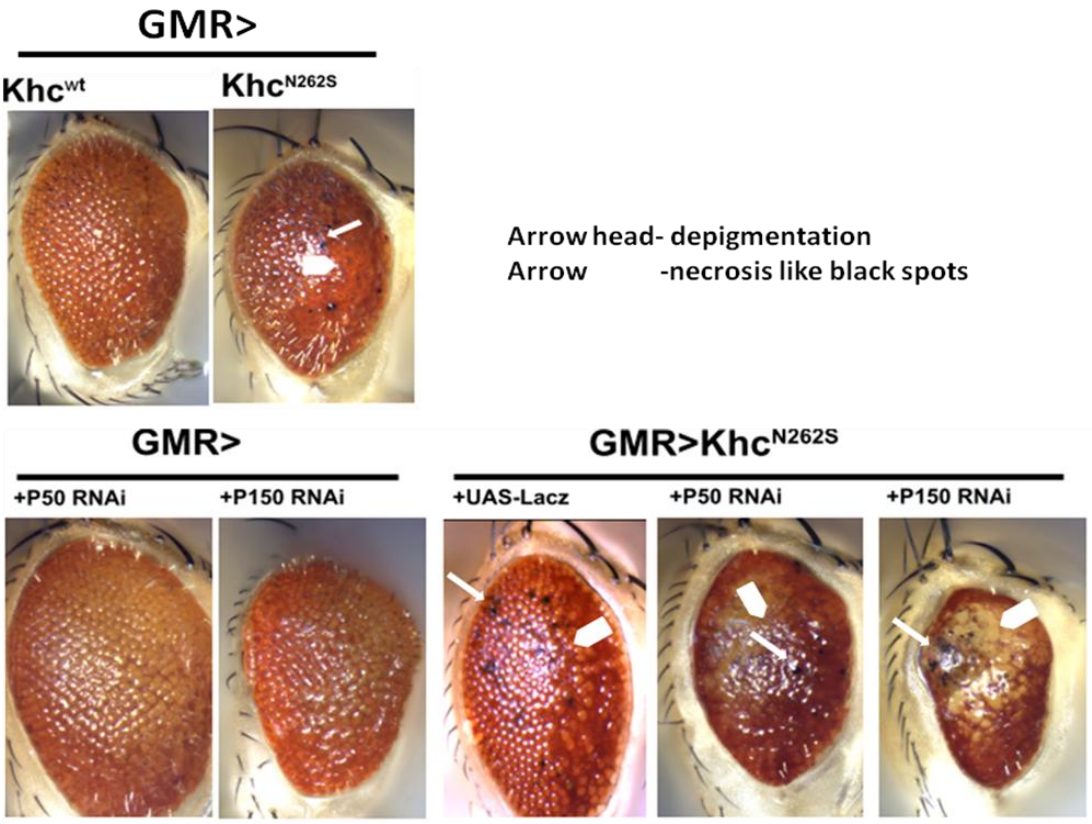

Figure 25: Screening rough eye phenotype. GMR-Gal4-induced rough eye phenotype (REP) in the eyes of Khc^{N262S}, Khcwt, Khc^{N262S}+LacZ as well as the retrograde blockers P50 RNAi and P150 RNAi both in the presence and absence of Khc^{N262S} mutation is shown. Depigmentation is indicated by white arrowhead and necrosis like black spot indicated by white arrow. Total of 10 flies per genotype was analyzed.

Table 7: Double blind scoring for rough eye phenotype.

Genotype		Feature	GMR score
GMR	**W^{1118}**	Control (native wild type kinesin expression)	-/+
GMR	**$Khc^{N262S+wt}$**	Ectopic co-expression of wild type and mutated kinesin in addition to native wild type kinesin	-/+
GMR	**Khc^{N262S}**	Ectopic expression of mutated kinesin in addition to native wild type kinesin	++
GMR	**$khc^{N262S+LacZ}$**	Ectopic expression of mutated kinesin and lacZ in addition to native wild type kinesin	++
GMR	**RNAi P50**	Retrograde transport blocker (RNAi Dynamitin)	-/+
GMR	**RNAi P150**	Retrograde transport blocker (RNAi Glued)	-/+
GMR+Khc^{N262S}	**RNAi P50**	Retrograde blocker in mutant kinesin background	+++
GMR+Khc^{N262S}	**RNAi P150**	Retrograde blocker in mutant kinesin background	+++

The table above represents the double blind score (by Junyi Zhu) for the severity of rough eye phenotype in flies GMR<w^{1118}, GMR<Khc^{N262S}, GMR<$Khc^{N262S+wt}$, GMR<$Khc^{N262S+LacZ}$, GMR<$Khc^{N262S<RNAiP50}$, GMR<$Khc^{N262S+RNAiP150}$, GMR<RNAiP50, GMR<RNAiP150. Completely normal eye phenotype was scored -/+, depigmentation along with black spots was scored ++ and severely affected eye accompanied by depigmentation and black spots were scored +++.

4.7.2 Expressing RNAi against retrograde motors with Khc^{N262S} worsened the mutant larval phenotype:

To further validate the effect of kinesin mutation and retrograde transport block, an additional behavioural screen was performed. Motor neuron specific expression of Khc^{N262S} in third instar larvae severely paralyzed them. Therefore, this model proved to be complex to evaluate any additional effect that the retrograde transport block could generate. The ideal model for studying this interaction would be the co expression model of wild type kinesin along with mutated kinesin ($Khc^{N262S+wt}$). Though these larvae showed the characteristic tail flip phenotype, yet they moved at a pace almost similar to the wild type larvae. Thus any changes induced by expressing additional genes in the mutant background could be clearly visualized using this less severe model. Possible gene dilution issue in the experiment was addressed using two additional controls - ($Khc^{N262S+wt+Lacz}$ and $Khc^{N262S+wt+CD8-GFP}$).

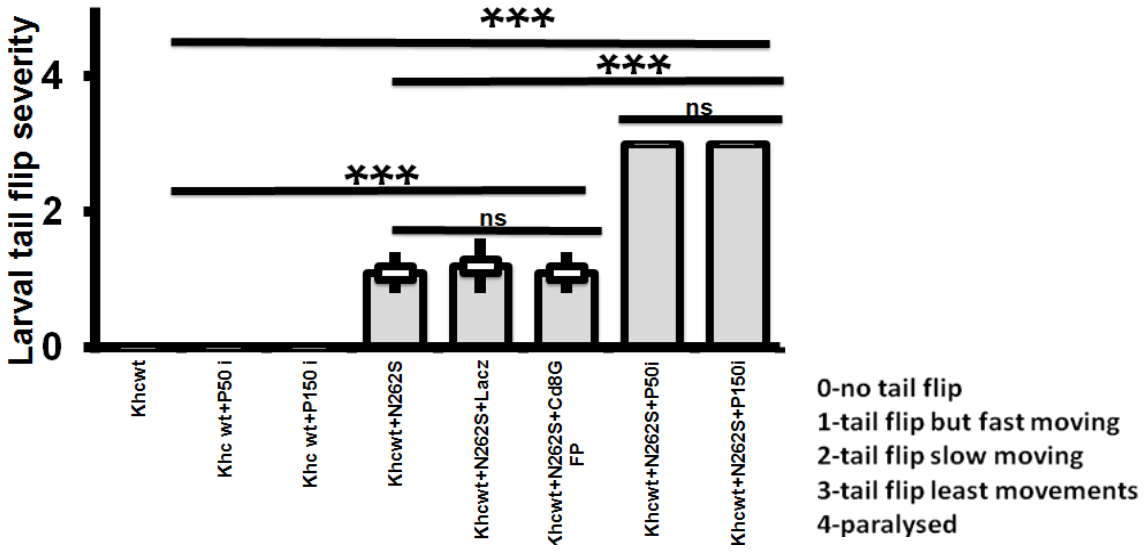

Figure 26 : Larval tail flip severity. D42<Khc^{wt}, D42<Khc$^{wt+RNAiP50}$, D42<Khc$^{wt+RNAiP150}$, D42< Khc$^{N262S+wt}$, D42<Khc$^{N262S+wt+LacZ}$, D42< Khc$^{N262S+wt+CD8-GFP}$, D42<Khc$^{N262S+wt+P50RNAi}$, D42<Khc$^{N262S+wt+P150\ RNAi}$ third instar larvae raised at 29°C were analysed for their severity of tail flip phenotype on apple juice agar plates.15 larvae per genotype were scored double blind (by Junyi Zhu). Healthy larvae without tail flip was scored 0, larvae displaying tail flip yet locomoting rapidly were scored 1, slow moving larvae displaying tail flip were scored 2, immobile larvae with tail flip was scored 3 and completely paralyzed larvae were scored 4. Statistical significance was determined using a Kruskal-Wallis H for comparisons between multiple groups. The standard error of the mean (s.e.m.) is shown as a box, the standard deviation (s.d.) as a black line. . * p<0.05; ** p<0.01, *** p<0.001.

The expression of both LacZ and CD8-GFP along with Khc^{wt} resulted in perfectly healthy larvae and its movement was no different from that of Khc^{wt} or w^{1118} larvae. But when expressed along with mutant kinesin (Khc$^{N262S+LacZ}$, Khc$^{N262S+CD8-GFP}$), the larvae exhibited phenotype similar to Khc$^{N262S+wt}$ larvae. Similarly, suppression of retrograde transporters dynein (P50) and dynactin (P150) and the expression of wild type kinesin (Khc^{wt+P50}, Khc$^{wt+P150}$) did not affect the locomotion. Nevertheless, when mutated kinesin was expressed additionally (Khc$^{N262S+wt+RNAiP50}$, Khc$^{N262S+wt+RNAiP150}$), the effect was dramatic (**Figure 26**). Larval movements were greatly reduced as these larvae were significantly weaker. This locomotive disability observed in larvae expressing mutated kinesin and blockers of retrograde motors was more pronounced than that observed in the kinesin mutants alone (Khc$^{N262S+wt}$), which was consistent with the GMR screen results.

4.8 BMP signaling is down regulated in Khc^{N262S} mutants

Our *Drosophila* model of SPG10 is characterized by axonal trafficking defects, synaptic defects, developmental defects, microtubular instability and behavioral impairments. The key features of BMP signaling defects and Khc^{N262S} mutants were similar. BMP signaling is the major retrograde signaling pathway that has crucial roles in developmental processes, axonal growth and synaptic function. Impairment of BMP signaling in *Drosophila* leads to axonal transport defects (Aberle, Haghighi et al. 2002; Ball, Warren-Paquin et al. 2010; Bayat, Jaiswal et al. 2011; Kang, Hansen et al. 2014). Kinesin mutation also affected retrograde transport (Fuger, Sreekumar et al. 2012) and since BMP is a retrograde signaling pathway, it was interesting to check if there existed a link between the two. The early evidence for the down regulation of BMP signaling in the Khc^{N262S} larvae comes from a previous study by Dr.Petra Füger in the lab. It was shown through her study that the pMad levels (the transcription factor in BMP signaling) were significantly down regulated in the brain of Khc^{N262S} mutant larvae. Nevertheless, the pMad levels were unaffected at the NMJs (Petra Füger, PhD thesis, 4.2.2.3).

Loss of BMP signaling affected synaptic structure and assembly (Ball, Warren-Paquin et al. 2010). Transgenic expression of Trio in Mad and Wit mutant larvae significantly restored NMJ structures in these mutants (Ball, Warren-Paquin et al. 2010). It was interesting to check if overexpressing either Trio or Tkv-CA (constitutively activate BMP receptor) in the kinesin mutant model could rescue the pathology induced by Khc^{N262S} mutation.

4.8.1 GMR screen - interaction between Khc^{N262S} mutants and BMP signaling genes revealed that Trio overxpression partially rescued the mutant rough eye phenotype

To further validate BMP signaling downregulation, interaction between Khc^{N262S} mutation and the positive and negative modifiers of BMP signaling were analysed through GMR screening. After expressing the desired proteins using the GMR-Gal4 driver at 29°C for 16 days post eclosion, the severity of depigmentation and necrosis in fly eyes were scored. No rough eye phenotype was observed in flies with wild type kinesin overexpression, but the expression of mutated kinesin (Khc^{N262S}) resulted in rough eye phenotype (**Figure 27A**). Both depigmentaion (**Figure 27**, **white arrowhead**) and necrosis-like black spots (**Figure 27, white arrow**) were observed in the Khc^{N262S} mutants. On the other hand, co-expression of wild type and mutated

kinesin ($Khc^{N262S+wt}$) rescued the rough eye phenotype which further confirmed the dominant negative nature of Khc^{N262S} mutation (**Table 8**).

Table 8: GMR eye phenotype score:

Genotype		GMR screen score
GMR	W^{1118}	-/-
GMR	$Khc^{N262S+wt}$	-/-
GMR	Khc^{N262S}	++
GMR	$khc^{N262S+LacZ}$	++
GMR+Khc^{N262S}	UAS Trio	-/+
GMR+Khc^{N262S}	UAS TKV- CA	++
GMR+Khc^{N262S}	UAS Wit-GFP	+
GMR+Khc^{N262S}	UAS Rac-V12	++
GMR+Khc^{N262S}	Tkv7	++
GMR+Khc^{N262S}	Trio6A	++
GMR+Khc^{N262S}	WitA12	++
GMR+Khc^{N262S}	WitB11	++
GMR+Khc^{N262S}	Gbb94	++

Table 8. GMR screening to validate BMP signalling in Khc^{N262S} mutants. Completely normal eye phenotype was scored -/-, mild phenotype accompanied by depigmentation alone was scored -/+, depigmentation along with fewer black spots was scored + and severely affected eye accompanied with depigmentation and black spots were scored ++. A total of 10 male fly raised at 29°C for 16 days were screened for each genotype and scored double blind by Junyi Zhu.

To compromise gene dilution issue, a control LacZ gene was co expressed with mutated kinesin which showed similar eye phenotype as observed in Khc^{N262S} mutant alone (**Figure 27 B**). Overexpression of BMP receptors like constitutively active thickveins (TKV-CA) or wishful thinking (Wit) along with Khc^{N262S} was not able to rescue the mutant eye phenotype (**Figure 27 B**). Similarly, as expected, the co-expression of receptor mutants like Tkv^{7}, Wit^{B11}, Wit^{A12} with Khc^{N262S} was unable to rescue the mutant eye phenotype (**Figure 27 C**). The eye phenotype observed in mutants was partially rescued by Trio (known target gene-BMP signaling) overexpression (**Figure 27 B**). In flies co-expressing Trio and Khc^{N262S} ($Khc^{N262S+Trio}$) the necrosis like black spots disappeared and the severity of depigmenation was also considerably

reduced. On the other hand, expression of mutant Trio ($Trio^{6A}$) along with Khc^{N262S} resulted in black spots and depigmentation as was observed in Khc^{N262S} mutants. The double blind scoring of the rough eye phenotype **(Table 8)** indicated that Trio overexpression with Khc^{N262S} showed reasonable rescue. The partial rescue in eye phenotype observed using the Trio overexpression led us to further investigate its effects on the behaviour of larvae.

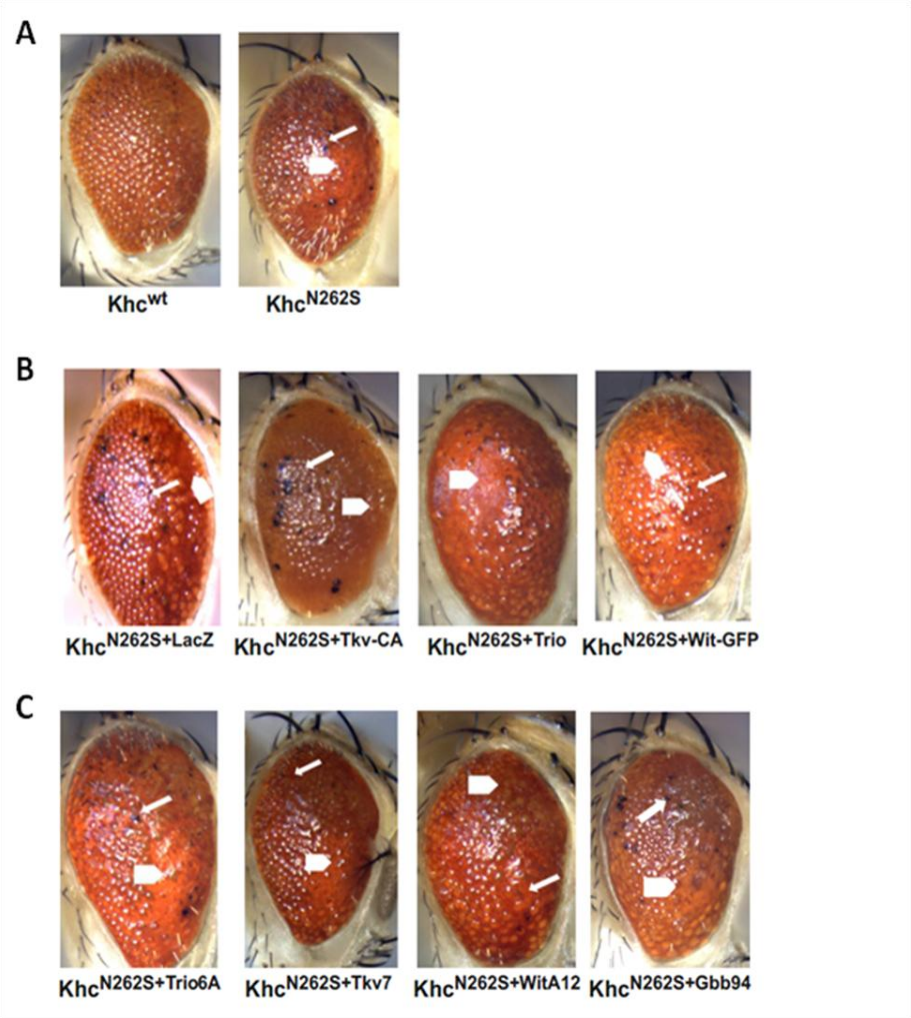

Figure 27: Rough eye phenotype: The figure shows the eye images for the genotypes depicted in **Table 8**. Depigmentation is shown using arrowheads and necrosis like black spots is shown by arrows.

4.9 Trio overexpression partially rescued trafficking of synaptic proteins

4.9.1 CSP and DV-Glut in the axonal swellings of Khc^{N262S} mutants

Impaired axonal transport of synaptic proteins has been one of the prominent cellular features of Khc^{N262S} model. Since ectopic expression of Trio and Khc^{N262S} partially rescued the rough eye phenotype, it was interesting to analyze if the upregulation of BMP signaling either at the receptor level (Tkv) or final target (Trio) could rescue the transport defects. To this aim, UAS-Tkv-CA and UAS-Trio was co-expressed with Khc^{N262S} in the motor neurons using the D42-Gal4 driver at 29°C. As observed before, the Khc^{N262S} mutants were marked with numerous immunoreactive clusters of HRP and synaptic proteins like CSP and DV-Glut. Likewise, co-expressing the control genes, UAS-LacZ or UAS-CD8-GFP in the Khc^{N262S} background resulted in axonal impairment as observed in Khc^{N262S} mutants alone. Overexpression of Tkv-CA in the mutant background ($Khc^{N262S+Tkv-CA}$) was not able to rescue the HRP or CSP accumulations (**Figure 28**). However, axonal trafficking was partially rescued by overexpression of UAS-Trio in the mutant background ($Khc^{N262S+UAS-Trio}$). The accumulation of CSP in the swellings in Trio overexpressing mutants were significantly reduced ($P<0.05$) when compared to Khc^{N262S} or the Lacz, CD8-GFP controls (**Figure 28B**). Nevertheless, there was no significant reduction observed in HRP accumulation or the distribution of swellings in the axonal segments (**Figure 28 C**).

Similarly, the accumulation of another synaptic protein DV-Glut was also significantly reduced in the nerve segments of $Khc^{N262S+Trio}$ ($P<0.05$) when compared to mutant groups (**Figure 29 B**). HRP accumulations in these larvae were not significantly reduced when compared to Khc^{N262S} or $Khc^{N262S+LacZ}$ and $Khc^{N262S+CD8-GFP}$ (**Figure 29 C**).

4.9.2 Trio overexpression partially rescued lysosomal marker (LAMP) accumulations in swellings of mutant nerve segments.

LAMP-GFP was used as a marker for late endosomes and lysosomal compartments in motor neurons. The GFP tagged LAMP was driven using D42-Gal4 driver in the motor neurons of Khc^{N262S},w^{1118}, $Khc^{N262S+Tkv-CA}$ and $Khc^{N262S+Trio}$ larvae. In the w^{1118} larvae with only the native kinesin expression no axonal swellings or LAMP-GFP accumulation was observed. Consistent

with our earlier results, Khc^{N262S} animals were characterised by swellings with trapped LAMP-GFP in axonal swellings (**Figure 21**). The accumulation of LAMP-GFP in the swellings were significantly reduced **($p<0.05$)** with Trio overexpression when compared to Khc^{N262S} or the controls ($Khc^{N262S+LacZ}$, $Khc^{N262S+CD8-GFP}$) **(Figure 30, B)**. Nevertheless, there was no significant reduction observed in HRP swellings in the axonal segments with Trio overexpression **(Figure 30, C)**. Overexpression of TKV-CA along with Khc^{N262S} ($Khc^{N262S+Tkv-CA}$) was not able to rescue LAMP-GFP in axonal swelling in the mutant background **(Figure 30, A, B)**.

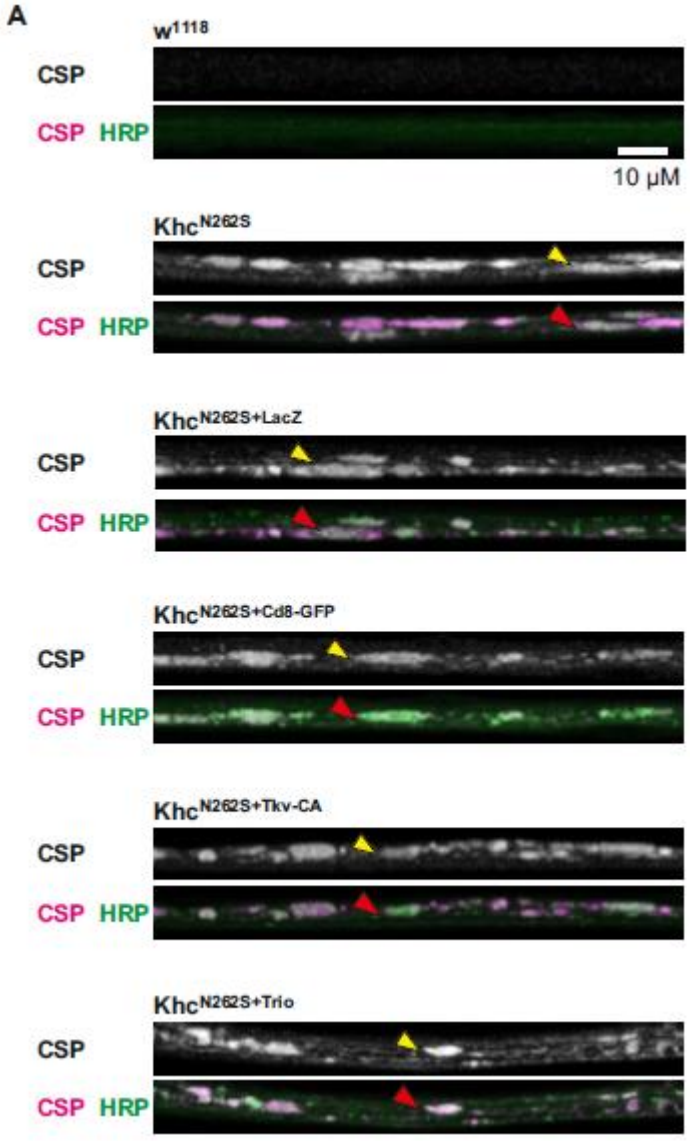

Figure 28: Axonal transport of CSP. Analysis of axonal cargo accumulation was performed by staining segmental nerves of third instar larva, (D42 <W^{1118}, D42 <Khc^{N262S}, D42 <$Khc^{N262S+LacZ}$, D42 <$Khc^{N262S+CD8-GFP}$, D42 <$Khc^{N262S+Tkv-CA}$, D42 <$Khc^{N262S+Trio}$ at 29°C) for the membrane marker anti-HRP and for Kinesin-1cargo CSP. **(A)** CSP accumulation in axonal segments shown by yellow arrowheads and HRP accumulation shown by red arrowheads. **(B)** Percentage of Area fraction CSP and **(C)** percentage of area fraction HRP is shown. Scale bar: 10 µm. For all quantifications, n = 45 axons per genotype were used. Statistical significance was determined by using a Kruskal-WallisH-test. The standard error of the mean (s.e.m.) is shown as a box, the standard deviation (s.d.) as a black line. * $p<0.05$; ** $p<0.01$, *** $p<0.001$.

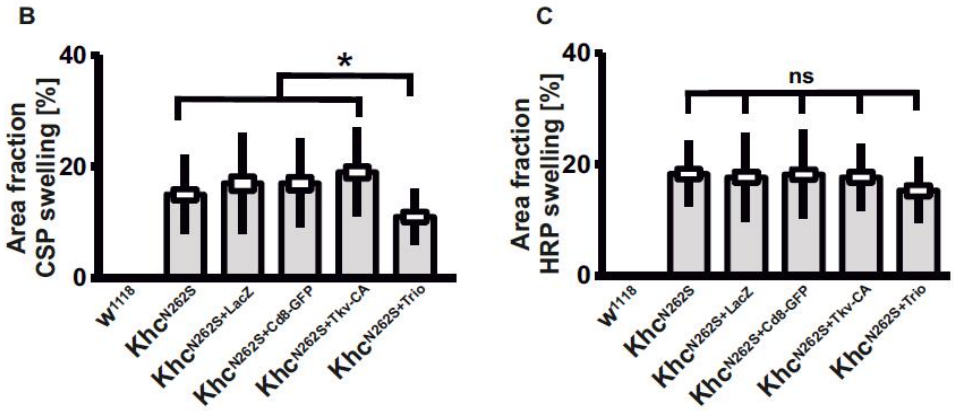

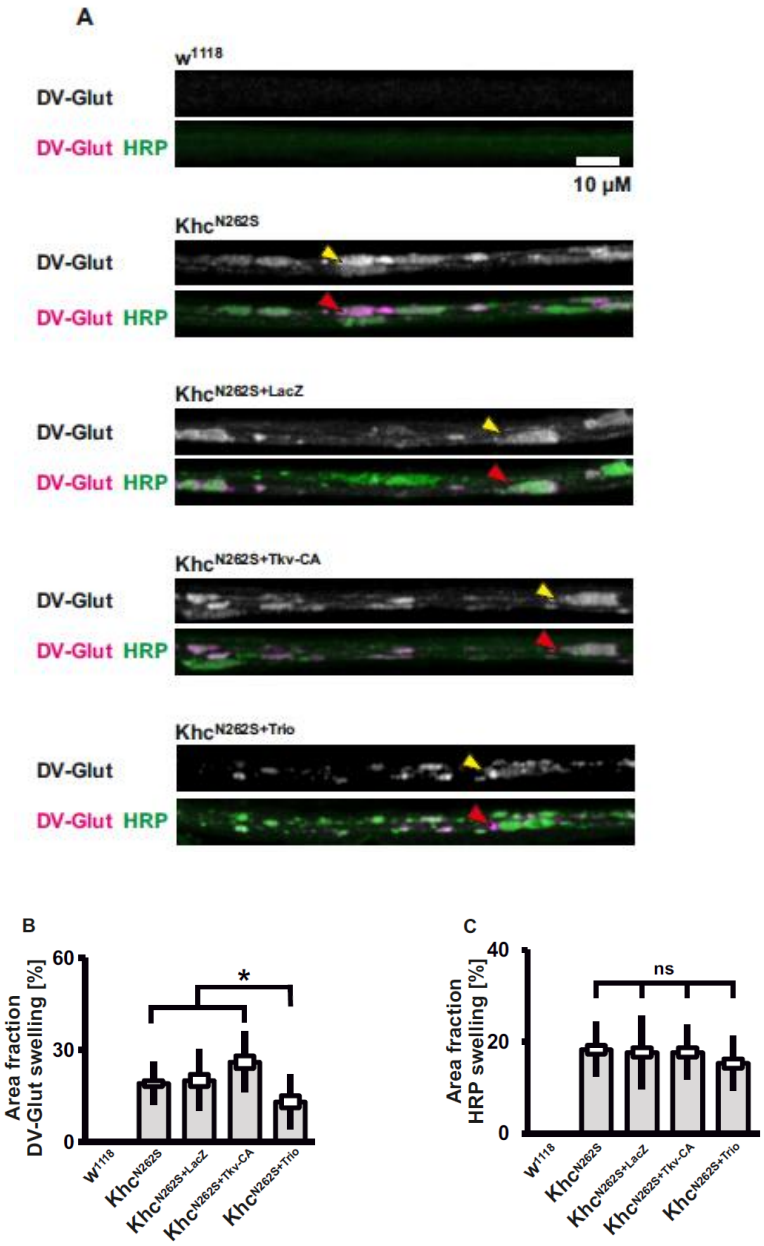

Figure 29: Trafficking of DV-Glut in axonal segments. Analysis of axonal cargo accumulation of third instar larva (D42<W^{1118},D42<Khc^{N262S},D42<$Khc^{N262S+LacZ}$,D42<$Khc^{N262S+CD8GFP}$,D42<$Khc^{N262S+Tkv-CA}$,D42<$Khc^{N262S+Trio}$) at 29°C for the membrane marker anti-HRP and DV-Glut. **(A)** DV-Glut accumulation in axonal segments shown by yellow arrowheads and HRP accumulation shown by red arrowheads. **(B)** Percentage of Area fraction DV-Glut **(C)** percentage of area fraction HRP Scale bar: 10 µm. For all quantification n = 45 axons per genotype was used. Statistical significance was determined by using a Kruskal-WallisH-test. The standard error of the mean (s.e.m.) is shown as a box, the standard deviation (s.d.) as a black line. * $p<0.05$; ** $p<0.01$, *** $p<0.001$.

4.9.3 Trio overexpression unable to rescue autophagosomal marker (ATG8-mRFP) accumulation in swellings of mutant nerve segments.

The autosomal and autolysosomal marker ATG8-mRFP were localized in axonal swellings in the nerve segments of Khc^{N262S} larvae. But upregulation of BMP signaling did not influence the trapping of AT8-mRFP in axonal swellings when driven with motor neuron specific D42-Gal4 driver at 29°C.Trio overexpression in the mutant background ($Khc^{N262S+Trio}$) did not rescue the accumulation of ATG8-mRFP in axonal segments (p=1) (**figure 31**).The percentage of area fraction swelling of both ATG8-mRFP and HRP were not significantly different in mutants overexpressing Trio or Tkv-CA ($Khc^{N262S+Tkv-CA}$, $Khc^{N262S+Trio}$) when compared with the Khc^{N262S} or $Khc^{N262S+LacZ}$ larvae (**figure 31 B,C**).No such accumulations were observed with the native kinesin expression (w^{1118}).

4.10 Up regulating BMP signaling unable to rescue behavioral tail flip phenotype:

One of the most prominent behavioural phenotypes observed in Khc^{N262S} was the tail flip phenotype. I was interested to verify if the up regulation of BMP signaling enabled to rectify the phenotypic and behavioural defects observed in Khc^{N262S} mutants. Expression of Tkv-CA and Trio along with KhcN262S did not rescue the tail flip phenotype.

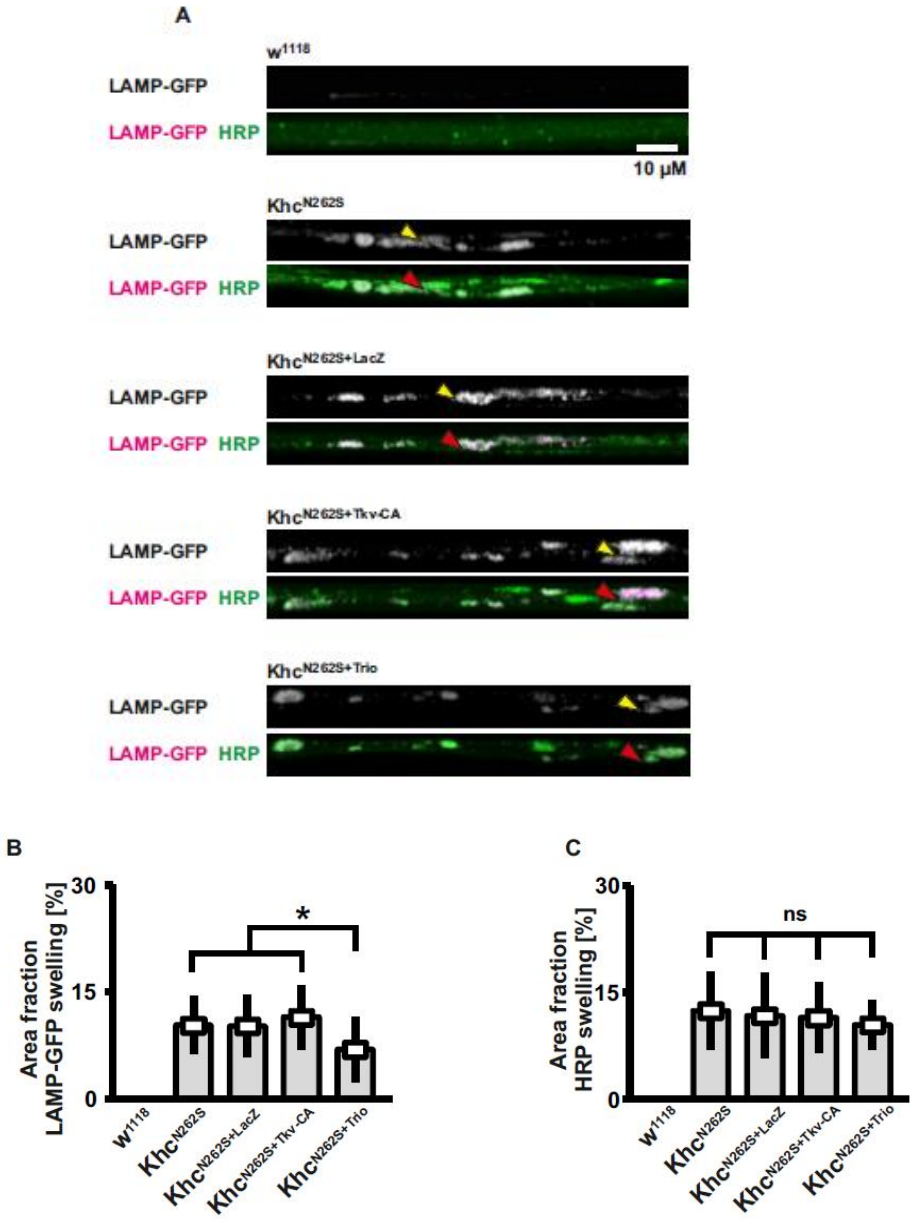

Figure 30: Trafficking of LAMP-GFP in axonal segments. Analysis of axonal cargo accumulation of third instarlarva,(D42<W^{1118},D42<Khc^{N262S},D42<$Khc^{N262S+LacZ}$,D42<$Khc^{N262S+Tkv-CA}$, D42<$Khc^{N262S+Trio}$ at 29°C) for the membrane marker anti-HRP and for lysosomal marker LAMP-GFP. **(A)** LAMP-GFP accumulation in axonal segments is shown by yellow arrowheads and HRP accumulation shown by red arrowhead. **(B)** Percentage of Area fraction LAMP-GFP and **(C)** percentage of area fraction HRP is shown. Scale bar: 10 µm. n = 45 axons per genotype. Statistical significance was determined by using a Kruskal-Wallis H-test for comparisons between multiple groups. The standard error of the mean (s.e.m.) is shown as a box, the standard deviation (s.d.) as a black line. * $p<0.05$; ** $p<0.01$, *** $p<0.001$.

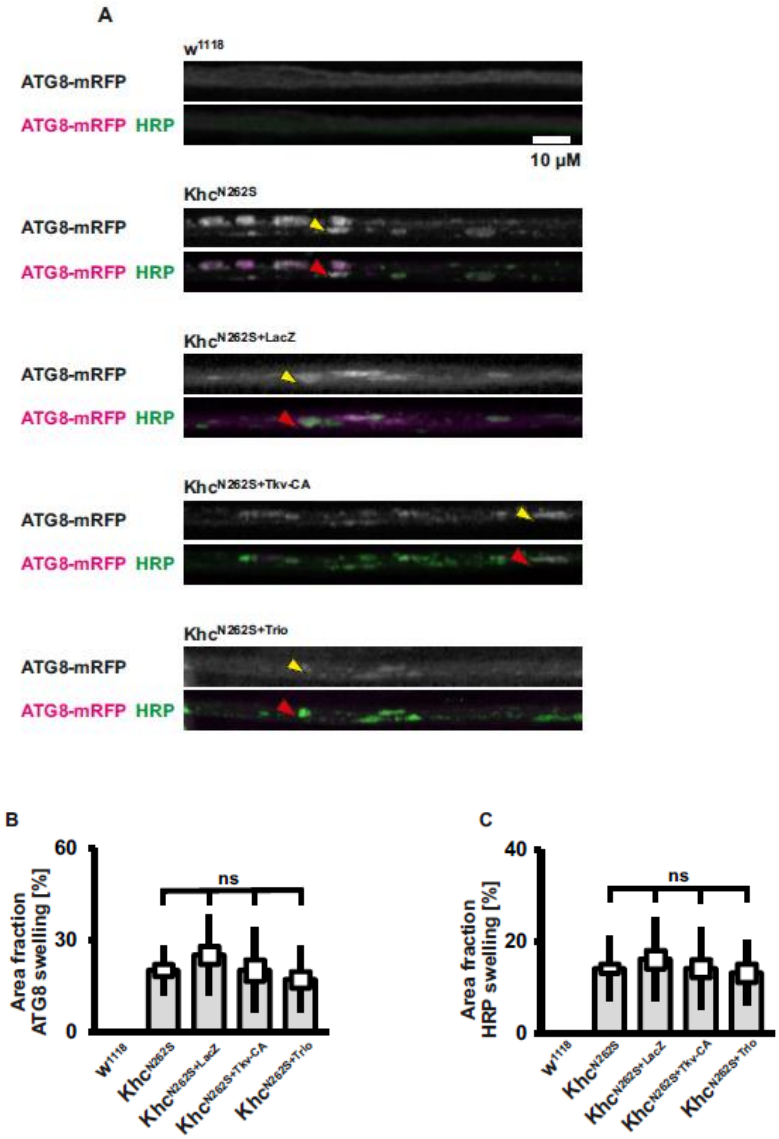

Figure 31: **ATG-mRFP trafficking in axonal segments**: Analysis of axonal cargo accumulation was performed by staining segmental nerves of third instar larva, (D42<W^{1118}, D42<Khc^{N262S},D42<$Khc^{N262S+LacZ}$,D42<$Khc^{N262S+CD8-GFP}$,D42<$Khc^{N262S+Tkv-CA}$, D42<$Khc^{N262S+Trio}$ at 29°C) for the membrane marker anti-HRP and for autophagosomal marker ATG8-mRFP. **(A)** ATG8-mRFP accumulation in axonal segments shown by yellow arrowheads and HRP accumulation shown by red arrowhead. **(B)** Percentage of Area fraction ATG8-mRFP and **(C)** percentage of area fraction HRP is shown. Scale bar: 10 µm. For all quantifications, n = 45 axons per genotype were used. Statistical significance was determined by using a Kruskal-Wallis H-test for comparisons between multiple groups. The standard error of the mean (s.e.m.) is shown as a box, the standard deviation (s.d.) as a black line. * $p<0.05$; ** $p<0.01$, *** $p<0.001$.

But surprisingly, UAS-Trio expression with Khc^{N262S} worsened the phenotype ($p<0.001$) (**figure 32**) as the larvae were paralyzed and death ensued in the L3 stage. On the other hand, mutant Khc^{N262S} larvae could survive to pupal stage. The partial rescue observed at axonal transport did not reflect on the behaviour of larvae. This could be due to the disruption of the tight regulation of Trio since it plays a very important role in development process. These larvae also showed signs of developmental issues as they transited from the second instar stage to the third instar stage.

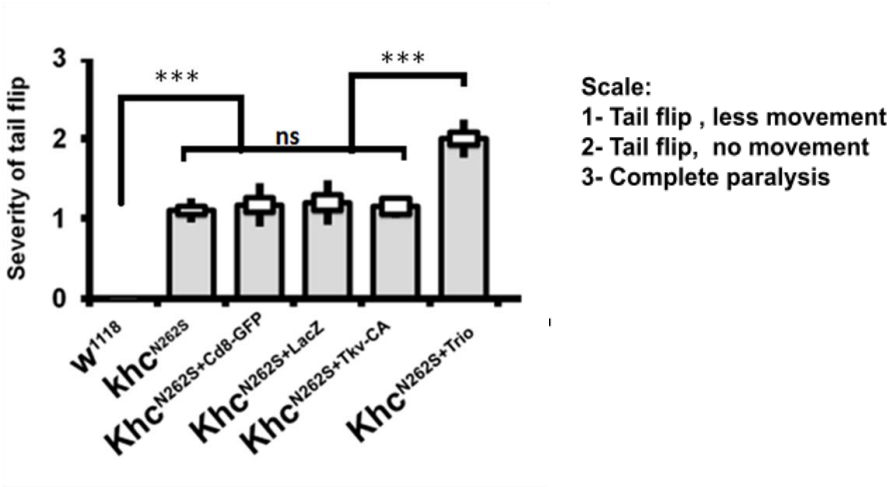

Figure 32: Tail flip behavior not rescued upon BMP signaling up regulation. The figure here depicts the severity of larval behavior observed in apple juice agar plates. Third instar larvae (w^{1118}, khc^{N262S}, $Khc^{N262S+CD8-GFP}$, $Khc^{N262S+LacZ}$, $Khc^{N262S+Tkv-CA}$, $Khc^{N262S+Trio}$) driven by D42-Gal4 at 25°C were used for analyzing the tail flip behavior. Larvae which locomoted slowly with tail flip were scored 1, larvae which were showed tail flip but scarcely moved were scored 2 and completely paralyzed larvae were scored 3. 15 larvae per genotype were used in the study. The scoring was done double blind by Junyi Zhu. Statistical significance was determined using a Kruskal-Wallis H for comparisons between multiple groups. The standard error of the mean (s.e.m.) is shown as a box, the standard deviation (s.d.) as a black line. .* $p<0.05$; ** $p<0.01$, *** $p<0.001$.

4.10.1 Khc^{N262S} induced fly behavior not rescued by Tkv or Trio overexpression:

Native kinesin expression (w^{1118}) as well as the expression of wild type kinesin (Khc^{wt}) using the motor neuron specific driver at 25°C or 29°C resulted in the emergence of healthy viable flies. As observed earlier no viable adult flies emerged when the mutated kinesin (Khc^{N262S}) was expressed using the D42 gal4 driver at either 25 or 29 °C (**Table 6**). But the addition of an extra

copy of wild type kinesin expressed ectopically along with mutated kinesin ($Khc^{N262S+wt}$) was able to rescue the dominant negative effect of the mutated protein and viable flies emerged at both temperatures.

Khc^{N262S} induced fly behavior				
Gal4-driver:	D42(25°C)	D42+khc^{wt}(25°C)	D42(29°C)	D42+khc^{wt} (29°C)
Expression:	motor neuron	motor neuron	motor neuron	motor neuron
w^{1118}	Healthy viable flies	Healthy viable flies	Healthy viable flies	Healthy viable flies
khc^{N262S}	Not viable	No tremoring flies; healthy	Not viable	No tremoring flies; healthy
$khc^{N262S+lacz}$	Not viable	No tremoring flies; healthy	Not viable	No tremoring flies; healthy
$khc^{N262s+Trio}$	Not viable	No tremoring flies; healthy	Not viable	Tremoring flies; unhealthy
$khc^{N262s+TKV-CA}$	Not viable	Not viable	Not viable	Not viable
UAS-Trio	Healthy viable flies	Healthy viable flies	Healthy viable flies	Healthy viable flies
UAS-TKV	Healthy viable flies	Healthy viable flies	Healthy viable flies	Healthy viable flies

Figure 33: Fly behaviour upon BMP signaling activation.

Similarly, viable flies emerged upon expression of LacZ together with wild type and mutated kinesin ($Khc^{N262S+wt+LacZ}$) at either temperatures but the expression of LacZ with Khc^{N262S} alone ($Khc^{N262S+LacZ}$) did not generate viable flies. The expression of neither Trio nor Tkv-CA along with Khc^{N262S} ($Khc^{N262S+Trio}$, $Khc^{N262S+Tkv-CA}$) at 25°C or 29°C could result in the eclosion of flies and the animals were lethal at pupal stage. On the other hand, when Khc^{wt} was additionally expressed in $Khc^{N262S+wt+Trio}$, though flies emerged, yet there were very weak, tremoring and short lived. The expression of Khc^{wt} and Tkv-CA along with mutant kinesin ($Khc^{N262S+wt+Tkv-CA}$) was lethal as no viable flies emerged. Expression of Trio or Tkv-CA in the absence of kinesin mutation (UAS-Trio,UAS-Tkv-CA) was not lethal with or without the co expression of wild type kinesin at either temperature **(Figure 33)**. Hence, it was clear from our behaviour studies that ectopic expression of either Trio or Tkv-CA with Khc^{N262S} was not able to rescue the mutant phenotype. Altering BMP signaling in an already diseased condition could be responsible for the enhanced severity. Likewise, Tkv and Trio could interfere with other signaling pathways which could have negatively affected the development of flies. This could explain the persistence of lethality of Trio and Tkv-CA overexpression even when the mutant kinesin was outnumbered by the wild type kinesin.

4.10.2 Mutants of BMP signaling make Khc^{N262S} phenotype worse:

Since the up regulation of the BMP signaling worsened the Khc^{N262S} phenotype as was observed with larvae and flies overexpressing either the BMP receptor (Tkv-CA) or the final target gene

(Trio), it was interesting to test the outcome of BMP signaling downregulation in the Khc^{N262S} mutants. Mutants of Tkv, Wit, Mad, Trio were characterized by severely affected synapses both structurally and functionally (Ball, Warren-Paquin et al. 2010). The mutants of BMP signaling receptors (Tkv) and (Wit) - Tkv^{7} and Wit^{A12}, mutant of BMP ligand Glass bottom boat (Gbb) - Gbb^{94} and the mutant for the target gene Trio –$Trio^{s}$ in the Khc^{N262S} background were analyzed for their characteristic tail flip behaviour. L3 larvae driven using D42-Gal4 driver at 29°C were scored double blind for their phenotypic severity on apple juice agar plates. Larvae overxpressing the wild type kinesin moved normally on the plates and displayed no tail flip. Similarly the BMP mutants Tkv^{7}, Wit^{A12}, Gbb^{94}, $Trio^{s}$ in the absence of the Khc^{N262S} moved not different from the wild type larvae and did not display tail flip. On the other hand, the locomotion was severely affected (mostly paralyzed) when expressed with Khc^{N262S} . Lethality was observed in these larvae by late L3 stage. The crawling ability of these BMP mutants in the Khc^{N262S} background was significantly worsened when compared to the $Khc^{N262S+Lacz}$, $Khc^{N262S+Cd8-GFP}$ as well as the Khc^{N262S} mutants (**Figure 34**). Hence, it was very evident that the down regulation of BMP signalling further worsened the Khc^{N262S} induced pathology.

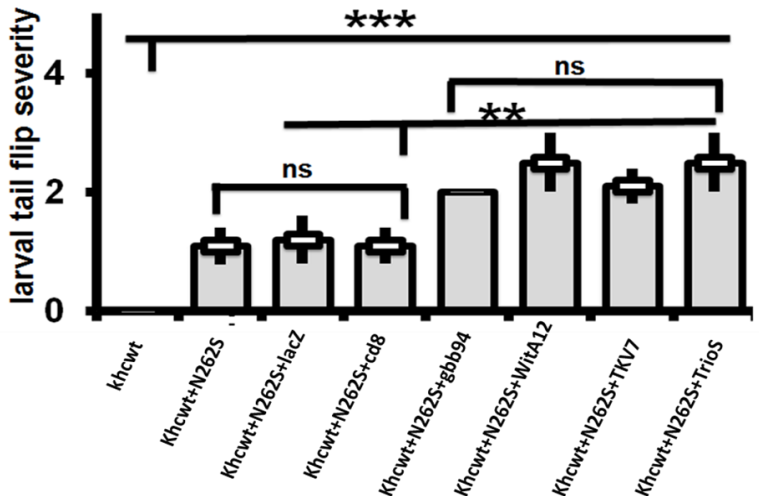

Figure 34: Tail flip behaviour not rescued upon BMP signaling down regulation. The graph depicts the severity of larval behaviour observed in apple juice agar plates. Third instar larvae (Khc^{wt}, $Khc^{N262S+wt}$, khc^{N262S}, $Khc^{N262S+wt+CD8-GFP}$, $Khc^{N262S+wt+LacZ}$, $Khc^{N262S+wt+Tkv-CA}$, $Khc^{N262S+wt+Trio}$) and BMP mutants driven by D42-Gal4 at 25°C were used for analyzing the tail flip behaviour. Larvae which locomoted slowly with tail flip were scored 1, larvae which were showed tail flip but scarcely moved were scored 2 and completely paralyzed larvae were scored 3. 15 larvae per genotype were used in the study. The scoring was done double blind by Junyi Zhu. Statistical significance was determined using a Kruskal-Wallis H for

comparisons between multiple groups. The standard error of the mean (s.e.m.) is shown as a box, the standard deviation (s.d.) as a black line. .* $p<0.05$; ** $p<0.01$, *** $p<0.001$.

4.11 Ectopic overexpression of Tkv-CA and Trio does not rescue the synaptic defects observed in Khc^{N262S} mutants.

Khc^{N262S} mutants were characterized by profound synaptic defects. Since axonal trafficking of synaptic proteins in Khc^{N262S} mutants was partially rescued by the overexpression of Trio, I wanted to assess if this partial rescue of axonal block would suffice for synaptic defect trounce.

4.11.1 Cytoskeletal disturbances persisted in Trio and Tkv-CA over expressing Khc^{N262S} mutants:

The regulation of microtubule dynamics depends of microtubule associated proteins. At the presynapse an atypical protein kinase C regulates the stability of microtubules by promoting the association of MAP1B related protein Futsch to microtubules. It has also been shown that mutations in Futsch disrupts synaptic microtubular organization and results in reduced synaptic bouton number (Roos, Hummel et al. 2000). The N- and C-terminal domains of Futsch are homologous to the vertebrate MAP1B microtubule-associated protein (Hummel, Krukkert et al. 2000). Expression of BMP target gene Trio can modulate cytoskeleton and is required in motor neurons for normal structural growth. Transgenic expression of Trio in motor neurons can partially restore NMJ defects in larvae mutant for BMP signalling (Ball, Warren-Paquin et al. 2010).

Khc^{N262S}, $Khc^{N262S+lacZ}$, $Khc^{N262S+Tkv\text{-}CA}$ and $Khc^{N262S+Trio}$ were expressed in motor neuron using D42-Gal4 driver at 29°C. The NMJ of muscle 6 and 7, segment A5 were analyzed for area fraction Futsch per NMJ. Ectopic overexpression of either Khc^{N262S} or LacZ in the mutant background resulted in the degeneration of NMJs in posterior segments (A5). These NMJs were much smaller and showed uneven HRP staining when compared to control ^{w1118}. NMJs of Khc^{N262S} mutants were characterized by very poor Futsch staining **(Figure 35, white arrowhead)** and intense HRP staining **(Figure 35, green arrowhead)** especially at the terminal boutons. This intense HRP staining at terminal boutons was consistent with our earlier experiments showing loss of synaptic proteins (**Section 4.3**) and hence might be an indication of dying synapses. This result was further supported by the poor acetylated tubulin staining observed in mutants as

described in **(Section 4.4).** Over expressing Trio or Tkv-CA in Khc^{N262S} mutants, both area fraction Futsch per NMJ as well as its intensity were significantly reduced ($P<0.05$) when compared to W^{1118} **(Figure 35)**. On the other hand, there was no significant difference observed in area fraction nor intensity of futsch in NMJs between the mutant groups (Khc^{N262S},$Khc^{N262S+lacZ}$, $Khc^{N262S+Tkv-CA}$ and $Khc^{N262S+Trio}$). These results indicate that upregulating BMP signaling in the mutants could not restore the cytoskeletal dynamics especially at the NMJs of posterior segments.

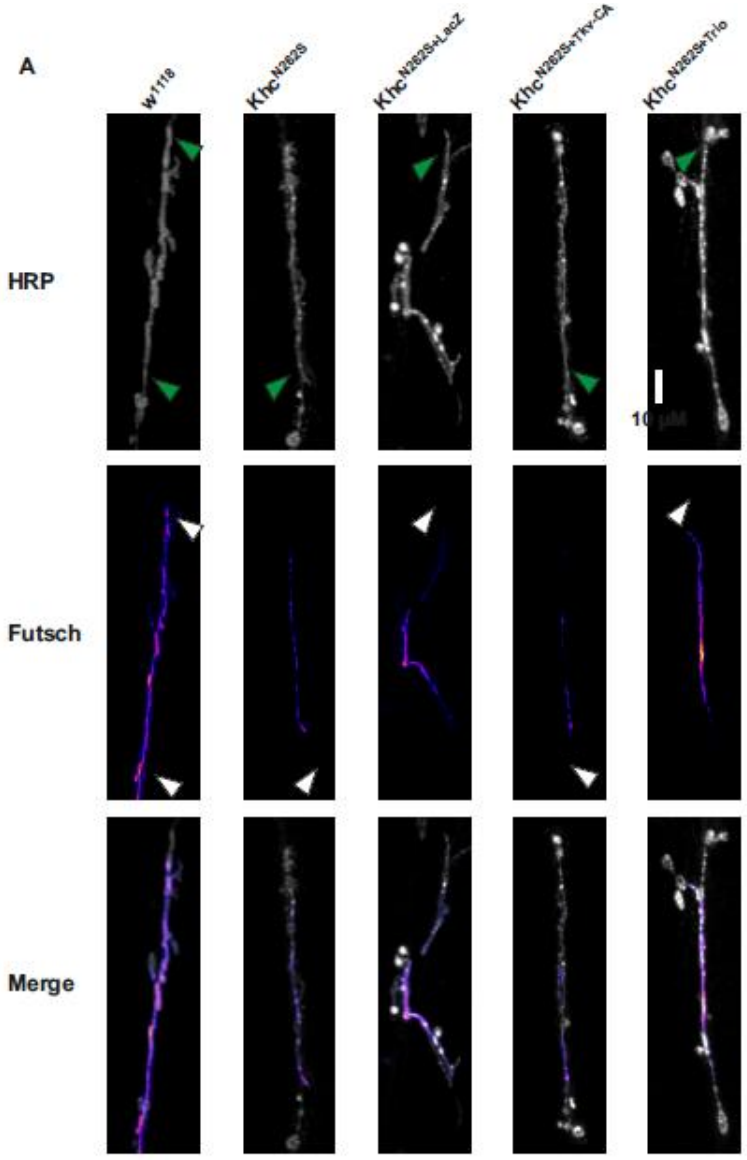

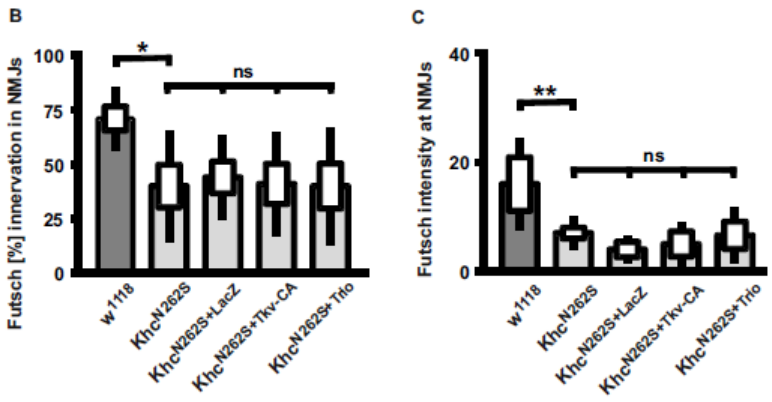

Figure 35: Persistence of cytoskeletal disturbances upon BMP activation in Khc^{N262S} mutants.

(A) Confocal images and quantification of immunofluorescent staining of Futsch and HRP in NMJs muscle 6/7, segment A5 of mid-third-instar *Drosophila* larva (D42<w^{1118}, D42<Khc^{N262S}, D42<Khc$^{N262S+LacZ}$, D42<Khc$^{N262S+TkvCA}$, D42<Khc$^{N262S+Trio}$).Terminal synapses of mutants show bright HRP staining (indicated by green arrowheads) and the loss of Futsch staining is shown by (white arrowheads). (B) Graph depicts the percentage of NMJ are innervated by Futsch. (C) Graph represents the intensity of Futsch staining in the NMJs.Scale bar: 10µm. For quantification, n = 8–10 NMJs were analyzed per genotype. Statistical significance was determined using a Kruskal-Wallis H for comparisons between multiple groups. The standard error of the mean (s.e.m.) is shown as a box, the standard deviation (s.d.) as a black line. * p<0.05; ** p<0.01, *** p<0.001.

4.11.2 Loss of synaptic proteins at the distal NMJ not rescued by Tkv-CA or Trio overexpression in the Khc^{N262S} mutants.

Next I tested if upregulating BMP signaling could rescue synaptic protein loss at distal NMJs. For this purpose Khc^{N262S}, Khc$^{N262S+LacZ}$, Khc$^{N262S+Cd8-GFP,}$Khc$^{N262S+Tkv-CA}$ and Khc$^{N262S+Trio}$ were expressed using D42-Gal4 driver at 29°C and the NMJs muscle 6/7 , distal segment A5 of third instar larve were immunostained with synaptic protein DV-GLUT and membrane marker HRP. W^{1118} NMJs showed homogenous staining of HRP and the synaptic proteins were distributed even to the most terminal ends of the NMJs. Consistent with earlier staining of Khc^{N262S} with DV-Glut (**Figure 22**), the NMJs were characterized by inhomogeneous HRP staining and reduced DV-Glut intensities when compared to the w^{1118} (p<0.001). Ectopic overexpression of Tkv-CA and Trio alongside Khc^{N262S} did not improve the abundance of synaptic proteins at NMJs (**Figure 36B**) as well as the intensity of DV-Glut which was significantly reduced (p<0.001) when compared to w^{1118}. Additionally, Khc$^{N262S+Tkv-CA}$ and Khc$^{N262S+Trio}$ NMJs were

characterised by regions (boutons) that were stained positive for HRP (green arrowhead) but either lacked or weakly stained for DV-Glut (white arrowhead)(**Figure 36A**),which was comparable to Khc^{N262S} mutants. Conversely, w^{1118} NMJs showed reasonable DV-Glut staining even at the terminal boutons.

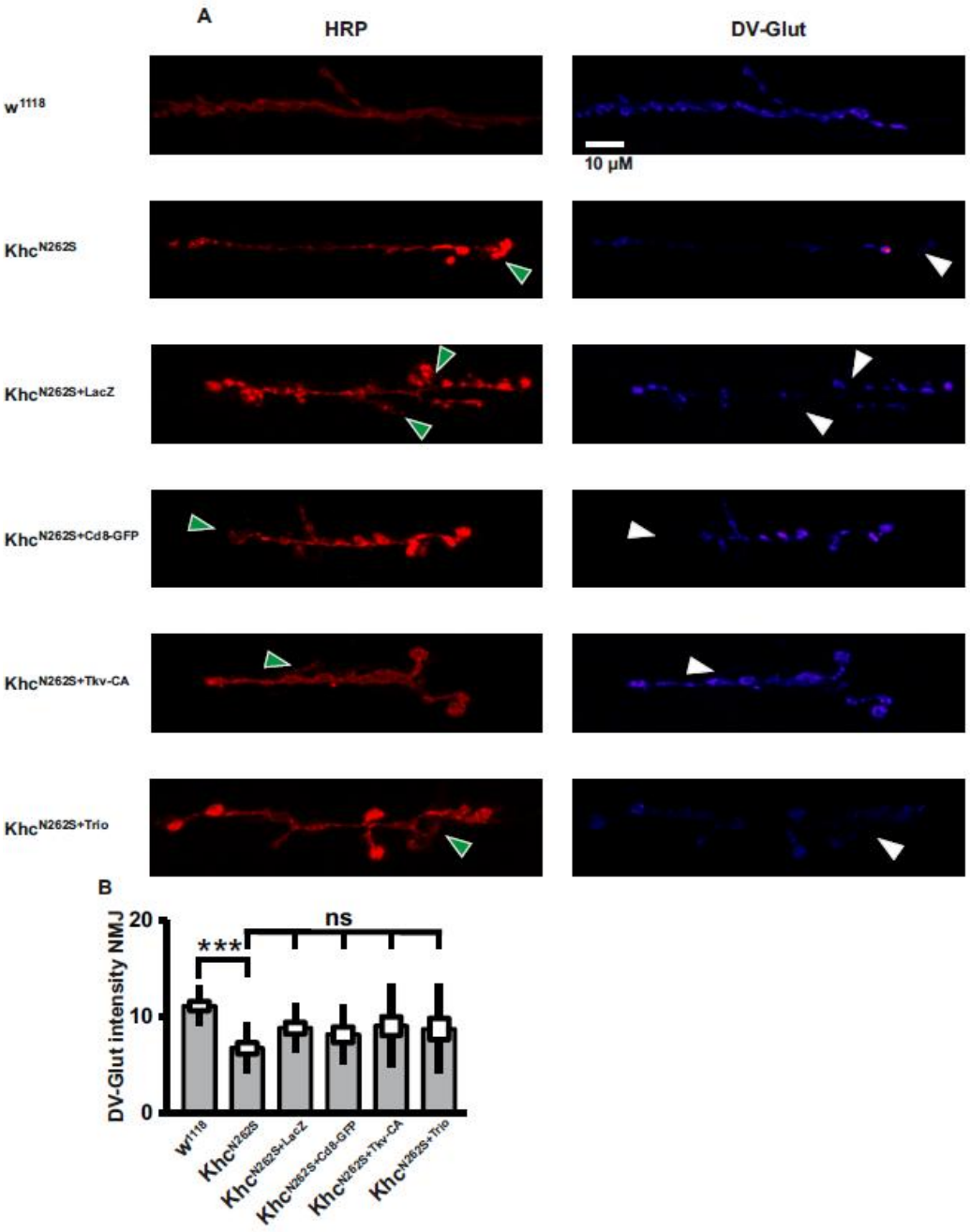

Figure 36 : Trio and Tkv-CA overexpression unable to rescue distal distribution of DV-Glut in mutant NMJs. (A) Confocal images and quantification of immunofluorescent staining of DV-Glut and HRP in NMJs of muscle 6/7, segment A5 of mid-third-instar *Drosophila* larva (D42<W^{1118},D42<Khc^{N262S},

D42<Khc$^{N262S+LacZ}$, D42<Khc$^{N262S+Cd8-GFP}$,D42<Khc$^{N262S+Tkv-CA}$ and D42<Khc$^{N262S+Trio}$). Terminal synapses of mutants show bright HRP staining (indicated by green arrowheads) and the loss of DV-Glut staining is shown by (white arrowheads). **(B)** Quantification of DV-Glut intensities in the NMJs**.** Scale bar: 10µm. For quantification, n = 10 NMJs were analyzed per genotype. Statistical significance was determined using a Kruskal-Wallis H for comparisons between multiple groups. The standard error of the mean (s.e.m.) is shown as a box, the standard deviation (s.d.) as a black line.. * $p<0.05$; ** $p<0.01$, *** $p<0.001$.

4.11.3 Lamp-GFP accumulation in Khc^{N262S} NMJs not rescued by Trio overexpression:

The axonal swellings of Khc^{N262S} larvae stained positive for LAMP-GFP which is a marker for PLVs (**Figure 21**). The accumulation of PLVs can be triggered by impairments in the retrograde transport of small prelysosomal organelles and moreover the retraction of synaptic terminals is associated with high lysosomal activity (Darabid, Perez-Gonzalez et al. 2014). A strong HRP staining at a subset of boutons at the NMJs of larvae expressing Khc^{N262S} suggested the local accumulation of membrane rich organelles. As lysosomal organelles were detected in axonal swellings, the strong HRP signal observed might be indicative of increased autophagy at the NMJ.

Motor neuron specific expression of LAMP-GFP in NMJ revealed that the Khc^{N262S} synapses were enriched with LAMP-GFP especially at the terminals (**Figure 37**). The bright HRP staining in boutons correlated with intense LAMP-GFP intensitiy (green arrowhead). Similar staining patterns were observed in NMJs of Khc$^{N262S+LacZ}$, Khc$^{N262S+Tkv-CA}$ and Khc$^{N262S+Trio}$ expressing larvae. An insignificant yet slight reduction in the intensities of LAMP-GFP was observed in Trio overexpressing Khc^{N262S} NMJs.

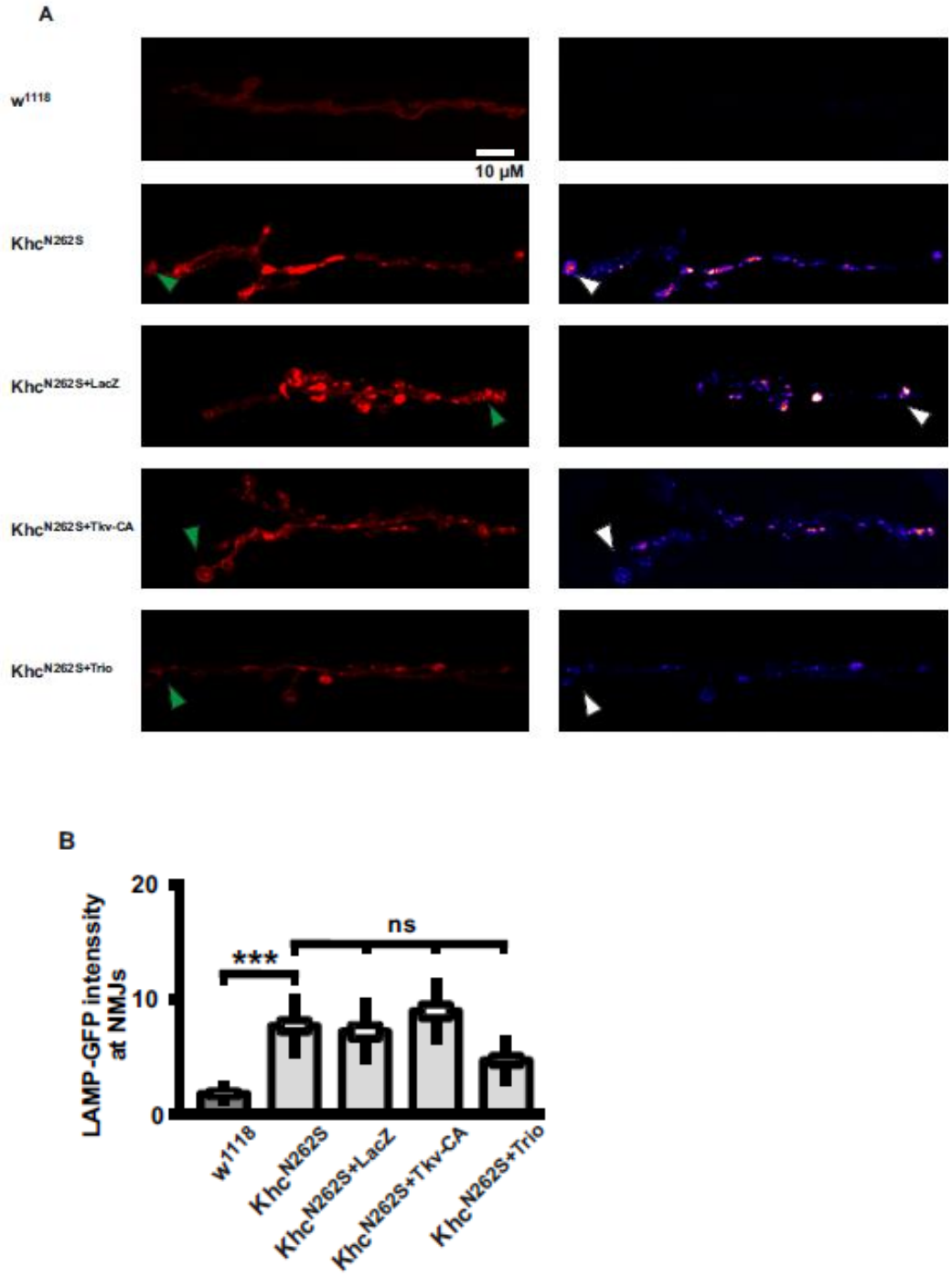

Figure 37: Trio and Tkv-CA overexpression unable to rescue distribution of LAMP-GFP in mutant NMJs. (A) Confocal images of immunofluorescent staining of LAMP-GFP and HRP in NMJs of muscle 6/7, segment A5 of mid-third-instar *Drosophila* larvae (D42<W^{1118}, D42<Khc^{N262S}, D42<$Khc^{N262S+LacZ}$,D 42<$Khc^{N262S+Cd8-GFP}$, D42<$Khc^{N262S+Tkv-CA}$and D42<$Khc^{N262S+Trio}$ at 29°C).Synapses with bright HRP staining and similar accumulation and bright staining of LAMP-GFP is indicated by green and white arrowheads respectively. **(B)** Quantification of LAMP-GFP intensities in the NMJs**.** Scale bar: 10µm. For

quantification, n = 20 NMJs were analyzed per genotype. Statistical significance was determined using a Kruskal-Wallis H for comparisons between multiple groups. The standard error of the mean (s.e.m.) is shown as a box, the standard deviation (s.d.) as a black line.. * $p<0.05$; ** $p<0.01$, *** $p<0.001$.

4.12 Overexpressing Tkv-CA in mutant background unable to rescue pMad levels in the Khc^{N262S} motor neuron cell bodies:

In the BMP signaling pathway, Tkv-CA causes the phosphorylation of Mad to pMad which further acts as a transcriptional factor for Trio in the cell bodies. The intensity of pMad levels in the cell bodies was analyzed upon overexpressing Tkv-CA in the Khc^{N262S} animals using the D42-Gal4 driver at 29°C. For quantification, a subset of motor-neuron cell bodies was stained for the transcription factor pMad and Even-skipped (Eve) (**Figure 38 A**). Even-skipped is expressed in the medially located aCC, RP2 motor neurons.$Khc^{N262S+Tkv-CA}$,$Khc^{N262S+LacZ}$, Khc^{N262S} and w^{1118} were driven using the motor neuron specific D42-Gal4 driver at 29°C and the motor neuron cell bodies were stained for Eve and pMad. The intensity of pMad in Khc^{N262S} mutants were significantly reduced when compared to w^{1118} control (**Figure 38B**). However, expression of Tkv-CA together with Khc^{N262S} did not rescue the pMad level. Failure to rescue pMad in the motor neuron cell bodies of Tkv-CA overexpressing Khc^{N262S} mutants could be due to hindrance in the retrograde transport of activated Tkv.

4.13 Khc^{N262S} mutation affects Retrograde transport TKV:

Since the overexpression of Tkv was unable to rescue the pMad levels in the motor neuron cell bodies, it was probable that the activated Tkv receptor was unable to reach the cell bodies to activate Mad to pMad. Therefore, the retrograde transport of Tkv in the axons of the mutant larvae were analyzed in-vivo. For this purpose, Tkv was tagged with yellow fluorescent protein and was expressed with the mutant ($Khc^{N262S+Tkv-YFP}$) and wild type kinesin ($Khc^{N262S+wt}$) using a D42-Gal4 driver at 25°C. The movement of the Tkv-YFP was then tracked in the axonal segments of anesthetised larvae. The relative speed of retrograde movement of Tkv in Khc^{N262S} axonal segments showed a 2.5 fold decrease when compared to wild type kinesin protein expression and similarly the relative retrograde flux (number of Tkv particles moving retrogradely in a given time) showed a 2.28 fold decrease which highly significant.

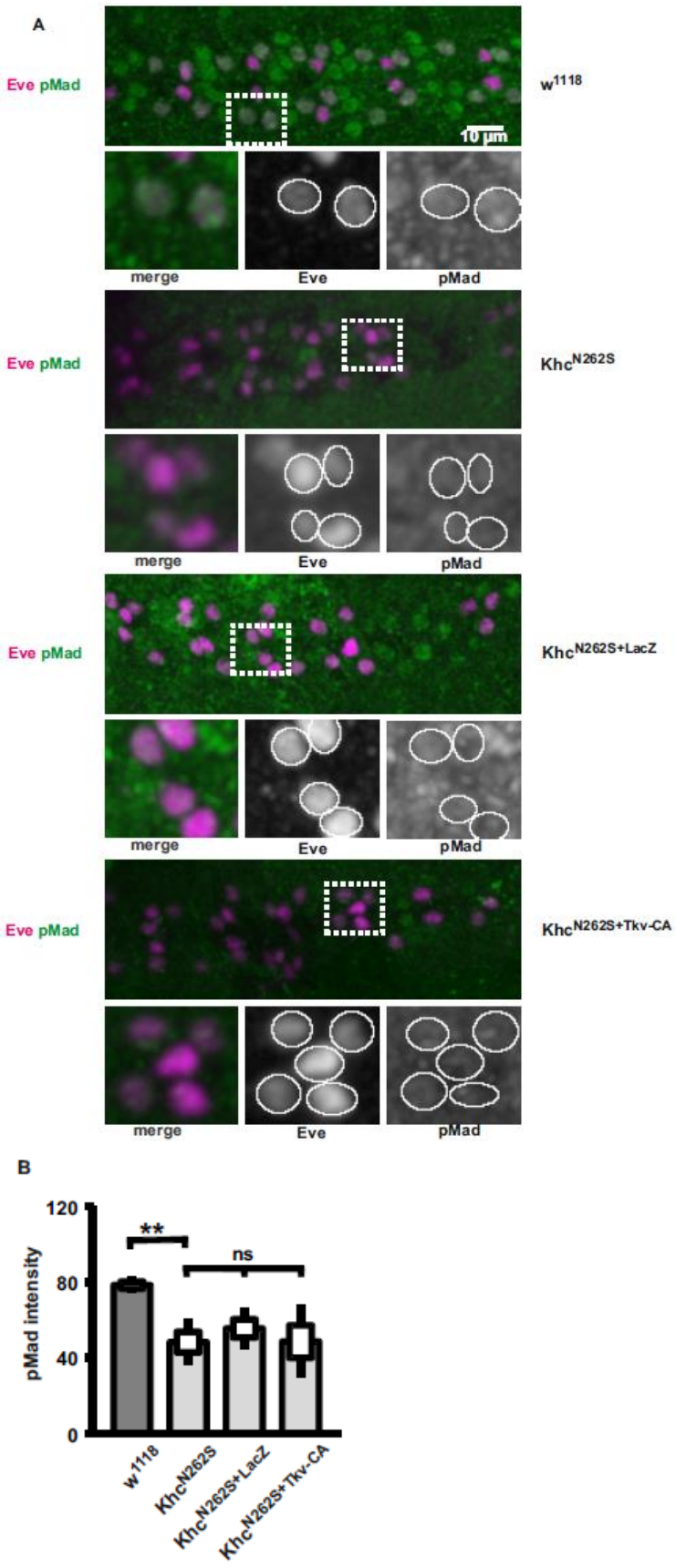

Figure 38: Tkv overexpression unable to rescue pMad levels in KhcN262S motor neuron cell bodies.

(A) Confocal images of immunofluorescent staining of Eve and pMad in motor neuron cell bodies of D42< W^{1118}, D42< Khc^{N262S}, D42< $Khc^{N262S+LacZ}$, D42< $Khc^{N262S+Cd8\text{-}GFP}$, D42< $Khc^{N262S+Tkv\text{-}CA}$. Motor neuron cell bodies show colocalised Eve (magenta) and pMad (green) staining. **(B)** Quantification of pMad intensities in the motor neuron cell bodies**.** Scale bar: 10µm. For quantification, n = 6-10 larval brain were analyzed per genotype. Statistical significance was determined using a Kruskal-Wallis H for comparisons between multiple groups. The standard error of the mean (s.e.m.) is shown as a box, the standard deviation (s.d.) as a black line.* $p<0.05$; ** $p<0.01$, *** $p<0.001$.

This significant reduction in relative retrograde flux and speed of Tkv could account for the reduced pMad levels observed in the motor neuron cell bodies of these mutants. Thus Khc^{N262S} mutants impaired the retrograde transport of activated receptors of the BMP signaling and leading to a possible downregulation.

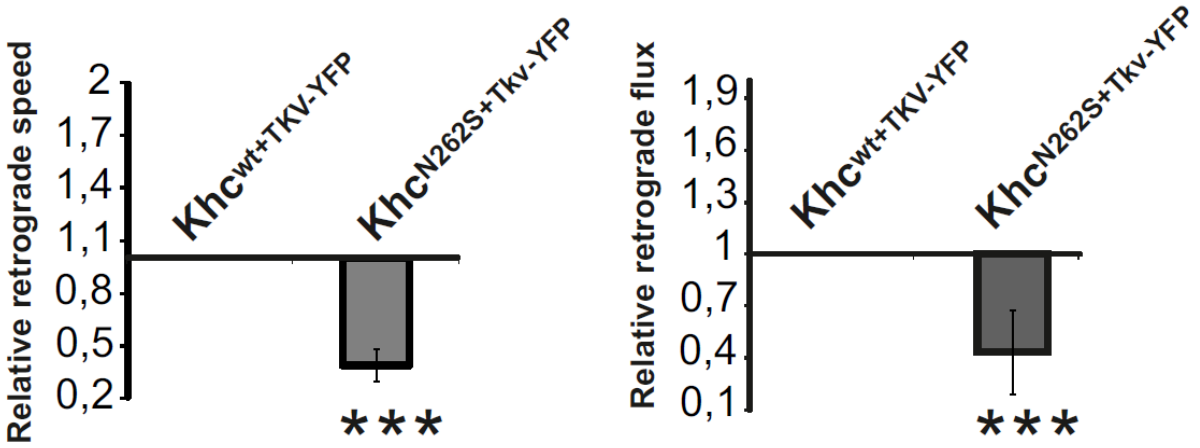

Figure 39: KhcN262S mutants display reduced relative retrograde speed and flux of Tkv-YFP in nerve segments. Graph depicts the relative retrograde speed and flux of Tkv-YFP in D42<Khc^{wt} and D42<Khc^{N262S} expressing L3 stage larvae at 25°C. KhcN262S larvae showed 2.5 fold decrease in retrograde speed and 2.28 fold decrease in the retrograde flux of BMP receptor Tkv. For quantification n = 3-5 animals per genotype were used in the study. Statistical significance was determined using a Kruskal-Wallis H for comparisons between multiple groups. The standard deviation is depicted (s.d.) as a black line.* $p<0.05$; ** $p<0.01$, *** $p<0.001$.

5 Discussion

5.1 Modeling human SPG10 in *Drosophila*: Khc^{N262S} mutation has a dominant negative nature

SPG10 is a subtype of HSP caused due to point mutations in KIF5A, a gene encoding neuronal kinesin heavy chain implicated in anterograde transport (Reid, Kloos et al. 2002). Our interest was in one particular point mutation N256S located on the loop connecting the microtubule binding site and the ATP binding site in the kinesin motor domain. Cargo bound kinesin dimers bind to microtubules at their microtubule binding site and glide to their destination by hydrolyzing ATP at each step. Previous studies confirmed that N256S kinesins exhibited significantly reduced gliding velocities along microtubules however its microtubule binding affinity was not affected when compared to wild type kinesin. The dominant nature of this mutation was evident from previous *in-vitro* studies by Ebbing et al (Ebbing, Mann et al. 2008). Attached to quantum dots as artificial cargo, mixtures involving N256S mutants produced slower cargo populations. N256S kinesins reduced the microtubule gliding velocity more than 2-fold at a 50:50 mixture of wild-type and mutant motor (Ebbing, Mann et al. 2008).This is because mutant kinesin could dimerise with wild type kinesin and render this heterodimer futile for transport.

To gain a better understanding of the pathophysiology and the dominant negative nature of SPG10, the *in- vivo drosophila* model was created with the human N256S mutation induced at the N262S position in *drosophila* kinesin heavy chain (Fuger, Sreekumar et al. 2012). Thus, Khc^{N262S} transgenic flies ectopically expressing mutated kinesin were created. These flies carried a copy of endogenous wild type kinesin and additionally an extra copy of mutated kinesin was expressed ectopically using tissue specific drivers. Our western blot analysis of flies developed at 29°C for 13days suggested nearly 3-4 fold excess expression of ectopic mutated kinesin (Khc^{N262S}) compared to endogenous wild type kinesin (Fuger, Sreekumar et al. 2012). However, human patients have a 1:2:1 ratio of (wild type kinesin homodimer, wild type mutant heterodimer and mutant homodimer) kinesin dimers. Consequently, to replicate the heterodimeric situation in HSP patients, both mutated and wild type kinesins were ectopically expressed ($Khc^{N262S+wt}$) so as to ensure the expression of approximately 1:1 ratio of wild type and mutated kinesin. It was clear

from my study that expression of wild type kinesin along with the mutated kinesin ($Khc^{N262S+wt}$) partially rescued the mutant kinesin (Khc^{N262S}) phenotype at both behavioral and cellular levels.

Upon expression of mutated kinesin in motor neurons (D42<Khc^{N262S}), extremely weak and short lived flies emerged. These flies held their wings at an abnormal upright position with respect to their body axis (**Section 4.1.2**). However, co expression of wild type and mutated kinesin D42<$Khc^{N262S+wt}$ significantly increased the median life expectancy of mutant flies from 5 days to 100 days, nevertheless the median life span was still significantly lower than control flies expressing wild type or endogenous kinesin (**Section 4.1.3**). These heterozygous flies did not exhibit abnormal wing posture and were capable of normal flight.

Upon motor neuron specific expression, Khc^{N262S} larvae suffered distal paralysis, characteristic of human HSP patients (**Section 4.1.1**). In humans, the distal paralysis is caused as a consequence of axonal degeneration of the longest cortico spinal track (Deluca, Ebers et al. 2004). Likewise, in *drosophila* larvae, the axons innervating the distal muscles, which are typically longer than the axons running to the anterior ends, are primarily affected. The expression of Khc^{N262S} in motor neurons resulted in the progression of the paralysis from the posterior ends to anterior segments since the pathology ranged from mere tail flip (mild) to overall paralysis (severe) as the larvae developed. But the addition of Khc^{wt} in the mutant background partially yet significantly limited the paralysis to distal ends and even restored the mobility of larvae though the tail flip persisted. At the stage where the Khc^{N262S} larvae were either paralyzed or dead, the $Khc^{N262S+wt}$ larvae were alive and mobile. The impaired motor function (climbing defect), observed in Khc^{N262S} mutants was significantly restored by the low expression of mutant kinesin (**Section 4.1.4**).

This partial rescue was not restricted to the phenotypic or behavioral aspects of the mutation but also had an influence at the cellular and molecular level. Axonal traffic jams were one of the characteristic cellular features of Khc^{N262S}larvae. These mutant larvae were marked by large clusters of axonal swellings which were significantly if not completely eliminated upon additional expression of wild type kinesin (**Section 4.2.2**). Similarly, the synaptic protein loss at distal synapses was also restored in heterozygous animals (**Section 4.6**). Another typical feature of Khc^{N262S} mutants was loss of microtubular stability (less acetylated microtubules) especially at the distal NMJs which were restored by additional expression of wild type kinesin (**Section 4.4**).

This partial, yet significant, rescue ofKhc^{N262S} induced phenotype by the overexpression of Khc wild type protein points towards several things. Firstly, if Khc^{N262S}protein was inherently toxic, then both Khc^{N262S}as well as $Khc^{N262S+wt}$ flies (having the same amount of the putative toxic Khc^{N262S}) should have displayed the phenotype with similar severity. Secondly, if Khc^{N262S} selectively disturbs kinesin function, the amount of wild type kinesin present would determine the severity of phenotype. $Khc^{N262S+wt}$as well as Khc^{N262S} animals have the same amount of mutant kineisn and the expression of additional Khc^{wt} could have increased the abundance of Khc^{wt} dimers which could then compensate for the axonal transport defect to a greater extent and thus must have partially rescued the mutant Khc^{N262S} phenotype.

5.2 Khc^{N262S} mutation resulted in non selective disturbance of axonal transport

Kinesins glide along the microtubule network and mediate the axonal transport of a multitude of cargo anterogradely and retrogradely, towards and away from the synapse, respectively (Dresbach, Torres et al. 2006; Fejtova and Gundelfinger 2006; Collins and DiAntonio 2007; Darabid, Perez-Gonzalez et al. 2014) and (Hirokawa 1998; Deacon, Serpinskaya et al. 2003; Chevalier-Larsen and Holzbaur 2006; Hirokawa, Niwa et al. 2010; Kang, Hansen et al. 2014). Proteins whose trafficking is negatively affected by impaired retrograde transport include those that are required for the maintenance of cytoskeletal integrity (e.g BMP receptors, Tkv, Wit, Sax, etc). Impairment of axonal transport is one of the key cellular features of HSP. *In- vitro* studies have shown that Khc^{N262S} mutation caused a reduction in the velocity of kinesins along the microtubules (Ebbing, Mann et al. 2008). Hence these slow moving Khc^{N262S} could create road blocks disrupting axonal trafficking. An autopsy of human SPG4 patients revealed the presence of axonal swellings (Kasher, De Vos et al. 2009). However, axonal swellings were also described in *Drosophila* larvae lacking Khc (Hurd and Saxton 1996). Likewise, considerable axonal swellings were also found in cultured motor neurons lacking KIF5A (Ferreirinha, Quattrini et al. 2004; Kasher, De Vos et al. 2009).These reports suggest that axonal swellings are established secondary to disrupted axonal transport, probably due to a depletion of a specific cargo or cargos at the synapse or due to the loss of cytoskeletal integrity. In order to clarify this point, axonal trafficking at an earlier larval developmental stage (L2) was analyzed. Here, axonal segments of Khc^{N262S} larvae were marked by relatively more cargo accumulations (indicated by Brp stainings)

(**Figure 24**) and comparatively less axonal swellings (indicated by HRP stainings). However, analysis of L3 stage larvae showed more pronounced axonal swellings which co-localized with cargo accumulations **(Figure 20).** Hence it could be concluded that the inability of mutant kinesins to carry cargos to the synapses could have triggered the axonal swellings by depleting the synapses of proteins. This could disrupt anterograde and retrograde signaling pathways, resulting in microtubular instability which further worsened transport.

When the proteins trapped in these swellings were probed it was found quite surprisingly that Khc^{N262S} mutation not only affected the trafficking of Kinesin-1 cargo, but on the other hand also affected the transport of Kinesin-3 cargo (**Section 4.2.3**). Additionally, markers of autolysosomal and PLVs were also trapped in these swellings (**Section 4.2.4**). The axonal segments of Khc^{N262S} mutants were characterized by regions with very strong HRP accumulations, which also co stained for kinesin -1 cargos like CSP and DV-Glut. On the contrary, axonal segments of w^{1118} and Khc^{wt} larvae showed uniform membrane staining (HRP) and were devoid of any cargo accumulations (**Figure 19**). Similarly, Kinesin-3 cargos like ANF-GFP and Brp were also found to be trapped in these swellings **(Figure 20).** LAMP-GFP, ATG8-mRFP the markers for PLVs and autophagosomes were also trapped in these swellings (**Figure 21**). Thus, Khc^{N262S} mutation causes non selective disturbance of axonal transport.

5.3 Disruption of axonal transport by Khc^{N262S} mutation impaired distal synaptic function:

Khc^{N262S} mutation affected both the structure and function of distal synapses. Abundance of synaptic proteins like Brp , DV-Glut, CSP was significantly reduced in the distal NMJs of Khc^{N262S} mutants (**Section 4.3**). These proteins are required at the presynapse for active zone formation and neurotransmission. Reduced synaptic proteins observed at the Khc^{N262S} distal NMJs correlated with the reduced synaptic activity as the number of vesicles released per action potential (quantal content) in these NMJs were significantly reduced(Fuger, Sreekumar et al. 2012).These distal NMJs in Khc^{N262S} were also characterized by significantly reduced NMJ area as well as post synaptic density(Fuger, Sreekumar et al. 2012) . At L3 stage, the mutant larvae were marked by strong paralysis and the distal synapses were already showing the signs of degeneration as there were significant amounts of destabilized microtubules (**Section 4.4**). The distal synapses in the segment A5 of Khc^{N262S} larvae were characterized by significantly less

acetylated tubulin (marker for long lived and stabilized microtubules) when compared to control animals expressing native kinesin (**Figure 23**). These synapses were also marked by thin microtubule network, a typical phenotype that has previously been reported in *spastin* mutants characterized by severe microtubular destabilization (Sherwood, Sun et al. 2004). Similarly, the distortion of MTs was further confirmed by poor Futsch staining observed in the distal synapses of Khc^{N262S} mutants (**Figure 35**). Synapse and axon loss may therefore be a primary step in the pathogenesis of the disease.

5.4 BMP signaling in the manifestation of HSP- Impaired BMP signaling in Khc^{N262S} mutants

BMP signaling is a highly conserved pathway that is essential for organized assembly of synapses during larval development of the *Drosophila* NMJs (Bayat, Jaiswal et al. 2011). BMP retrograde signaling is required for synaptic terminal growth and electrophysiological refinement. (Bayat, Jaiswal et al. 2011; Kang, Hansen et al. 2014). SPG3A (Atlastin), SPG4 (Spastin), SPG6 (NIPA1), and SPG20 (Spartin) have all been associated with impaired BMP signaling (Wang, Shaw et al. 2007).In the signaling pathway, BMP receptors (Wit, Sax, Tkv) at the NMJ are activated by postsynaptically released Glass-bottom boat resulting in the phosphorylation of Mad (pMad). This pMad in turn acts as a transcription factor for Trio in the nucleus. Trio is required in motor neurons for normal structural growth and is involved in the maintenance of proper cytoskeleton (Ball, Warren-Paquin et al. 2010). It was interesting to check if BMP signaling was altered in *Drosophila* model of SPG10. This would be an additional factor in establishing altered BMP signaling as a unifying mechanism in development of HSP.

The regulation of BMP signaling in the Khc^{N262S} mutants was investigated primarily due to 4 reasons. Firstly, the key pathological features of Khc^{N262S} *Drosophila* model were similar to the pathology observed in larvae where BMP signaling was down regulated (Ball, Warren-Paquin et al. 2010). One of the characteristic features of SPG10 is axonal transport block. Interestingly, impairment of BMP signaling in *Drosophila* leads to axon transport defects(Blackstone, O'Kane et al. 2011). Likewise, BMP signaling plays an important role in development, maintaining cytoskeletal dynamics, axon guidance and structural growth of synapses (Keshishian and Kim 2004; Blackstone, O'Kane et al. 2011). All these functions are negatively affected in the Khc^{N262S} larvae.

SecondlyKhc^{N262S} mutation also impaired retrograde transport in addition to anterograde transport (Fuger, Sreekumar et al. 2012). And since, BMP signaling is the major retrograde signaling pathway, is also primarily affected. Kinesins are involved in the transport retrograde motors to the synaptic ends and hence impairment in anterograde transport would affect the retrograde transport indirectly (Yamada, Toba et al. 2010).

Thirdly, BMP signaling transcription factor pMad levels in the motor neuron cell bodies of Khc^{N262S} larvae were significantly reduced compared to w^{1118} (PertaFüger, PhD thesis**, Section 4.2.2.3**).

Finally, GMR eye screen for the activators and negative regulators of BMP signaling in the mutant background showed that Trio overexpression was able to partially rescue the rough eye phenotype observed in Khc^{N262S} mutants (**Section 4.8.1**).

Since these early evidences linked to a probable negative regulation of BMP signaling in Khc^{N262S} mutants, it prompted us to check if an upregulation of BMP signaling at either the receptor level using a constitutively active Tkv or at gene level by overexpressing Trio is able to rescue the pathological phenotype observed in Khc^{N262S} mutants. For this purpose transgenic Khc^{N262S} flies co-expressing Tkv-CA, Trio, Rac^{V12}, Mad-GFP as activators of BMP signaling and flies co-expressing mutants of BMP signaling mediators Tkv^{7}, Gbb^{94}, Trio^{S}, Wit^{A12} and Wit^{B11} as negative regulators of BMP signaling were analyzed for axonal trafficking, cytoskeletal dynamics, synaptic and behavioral rescue.

5.5 Overexpression of Tkv-CA and Trio in Khc^{N262S} mutants unable to rescue the pathological phenotype:

BMP signaling mediators like the receptor Tkv-CA and the target gene Trio were upregulated in the KhcN262S mutants to check if this overexpression could ameliorate the mutant phenotype. Ectopic expression of Tkv-CA in the mutant background did not rescue the axonal traffic jams (**Section 4.9.1,2,3**), loss of synaptic proteins in distal synapses (**Section 4.11.2**) or cytoskeletal integrity (**Section 4.11.1**). Tkv is responsible for the activation of Mad to pMad that acts as transcriptional activator of Trio. When pMad levels in the motor cell bodies in *Drosophila* mutant brain were analysed, Tkv-CA overexpression was unable to restore the levels when compared to controls (**Figure 38**). This could be due to the disruption of retrograde transport of Tkv to the cell bodies to activate Trio. Activated receptors of BMP signaling are carried via

endosomes and retrogradely transported to the cell bodies where it phosphorylates Mad (Smith, Machamer et al. 2012). It has also been shown that the activated receptors Tkv and Wit often co-localized in these endosomes. It has been suggested that both receptors might be acting together in Mad phosphorylation (Smith, Machamer et al. 2012). *In- vivo* studies using YFP tagged Tkv in the nerve segments of Khc^{N262S} larvae enabled to understand the affliction of retrograde transport as fewer Tkv moved retrogradely and when they did, the speed was severely reduced (**Section 4.13**). The negative effect of Khc^{N262S} mutation on retrograde transport must have affected the transport of activated Tkv (**Figure 39**) and this is further supported by significantly decreased amounts of pMad observed in the motor neuron cell bodies of $Khc^{N262S\ +Tkv\text{-}CA}$ animals (**Figure 38**).

Trio acts as the molecular link between retrograde signaling and cytoskeletal arrangement. Trio modulates actin cytoskeleton by activating members of the Rho family of small GTPases like Rho, Rac, and Cdc42 (Ball, Warren-Paquin et al. 2010).Trio interacts with several members of a subfamily of MT-associated proteins called "MT plus-end tracking proteins" (+TIPs) like NAV1 (Navigator 1) and EB1 (End-Binding protein 1) (van Haren, Boudeau et al. 2014). Dynamic behavior of MTs is controlled by the binding of +TIPs to the plus end of MTs and Trio interacts with +TIPs. Overexpression of Trio in the mutant background ($Khc^{N262S+Trio}$) showed a partial rescue in axonal impairment of cargo transport (**Section 4.9, 4.9.1, 4.9.2, 4.9.3, 4.9.4**). Motor neuron specific expression of Trio in Khc^{N262S} mutants significantly reduced the DV-Glut and CSP accumulations in the swellings however the HRP accumulations and swelling densities remained unaffected (**Figure 28 - Figure 31**). It is possible that Trio overexpression has modulated the cytoskeleton slightly which enabled a significant movement of cargo but was not sufficient to eliminate the swellings. However, the synaptic protein depletion observed in the mutant distal NMJs were not rescued upon Trio overexpression (**Figure 36**). Similarly, when the microtubular integrity at the distal synapses were analyzed, $Khc^{N262S+Trio}$ mutant NMJs were marked with poor Futsch staining and loss of Futsch at the terminal boutons (**Figure 35**). There was an also considerable amount of LAMP observed in Trio overexpressing Khc^{N262S} mutants (**Figure 37**) which was indicative of stress related to synapse retraction.

Upregulation of BMP signaling mediators did not rescue the Khc^{N262S} induced behavioral defects (**Section 4.10, Figure 32**). But all these does not exclude the downregulation of BMP signaling in the mutants, it just suggests that the molecular mechanism involved could be much more

complex and BMP signaling could only be one among the many factors that caused the observed phenotype. Trio is the only known gene that is found till date to be the gene target of BMP signaling but that does not exclude the possibility of more targets. Since anterograde and retrograde transport is affected in Khc^{N262S} mutants, multiple signaling pathways might have been implicated and upregulating BMP signaling alone would not suffice.

5.6 Future outlook

Our studies show that axonal trafficking and synaptic defects could be the early cellular mechanisms leading to the development of SPG10 pathology. Hence, treatment aimed at axonal and synaptic rescue could be effective. It may not be helpful in completely eliminating the pathology but at least might help in prolonging the onset of the disease. Further studies should be aimed at identifying cargos that accumulate first in the swellings so as to understand the temporal sequence of HSP pathogenesis.

It is very clear from my study that outnumbering the mutant kinesin with wild type kinesin showed a significant rescue in pathology at behavioral and cellular levels and hence treatments could also aim at diluting the mutant kinesin in the system. It could be done using recombinant kinesin heavy chain that would specifically bind to it but not the mutated ones and thereby outnumbering the mutant kinesins. At the same time, stabilizing microtubules could also allow more non mutant kinesin dimers and other compensating kinesin family members to carry cargos whereby the onset of the disease could be delayed. Maybe the combination of recombinant kinesin delivery and site specific injection of microtubule stabilizing drugs could prove very effective.

6 References

Aberle, H., A. P. Haghighi, et al. (2002). "wishful thinking encodes a BMP type II receptor that regulates synaptic growth in Drosophila." Neuron **33**(4): 545-558.

Andretic, R., Y. C. Kim, et al. (2008). "Drosophila D1 dopamine receptor mediates caffeine-induced arousal." Proc Natl Acad Sci U S A **105**(51): 20392-20397.

Atorino, L., L. Silvestri, et al. (2003). "Loss of m-AAA protease in mitochondria causes complex I deficiency and increased sensitivity to oxidative stress in hereditary spastic paraplegia." J Cell Biol **163**(4): 777-787.

Bainton, R. J., L. T. Tsai, et al. (2000). "Dopamine modulates acute responses to cocaine, nicotine and ethanol in Drosophila." Curr Biol **10**(4): 187-194.

Ball, R. W., M. Warren-Paquin, et al. (2010). "Retrograde BMP signaling controls synaptic growth at the NMJ by regulating trio expression in motor neurons." Neuron **66**(4): 536-549.

Barry, D. M., S. Millecamps, et al. (2007). "New movements in neurofilament transport, turnover and disease." Exp Cell Res **313**(10): 2110-2120.

Bayat, V., M. Jaiswal, et al. (2011). "The BMP signaling pathway at the Drosophila neuromuscular junction and its links to neurodegenerative diseases." Curr Opin Neurobiol **21**(1): 182-188.

Bellen, H. J., C. Tong, et al. (2010). "100 years of Drosophila research and its impact on vertebrate neuroscience: a history lesson for the future." Nat Rev Neurosci **11**(7): 514-522.

Berg, I., S. Thor, et al. (2009). "Modeling familial amyloidotic polyneuropathy (Transthyretin V30M) in Drosophila melanogaster." Neurodegener Dis **6**(3): 127-138.

Bhat, K. M., I. Gaziova, et al. (2007). "Regulation of axon guidance by slit and netrin signaling in the Drosophila ventral nerve cord." Genetics **176**(4): 2235-2246.

Blackstone, C., C. J. O'Kane, et al. (2011). "Hereditary spastic paraplegias: membrane traffic and the motor pathway." Nat Rev Neurosci **12**(1): 31-42.

Bonnet, C., D. Boucher, et al. (2001). "Differential binding regulation of microtubule-associated proteins MAP1A, MAP1B, and MAP2 by tubulin polyglutamylation." J Biol Chem **276**(16): 12839-12848.

Brady, S. T., R. J. Lasek, et al. (1982). "Fast axonal transport in extruded axoplasm from squid giant axon." Science **218**(4577): 1129-1131.

Brand, A. H. and N. Perrimon (1993). "Targeted gene expression as a means of altering cell fates and generating dominant phenotypes." Development **118**(2): 401-415.

Bulat, V., M. Rast, et al. (2014). "Presynaptic CK2 promotes synapse organization and stability by targeting Ankyrin2." J Cell Biol **204**(1): 77-94.

Cai, D., D. P. McEwen, et al. (2009). "Single molecule imaging reveals differences in microtubule track selection between Kinesin motors." PLoS Biol **7**(10): e1000216.

Cao, W., H. J. Song, et al. (2008). "Identification of novel genes that modify phenotypes induced by Alzheimer's beta-amyloid overexpression in Drosophila." Genetics **178**(3): 1457-1471.

Chan, Y. B., I. Miguel-Aliaga, et al. (2003). "Neuromuscular defects in a Drosophila survival motor neuron gene mutant." Hum Mol Genet **12**(12): 1367-1376.

Chevalier-Larsen, E. and E. L. Holzbaur (2006). "Axonal transport and neurodegenerative disease." Biochim Biophys Acta **1762**(11-12): 1094-1108.

Collins, C. A. and A. DiAntonio (2007). "Synaptic development: insights from Drosophila." Curr Opin Neurobiol **17**(1): 35-42.

Conde, C. and A. Caceres (2009). "Microtubule assembly, organization and dynamics in axons and dendrites." Nat Rev Neurosci **10**(5): 319-332.

Dagenbach, E. M. and S. A. Endow (2004). "A new kinesin tree." J Cell Sci **117**(Pt 1): 3-7.

Darabid, H., A. P. Perez-Gonzalez, et al. (2014). "Neuromuscular synaptogenesis: coordinating partners with multiple functions." Nat Rev Neurosci **15**(11): 703-718.

De Vos, K. J., A. J. Grierson, et al. (2008). "Role of axonal transport in neurodegenerative diseases." Annu Rev Neurosci **31**: 151-173.

Deacon, S. W., A. S. Serpinskaya, et al. (2003). "Dynactin is required for bidirectional organelle transport." J Cell Biol **160**(3): 297-301.

DeBoer, S. R., Y. You, et al. (2008). "Conventional kinesin holoenzymes are composed of heavy and light chain homodimers." Biochemistry **47**(15): 4535-4543.
Deluca, G. C., G. C. Ebers, et al. (2004). "The extent of axonal loss in the long tracts in hereditary spastic paraplegia." Neuropathol Appl Neurobiol **30**(6): 576-584.
Desai, A. and T. J. Mitchison (1997). "Microtubule polymerization dynamics." Annu Rev Cell Dev Biol **13**: 83-117.
Desset, S., N. Buchon, et al. (2008). "In Drosophila melanogaster the COM locus directs the somatic silencing of two retrotransposons through both Piwi-dependent and -independent pathways." PLoS One **3**(2): e1526.
Dietzl, G., D. Chen, et al. (2007). "A genome-wide transgenic RNAi library for conditional gene inactivation in Drosophila." Nature **448**(7150): 151-156.
Dion, P. A., H. Daoud, et al. (2009). "Genetics of motor neuron disorders: new insights into pathogenic mechanisms." Nat Rev Genet **10**(11): 769-782.
Dompierre, J. P., J. D. Godin, et al. (2007). "Histone deacetylase 6 inhibition compensates for the transport deficit in Huntington's disease by increasing tubulin acetylation." J Neurosci **27**(13): 3571-3583.
Dresbach, T., V. Torres, et al. (2006). "Assembly of active zone precursor vesicles: obligatory trafficking of presynaptic cytomatrix proteins Bassoon and Piccolo via a trans-Golgi compartment." J Biol Chem **281**(9): 6038-6047.
Dunn, S., E. E. Morrison, et al. (2008). "Differential trafficking of Kif5c on tyrosinated and detyrosinated microtubules in live cells." J Cell Sci **121**(Pt 7): 1085-1095.
Eaton, B. A. and G. W. Davis (2005). "LIM Kinase1 controls synaptic stability downstream of the type II BMP receptor." Neuron **47**(5): 695-708.
Ebbing, B., K. Mann, et al. (2008). "Effect of spastic paraplegia mutations in KIF5A kinesin on transport activity." Hum Mol Genet **17**(9): 1245-1252.
Falcon-Perez, J. M., R. Romero-Calderon, et al. (2007). "The Drosophila pigmentation gene pink (p) encodes a homologue of human Hermansky-Pudlak syndrome 5 (HPS5)." Traffic **8**(2): 154-168.
Feany, M. B. and W. W. Bender (2000). "A Drosophila model of Parkinson's disease." Nature **404**(6776): 394-398.
Fejtova, A. and E. D. Gundelfinger (2006). "Molecular organization and assembly of the presynaptic active zone of neurotransmitter release." Results Probl Cell Differ **43**: 49-68.
Ferreirinha, F., A. Quattrini, et al. (2004). "Axonal degeneration in paraplegin-deficient mice is associated with abnormal mitochondria and impairment of axonal transport." J Clin Invest **113**(2): 231-242.
Finsterer, J., W. Loscher, et al. (2012). "Hereditary spastic paraplegias with autosomal dominant, recessive, X-linked, or maternal trait of inheritance." J Neurol Sci **318**(1-2): 1-18.
Fuger, P., V. Sreekumar, et al. (2012). "Spastic paraplegia mutation N256S in the neuronal microtubule motor KIF5A disrupts axonal transport in a Drosophila HSP model." PLoS Genet **8**(11): e1003066.
Goizet, C., A. Boukhris, et al. (2009). "Complicated forms of autosomal dominant hereditary spastic paraplegia are frequent in SPG10." Hum Mutat **30**(2): E376-385.
Goldstein, L. S. (2001). "Kinesin molecular motors: transport pathways, receptors, and human disease." Proc Natl Acad Sci U S A **98**(13): 6999-7003.
Graf, E. R., R. W. Daniels, et al. (2009). "Rab3 dynamically controls protein composition at active zones." Neuron **64**(5): 663-677.
Grafstein, B. and D. S. Forman (1980). "Intracellular transport in neurons." Physiol Rev **60**(4): 1167-1283.
Hall, A. C., F. R. Lucas, et al. (2000). "Axonal remodeling and synaptic differentiation in the cerebellum is regulated by WNT-7a signaling." Cell **100**(5): 525-535.
Harding, A. E. (1983). "Classification of the hereditary ataxias and paraplegias." Lancet **1**(8334): 1151-1155.
Hirokawa, N. (1982). "Cross-linker system between neurofilaments, microtubules, and membranous organelles in frog axons revealed by the quick-freeze, deep-etching method." J Cell Biol **94**(1): 129-142.

Hirokawa, N. (1994). "Microtubule organization and dynamics dependent on microtubule-associated proteins." Curr Opin Cell Biol **6**(1): 74-81.
Hirokawa, N. (1998). "Kinesin and dynein superfamily proteins and the mechanism of organelle transport." Science **279**(5350): 519-526.
Hirokawa, N., R. Nitta, et al. (2009). "The mechanisms of kinesin motor motility: lessons from the monomeric motor KIF1A." Nat Rev Mol Cell Biol **10**(12): 877-884.
Hirokawa, N., S. Niwa, et al. (2010). "Molecular motors in neurons: transport mechanisms and roles in brain function, development, and disease." Neuron **68**(4): 610-638.
Hirokawa, N. and Y. Noda (2008). "Intracellular transport and kinesin superfamily proteins, KIFs: structure, function, and dynamics." Physiol Rev **88**(3): 1089-1118.
Hirokawa, N., Y. Noda, et al. (1998). "Kinesin and dynein superfamily proteins in organelle transport and cell division." Curr Opin Cell Biol **10**(1): 60-73.
Hirokawa, N., Y. Noda, et al. (2009). "Kinesin superfamily motor proteins and intracellular transport." Nat Rev Mol Cell Biol **10**(10): 682-696.
Hirokawa, N., K. K. Pfister, et al. (1989). "Submolecular domains of bovine brain kinesin identified by electron microscopy and monoclonal antibody decoration." Cell **56**(5): 867-878.
Hummel, T., K. Krukkert, et al. (2000). "Drosophila Futsch/22C10 is a MAP1B-like protein required for dendritic and axonal development." Neuron **26**(2): 357-370.
Hurd, D. D. and W. M. Saxton (1996). "Kinesin mutations cause motor neuron disease phenotypes by disrupting fast axonal transport in Drosophila." Genetics **144**(3): 1075-1085.
Imlach, W. and B. D. McCabe (2009). "Electrophysiological methods for recording synaptic potentials from the NMJ of Drosophila larvae." J Vis Exp(24).
Inomata, H., Y. Nakamura, et al. (2003). "A scaffold protein JIP-1b enhances amyloid precursor protein phosphorylation by JNK and its association with kinesin light chain 1." J Biol Chem **278**(25): 22946-22955.
Jackson, G. R., I. Salecker, et al. (1998). "Polyglutamine-expanded human huntingtin transgenes induce degeneration of Drosophila photoreceptor neurons." Neuron **21**(3): 633-642.
Joshi, H. C. (1994). "Microtubule organizing centers and gamma-tubulin." Curr Opin Cell Biol **6**(1): 54-62.
Kanai, Y., Y. Okada, et al. (2000). "KIF5C, a novel neuronal kinesin enriched in motor neurons." J Neurosci **20**(17): 6374-6384.
Kang, M. J., T. J. Hansen, et al. (2014). "Disruption of Axonal Transport Perturbs Bone Morphogenetic Protein (BMP) - Signaling and Contributes to Synaptic Abnormalities in Two Neurodegenerative Diseases." PLoS One **9**(8): e104617.
Karle, K. N., D. Mockel, et al. (2012). "Axonal transport deficit in a KIF5A(-/-) mouse model." Neurogenetics **13**(2): 169-179.
Kasher, P. R., K. J. De Vos, et al. (2009). "Direct evidence for axonal transport defects in a novel mouse model of mutant spastin-induced hereditary spastic paraplegia (HSP) and human HSP patients." J Neurochem **110**(1): 34-44.
Kawaguchi, K. (2013). "Role of kinesin-1 in the pathogenesis of SPG10, a rare form of hereditary spastic paraplegia." Neuroscientist **19**(4): 336-344.
Keshishian, H. and Y. S. Kim (2004). "Orchestrating development and function: retrograde BMP signaling in the Drosophila nervous system." Trends Neurosci **27**(3): 143-147.
Kimura, T., H. Watanabe, et al. (2005). "Tubulin and CRMP-2 complex is transported via Kinesin-1." J Neurochem **93**(6): 1371-1382.
Kohler, K., E. Brunner, et al. (2009). "A combined proteomic and genetic analysis identifies a role for the lipid desaturase Desat1 in starvation-induced autophagy in Drosophila." Autophagy **5**(7): 980-990.
Konishi, Y. and M. Setou (2009). "Tubulin tyrosination navigates the kinesin-1 motor domain to axons." Nat Neurosci **12**(5): 559-567.
Kozielski, F., S. Sack, et al. (1997). "The crystal structure of dimeric kinesin and implications for microtubule-dependent motility." Cell **91**(7): 985-994.

Kreitzer, G., G. Liao, et al. (1999). "Detyrosination of tubulin regulates the interaction of intermediate filaments with microtubules in vivo via a kinesin-dependent mechanism." Mol Biol Cell **10**(4): 1105-1118.

Krylova, O., J. Herreros, et al. (2002). "WNT-3, expressed by motoneurons, regulates terminal arborization of neurotrophin-3-responsive spinal sensory neurons." Neuron **35**(6): 1043-1056.

Larcher, J. C., D. Boucher, et al. (1996). "Interaction of kinesin motor domains with alpha- and beta-tubulin subunits at a tau-independent binding site. Regulation by polyglutamylation." J Biol Chem **271**(36): 22117-22124.

Lawrence, P. A. and P. Johnston (1989). "Pattern formation in the Drosophila embryo: allocation of cells to parasegments by even-skipped and fushi tarazu." Development **105**(4): 761-767.

Li, H., S. H. Li, et al. (2001). "Huntingtin aggregate-associated axonal degeneration is an early pathological event in Huntington's disease mice." J Neurosci **21**(21): 8473-8481.

Liao, G. and G. G. Gundersen (1998). "Kinesin is a candidate for cross-bridging microtubules and intermediate filaments. Selective binding of kinesin to detyrosinated tubulin and vimentin." J Biol Chem **273**(16): 9797-9803.

Lindsay, S. A. and S. A. Wasserman (2014). "Conventional and non-conventional Drosophila Toll signaling." Dev Comp Immunol **42**(1): 16-24.

Lo Giudice, T., F. Lombardi, et al. (2014). "Hereditary spastic paraplegia: Clinical-genetic characteristics and evolving molecular mechanisms." Exp Neurol.

Lodish H, B. A., Zipursky SL, et al. (2000). Molecular Cell Biology.

Lohr, D., P. Venkov, et al. (1995). "Transcriptional regulation in the yeast GAL gene family: a complex genetic network." FASEB J **9**(9): 777-787.

Mahr, A. and H. Aberle (2006). "The expression pattern of the Drosophila vesicular glutamate transporter: a marker protein for motoneurons and glutamatergic centers in the brain." Gene Expr Patterns **6**(3): 299-309.

Mandelkow, E. and E. M. Mandelkow (1995). "Microtubules and microtubule-associated proteins." Curr Opin Cell Biol **7**(1): 72-81.

Marques, G., H. Bao, et al. (2002). "The Drosophila BMP type II receptor Wishful Thinking regulates neuromuscular synapse morphology and function." Neuron **33**(4): 529-543.

McCabe, B. D., S. Hom, et al. (2004). "Highwire regulates presynaptic BMP signaling essential for synaptic growth." Neuron **41**(6): 891-905.

McCabe, B. D., G. Marques, et al. (2003). "The BMP homolog Gbb provides a retrograde signal that regulates synaptic growth at the Drosophila neuromuscular junction." Neuron **39**(2): 241-254.

McClung, C. and J. Hirsh (1998). "Stereotypic behavioral responses to free-base cocaine and the development of behavioral sensitization in Drosophila." Curr Biol **8**(2): 109-112.

McGuire, S. E., M. Deshazer, et al. (2005). "Thirty years of olfactory learning and memory research in Drosophila melanogaster." Prog Neurobiol **76**(5): 328-347.

Mockett, R. J., S. N. Radyuk, et al. (2003). "Phenotypic effects of familial amyotrophic lateral sclerosis mutant Sod alleles in transgenic Drosophila." Proc Natl Acad Sci U S A **100**(1): 301-306.

Montell, C. (2005). "TRP channels in Drosophila photoreceptor cells." J Physiol **567**(Pt 1): 45-51.

Moore, L. A., H. T. Broihier, et al. (1998). "Identification of genes controlling germ cell migration and embryonic gonad formation in Drosophila." Development **125**(4): 667-678.

Morton, A. M., A. L. Cunningham, et al. (2010). "Kinesin-1 plays a role in transport of SNAP-25 to the plasma membrane." Biochem Biophys Res Commun **391**(1): 388-393.

Moses, K., M. C. Ellis, et al. (1989). "The glass gene encodes a zinc-finger protein required by Drosophila photoreceptor cells." Nature **340**(6234): 531-536.

Mudher, A., D. Shepherd, et al. (2004). "GSK-3beta inhibition reverses axonal transport defects and behavioural phenotypes in Drosophila." Mol Psychiatry **9**(5): 522-530.

Newfeld, S. J., R. G. Wisotzkey, et al. (1999). "Molecular evolution of a developmental pathway: phylogenetic analyses of transforming growth factor-beta family ligands, receptors and Smad signal transducers." Genetics **152**(2): 783-795.

Newsome, T. P., B. Asling, et al. (2000). "Analysis of Drosophila photoreceptor axon guidance in eye-specific mosaics." Development **127**(4): 851-860.

Nichols, R., W. G. Bendena, et al. (2002). "Myotropic peptides in Drosophila melanogaster and the genes that encode them." J Neurogenet **16**(1): 1-28.
Niclas, J., F. Navone, et al. (1994). "Cloning and localization of a conventional kinesin motor expressed exclusively in neurons." Neuron **12**(5): 1059-1072.
Ohtsuka, T., E. Takao-Rikitsu, et al. (2002). "Cast: a novel protein of the cytomatrix at the active zone of synapses that forms a ternary complex with RIM1 and munc13-1." J Cell Biol **158**(3): 577-590.
Pandey, U. B. and C. D. Nichols (2011). "Human disease models in Drosophila melanogaster and the role of the fly in therapeutic drug discovery." Pharmacol Rev **63**(2): 411-436.
Panzer, S., D. Weigel, et al. (1992). "Organogenesis in Drosophila melanogaster: embryonic salivary gland determination is controlled by homeotic and dorsoventral patterning genes." Development **114**(1): 49-57.
Petersen, S. A., R. D. Fetter, et al. (1997). "Genetic analysis of glutamate receptors in Drosophila reveals a retrograde signal regulating presynaptic transmitter release." Neuron **19**(6): 1237-1248.
Phelps, C. B. and A. H. Brand (1998). "Ectopic gene expression in Drosophila using GAL4 system." Methods **14**(4): 367-379.
Pokrzywa, M., I. Dacklin, et al. (2007). "Misfolded transthyretin causes behavioral changes in a Drosophila model for transthyretin-associated amyloidosis." Eur J Neurosci **26**(4): 913-924.
Prussing, K., A. Voigt, et al. (2013). "Drosophila melanogaster as a model organism for Alzheimer's disease." Mol Neurodegener **8**: 35.
Ptashne, M. (1988). "How eukaryotic transcriptional activators work." Nature **335**(6192): 683-689.
Pulipparacharuvil, S., M. A. Akbar, et al. (2005). "Drosophila Vps16A is required for trafficking to lysosomes and biogenesis of pigment granules." J Cell Sci **118**(Pt 16): 3663-3673.
Raftery, L. A., V. Twombly, et al. (1995). "Genetic screens to identify elements of the decapentaplegic signaling pathway in Drosophila." Genetics **139**(1): 241-254.
Rawson, J. M., M. Lee, et al. (2003). "Drosophila neuromuscular synapse assembly and function require the TGF-beta type I receptor saxophone and the transcription factor Mad." J Neurobiol **55**(2): 134-150.
Ready, D. F., T. E. Hanson, et al. (1976). "Development of the Drosophila retina, a neurocrystalline lattice." Dev Biol **53**(2): 217-240.
Reed, N. A., D. Cai, et al. (2006). "Microtubule acetylation promotes kinesin-1 binding and transport." Curr Biol **16**(21): 2166-2172.
Reid, E. (2003). "Science in motion: common molecular pathological themes emerge in the hereditary spastic paraplegias." J Med Genet **40**(2): 81-86.
Reid, E., A. M. Dearlove, et al. (1999). "A new locus for autosomal dominant "pure" hereditary spastic paraplegia mapping to chromosome 12q13, and evidence for further genetic heterogeneity." Am J Hum Genet **65**(3): 757-763.
Reid, E., M. Kloos, et al. (2002). "A kinesin heavy chain (KIF5A) mutation in hereditary spastic paraplegia (SPG10)." Am J Hum Genet **71**(5): 1189-1194.
Reiter, L. T., L. Potocki, et al. (2001). "A systematic analysis of human disease-associated gene sequences in Drosophila melanogaster." Genome Res **11**(6): 1114-1125.
Roos, J., T. Hummel, et al. (2000). "Drosophila Futsch regulates synaptic microtubule organization and is necessary for synaptic growth." Neuron **26**(2): 371-382.
Rorth, P. (1996). "A modular misexpression screen in Drosophila detecting tissue-specific phenotypes." Proc Natl Acad Sci U S A **93**(22): 12418-12422.
Saitoe, M., T. L. Schwarz, et al. (2001). "Absence of junctional glutamate receptor clusters in Drosophila mutants lacking spontaneous transmitter release." Science **293**(5529): 514-517.
Salinas, P. C. (2012). "Wnt signaling in the vertebrate central nervous system: from axon guidance to synaptic function." Cold Spring Harb Perspect Biol **4**(2).
Salinas, S., C. Proukakis, et al. (2008). "Hereditary spastic paraplegia: clinical features and pathogenetic mechanisms." Lancet Neurol **7**(12): 1127-1138.
Sanchez-Ferrero, E., E. Coto, et al. (2012). "Mitochondrial DNA polymorphisms/haplogroups in hereditary spastic paraplegia." J Neurol **259**(2): 246-250.

Satta, R., N. Dimitrijevic, et al. (2003). "Drosophila metabolize 1,4-butanediol into gamma-hydroxybutyric acid in vivo." Eur J Pharmacol **473**(2-3): 149-152.
Schulze, E., D. J. Asai, et al. (1987). "Posttranslational modification and microtubule stability." J Cell Biol **105**(5): 2167-2177.
Sherwood, N. T., Q. Sun, et al. (2004). "Drosophila spastin regulates synaptic microtubule networks and is required for normal motor function." PLoS Biol **2**(12): e429.
Siksou, L., P. Rostaing, et al. (2007). "Three-dimensional architecture of presynaptic terminal cytomatrix." J Neurosci **27**(26): 6868-6877.
Simon, A. F., D. T. Liang, et al. (2006). "Differential decline in behavioral performance of Drosophila melanogaster with age." Mech Ageing Dev **127**(7): 647-651.
Smith, R. B., J. B. Machamer, et al. (2012). "Relay of retrograde synaptogenic signals through axonal transport of BMP receptors." J Cell Sci **125**(Pt 16): 3752-3764.
Snow, P. M., N. H. Patel, et al. (1987). "Neural-specific carbohydrate moiety shared by many surface glycoproteins in Drosophila and grasshopper embryos." J Neurosci **7**(12): 4137-4144.
Song, Y. H., A. Marx, et al. (2001). "Structure of a fast kinesin: implications for ATPase mechanism and interactions with microtubules." EMBO J **20**(22): 6213-6225.
Speese, S. D. and V. Budnik (2007). "Wnts: up-and-coming at the synapse." Trends Neurosci **30**(6): 268-275.
Strauss, R. (2002). "The central complex and the genetic dissection of locomotor behaviour." Curr Opin Neurobiol **12**(6): 633-638.
Su, Q., Q. Cai, et al. (2004). "Syntabulin is a microtubule-associated protein implicated in syntaxin transport in neurons." Nat Cell Biol **6**(10): 941-953.
Takasu-Ishikawa, E., M. Yoshihara, et al. (2001). "Screening for synaptic defects revealed a locus involved in presynaptic and postsynaptic functions in Drosophila embryos." J Neurobiol **48**(2): 101-119.
Tanaka, Y., Y. Kanai, et al. (1998). "Targeted disruption of mouse conventional kinesin heavy chain, kif5B, results in abnormal perinuclear clustering of mitochondria." Cell **93**(7): 1147-1158.
Terada, S., M. Kinjo, et al. (2010). "Kinesin-1/Hsc70-dependent mechanism of slow axonal transport and its relation to fast axonal transport." EMBO J **29**(4): 843-854.
Terada, S., M. Kinjo, et al. (2000). "Oligomeric tubulin in large transporting complex is transported via kinesin in squid giant axons." Cell **103**(1): 141-155.
Tsang, H. T., T. L. Edwards, et al. (2009). "The hereditary spastic paraplegia proteins NIPA1, spastin and spartin are inhibitors of mammalian BMP signalling." Hum Mol Genet **18**(20): 3805-3821.
Uchida, A., N. H. Alami, et al. (2009). "Tight functional coupling of kinesin-1A and dynein motors in the bidirectional transport of neurofilaments." Mol Biol Cell **20**(23): 4997-5006.
Vale, R. D. (1996). "Switches, latches, and amplifiers: common themes of G proteins and molecular motors." J Cell Biol **135**(2): 291-302.
Vale, R. D. (2003). "The molecular motor toolbox for intracellular transport." Cell **112**(4): 467-480.
Vale, R. D., T. S. Reese, et al. (1985). "Identification of a novel force-generating protein, kinesin, involved in microtubule-based motility." Cell **42**(1): 39-50.
van Haren, J., J. Boudeau, et al. (2014). "Dynamic microtubules catalyze formation of navigator-TRIO complexes to regulate neurite extension." Curr Biol **24**(15): 1778-1785.
Venken, K. J. and H. J. Bellen (2007). "Transgenesis upgrades for Drosophila melanogaster." Development **134**(20): 3571-3584.
Verhey, K. J., D. Meyer, et al. (2001). "Cargo of kinesin identified as JIP scaffolding proteins and associated signaling molecules." J Cell Biol **152**(5): 959-970.
Verstreken, P., T. Ohyama, et al. (2008). "FM 1-43 labeling of synaptic vesicle pools at the Drosophila neuromuscular junction." Methods Mol Biol **440**: 349-369.
Vosshall, L. B. and R. F. Stocker (2007). "Molecular architecture of smell and taste in Drosophila." Annu Rev Neurosci **30**: 505-533.
Wagh, D. A., T. M. Rasse, et al. (2006). "Bruchpilot, a protein with homology to ELKS/CAST, is required for structural integrity and function of synaptic active zones in Drosophila." Neuron **49**(6): 833-844.

Walker, R. A., E. T. O'Brien, et al. (1988). "Dynamic instability of individual microtubules analyzed by video light microscopy: rate constants and transition frequencies." J Cell Biol **107**(4): 1437-1448.
Wang, J. T., Z. A. Medress, et al. (2012). "Axon degeneration: molecular mechanisms of a self-destruction pathway." J Cell Biol **196**(1): 7-18.
Wang, L. and A. Brown (2010). "A hereditary spastic paraplegia mutation in kinesin-1A/KIF5A disrupts neurofilament transport." Mol Neurodegener **5**: 52.
Wang, X., W. R. Shaw, et al. (2007). "Drosophila spichthyin inhibits BMP signaling and regulates synaptic growth and axonal microtubules." Nat Neurosci **10**(2): 177-185.
Warrick, J. M., H. Y. Chan, et al. (1999). "Suppression of polyglutamine-mediated neurodegeneration in Drosophila by the molecular chaperone HSP70." Nat Genet **23**(4): 425-428.
Waterman-Storer, C. M. and E. L. Holzbaur (1996). "The product of the Drosophila gene, Glued, is the functional homologue of the p150Glued component of the vertebrate dynactin complex." J Biol Chem **271**(2): 1153-1159.
Watson, M. R., R. D. Lagow, et al. (2008). "A drosophila model for amyotrophic lateral sclerosis reveals motor neuron damage by human SOD1." J Biol Chem **283**(36): 24972-24981.
Yamada, M., S. Toba, et al. (2010). "mNUDC is required for plus-end-directed transport of cytoplasmic dynein and dynactins by kinesin-1." EMBO J **29**(3): 517-531.
Yang, J. T., W. M. Saxton, et al. (1988). "Isolation and characterization of the gene encoding the heavy chain of Drosophila kinesin." Proc Natl Acad Sci U S A **85**(6): 1864-1868.
Yao, C. K., Y. Q. Lin, et al. (2009). "A synaptic vesicle-associated Ca2+ channel promotes endocytosis and couples exocytosis to endocytosis." Cell **138**(5): 947-960.
Yoshihara, M., A. W. Ensminger, et al. (2001). "Neurobiology and the Drosophila genome." Funct Integr Genomics **1**(4): 235-240.
Zeidler, M. P., C. Tan, et al. (2004). "Temperature-sensitive control of protein activity by conditionally splicing inteins." Nat Biotechnol **22**(7): 871-876.
Zhao, J. and P. Hedera (2013). "Hereditary spastic paraplegia-causing mutations in atlastin-1 interfere with BMPRII trafficking." Mol Cell Neurosci **52**: 87-96.